Dynamics of the Jovian magnetotail

Von der Fakultät für Physik und Geowissenschaften
der Technischen Universität Carolo-Wilhelmina
zu Braunschweig
zur Erlangung des Grades einer
Doktorin der Naturwissenschaften
(Dr.rer.nat.)
genehmigte
Dissertation

von Elena Aleksandrovna Kronberg
aus Barnaul/Russia

Bibliografische Information Der Deutschen Bibliothek

Die Deutsche Bibliothek verzeichnet diese Publikation in der Deutschen Nationalbibliografie; detaillierte bibliografische Daten sind im Internet über `http://dnb.ddb.de` abrufbar.

1. Referentin oder Referent: Prof. Dr. K.-H. Glassmeier
2. Referentin oder Referent: Prof. Dr. M. K. Dougherty
eingereicht am: 13 Februar
mündliche Prüfung (Disputation) am: 2 Mai 2006

Copyright © Copernicus GmbH 2006

ISBN 3-936586-55-1

Copernicus GmbH, Katlenburg-Lindau
Druck: Schaltungsdienst Lange, Berlin

Printed in Germany

Vorveröffentlichungen der Dissertation

Teilergebnisse aus dieser Arbeit wurden mit Genehmigung der Fakultät für Physik und Geowissenschaften, vertreten durch den Mentor oder den Betreuer der Arbeit, in folgenden Beiträgen vorab veröffentlicht:

Publikationen

Kronberg E. A., J. Woch, N. Krupp, A. Lagg, K. K. Khurana, and K.-H. Glassmeier, *Mass release at Jupiter - substorm-like processes in the Jovian magnetotail*. J. Geophys. Res., 110, A03211, doi:10.1029/2004JA010777, 2005.

Tagungsbeiträge

Kronberg E. A., J. Woch, N. Krupp, A. Lagg, and K.-H. Glassmeier, *Bursty bulk flow events as a signature for magnetic reconnection in the Jovian magnetosphere* (Poster), Magnetic Reconnection and the Dynamic Sun, St Andrews, Great Britain, 8 - 10 September, 2003.

Kronberg E. A., J. Woch, N. Krupp, A. Lagg, and K.-H. Glassmeier, *Substorms at Jupiter?* (Talk), Deutsche Physikalische Gesellschaft (DPG)- Arbeitsgemeinschaft Extraterrestrische Forschung (AEF), Frühjahrstagung, Kiel, Germany, 8 - 11 March, 2004.

Kronberg E. A., J. Woch, N. Krupp, A. Lagg, K.-H. Glassmeier, and K. K. Khurana, *Substorms at Jupiter?* (Talk), European Geophysical Union (EGU), First General Assembly, Nice, France, 25 - 30 April, 2004.

Kronberg E. A., K.-H. Glassmeier, J. Woch, N. Krupp, A. Lagg, *Why is the dynamics of the Jovian magnetosphere quasi-periodical?* (Talk), European Geophysical Union (EGU), Vienna, Austria, 24 - 29 April, 2005.

Kronberg E. A., J. Woch, N. Krupp, A. Lagg, and K.-H. Glassmeier, *Periodical substorms at Jupiter and Earth* (Talk), International Association of Geomagnetism and Aeronomy (IAGA), Toulouse, France, 20 - 29 July, 2005.

Contents

List of Figures

List of Tables

Abstract

The Jupiter orbiting spacecraft Galileo has provided evidence that the Jovian magnetotail is subject to a periodic process with a typical timescale of several days by which the Jovian system is presumably releasing its excess iogenic mass. This process is analyzed using data returned from the Energetic Particles Detector (EPD), the magnetometer and plasma wave experiment on Galileo. The mass release process resembles a terrestrial substorm in the sense of a global reconfiguration of the magnetotail. During the initial "loading" phase the plasma convection is at a moderate speed in the corotational direction, and the Jovian plasma sheet appears to be in a stable configuration. In the release phase reconnection through a thinned current sheet leads to radially inward and outward plasma flows and the ejection of plasmoids. The striking difference from terrestrial substorms is the periodical appearance of the reconfiguration events. Such an intrinsic periodic behavior cannot readily be explained by a solar wind driven process. Therefore the role of the solar wind as energy source is of less importance than for terrestrial substorms. Instead, ion mass-loading from internal plasma sources and fast planetary rotation causes stretching of magnetotail field lines. The resulting magnetotail configuration favors magnetic reconnection. This leads to the formation and release of plasmoids. Continued mass-loading then again leads to stretching of tail field lines. Thus assuming that this quasi-periodical process is internally driven, a simple conceptual model to estimate the time period of the periodic reconfiguration process is constructed. The model shows that the suggested intrinsic mechanism can explain the observed several days periodicities of Jovian substorm-like processes.

1 Introduction

1.1 Jupiter and its dynamical surrounding

Jupiter in many aspects is the most outstanding planet in our solar system. Jupiter is the biggest planet with a radius of R_J =7.1 $\cdot 10^7$ m and a mass of $\sim$ 1.8987 $\cdot$ 10^{27} kg. Jupiter also has the fastest rotation period of $\sim$ 9 h 55 min and the largest magnetic moment of $\sim$ $4.2 \cdot 10^{-4}$ T R_J^3. The radiation belts of Jupiter are the most intense and the radio emissions are the strongest. Jupiter has the largest moon of the solar system Ganymede, and the strongest source of plasma located deep in the inner magnetosphere, the moon Io, releasing about 1000 kg s^{-1} of material.

This fascinating solar system body is embedded in a very dynamical plasma and magnetic environment. An example of its dynamical behavior are sudden changes in the circulation of plasma and corresponding topological changes in the magnetic field.

One external factor which influences the dynamics is the solar wind. Its dynamic pressure shapes the planetary field lines forming a cavity which contains a low-density hot plasma that comes from internal and external sources. This cavity is called a magnetosphere. Jupiter has the largest magnetosphere in our solar system which is so large that, if it could be observed from the Earth, it would appear larger than the Earth's moon. The size of the Jovian magnetosphere is defined by a balance between the dynamic pressure of the solar wind, the magnetic pressure of the planet and the plasma pressure from internal sources. The reason of the gigantic size is that the solar wind mass density and hence its dynamic pressure decreases as the inverse square of the distance from the Sun. Consequently the dynamic solar wind pressure at Jupiter is 27 times smaller than at Earth (Russell 2001). Specifically this affects the size of the magnetosphere's outer boundary which is called magnetopause. Thus the dayside magnetopause of Jupiter was observed at distances from $\sim$ 45 to over 100 R_J (Joy et al. 2002).

Further factors, which make the Jovian magnetosphere strikingly different from the Earth, are the presence of the internal mass source Io and the fast planetary rotation. Jupiter's rotation is the engine that drives its magnetosphere and the mass addition from Io is the fuel that powers the magnetosphere. This leads to additional stress which stretches out the magnetic field forming a magnetodisc beyond about 24 R_J (Smith et al. 1975). The plasma (mainly consisting of oxygen, sulfur, protons and helium) generates an azimuthal current in the equatorial region of the Jovian magnetosphere which is confined to a thin current sheet with a thickness of $\sim$ 4 R_J in the dawn sector and around 7.6 R_J in the dusk sector (Khurana et al. 2004). Plasma is confined in the magnetodisc region where the loss cone is small. Thus the plasma and currents are found approximately in the same sheet-like region. Therefore the terms current sheet and plasma sheet can be used equally.

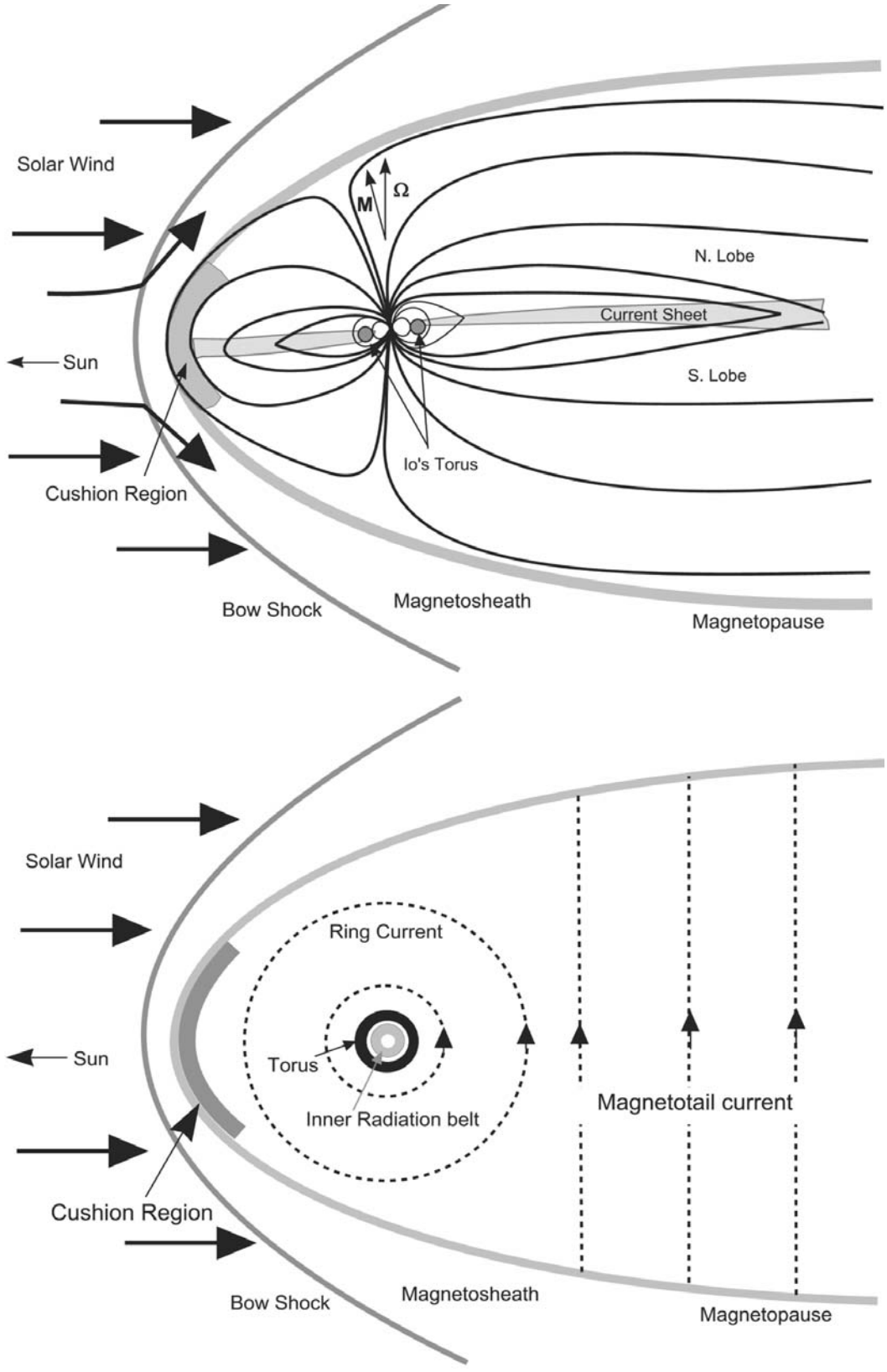

Figure 1.1: A scheme of Jupiter's magnetosphere in the noon-midnight meridian surface (top) and the equatorial cross-section (bottom), from Khurana et al. (2004).

The magnetic dipole tilt is $\sim 9.8^\circ$ and the 10-hour planetary rotation leads to periodical modulation (latitudinal motion) of the plasma sheet (see example in Figure 3.1).

The orientation of the planetary magnetic dipole is directed as the rotation axis and the field inside the plasma sheet is mainly southward orientated.

In Figure 1.1 this magnetic configuration is presented as a sketch of the Jovian magnetic field in the noon-midnight meridian plane. The boundary in front of the dayside magnetopause is called the bow shock, which reduces the speed and changes the direction of motion of solar wind particles. The region between the bow shock and the magnetopause is called the magnetosheath. A so called cushion region separates the magnetodisc from the magnetopause on the dayside. The magnetospheric regions above and below the current sheet are called lobes.

The Jovian magnetosphere is usually divided into three basic regions: the inner (< 10 R_J), the middle (10 - 40 R_J) and the outer (> 40 R_J) magnetosphere.

1.1.1 The inner magnetosphere: Region of plasma sources

The inner magnetosphere is the location of the inner radiation belts and the plasma sources. The magnetic field in this region is in first order produced by sources in the interior of the planet, i.e. the configuration is mostly dipole-like.

At 5.9 R_J , i. e. within the inner magnetosphere the moon Io is orbiting Jupiter. More than 100 active volcanoes have been discovered on Io releasing a mixture of ions and neutrals (mainly SO_2) through the Io atmosphere (for a review see Saur et al. 2004). The neutrals are ionized by electron impact ionization, charge exchange or by UV radiation. Thus the plasma composition in the Jovian magnetosphere is different from Earth, since it contains mainly heavy ions. The main mass loading region is about 2 Io diameters (5000 km) around the moon and is called Io torus. Io's orbital velocity is 17 km s^{-1} and the plasma at Io orbit corotates with a speed of 74 km s^{-1}. For example, the acceleration of ions released with a rate of 800 kg s^{-1} from orbital energies to corotational energies by the Io-torus interaction is equivalent to the power transferred into the Earth's magnetosphere during the storms, whereas at Jupiter this energy transfer is active continuously. The amount of magnetic flux convected into the region between $\sim$ 5.2 and $\sim$ 10 R_J is about 80 000 Wb s^{-1} (Russell 2001). The Io torus contains several million tons of plasma which slowly moves outward by the centrifugal force. Radial transport from Io is a possible loss mechanism which is usually associated with the interchange instability. A mass-loaded inner flux tube interchanges radially with an "empty" outer flux tube so that the heavily loaded tube moves outward (Hill et al. 1981, Thorne et al. 1997, Kivelson et al. 1997). This process preserves the magnetic flux and transports ions outward. If interchange is not accompanied by scattering, flux tubes will keep their total content until they get emptied at some very large distance. An example is the loss of ions in the magnetotail. The loss mechanism in the magnetotail is the main topic of this work.

Different estimates for the total mass-loading rate of ions from Io into the magnetosphere exist. Using a simplified model based on Galileo data of the plasma perturbations in Io's wake Bagenal (1997) estimated the Io source of ions within $5R_{Io}$ to 180 - 580 kg s^{-1}. Saur et al. (2003) reanalysed the work mentioned above, incorporated Hubble Space Telescope UV measurements and model calculations and concluded that Io supplies at most 200 kg s^{-1} in form of ions. From three-dimensional calculations Smyth and Mar-

coni (2003) derived a total mass-loading rate of ions (due to electron impact and charge exchange) as large as 275 kg s^{-1}. Thus Io is the main source of plasma in the Jovian magnetosphere. If mass-loading would be totally absent the magnetopause standoff distance would be only 40 R_J.

The second important source of ions in Jupiter's magnetosphere is the solar wind. The solar wind particle source is estimated by a consideration of the solar wind mass flux incident on the Jovian magnetopause to a maximum of $<$ 100 kg s $^{-1}$ of protons (Hill et al. 1983), which is relatively small compared with the Io mass source.

Ionization in the upper atmosphere by precipitating particles and subsequent acceleration by an electric field into the magnetosphere is the source for additional ~ 20 kg s $^{-1}$ ions, assuming that most of these ions are protons (Krimigis et al. 1981).

The Jovian moons Europa, Ganymede and Callisto presumably produce around 50 kg s^{-1} of oxygen ions (Schreier et al. 1993, Saur et al. 1998, Cooper et al. 2001).

1.1.2 The middle magnetosphere: Rotation effects

The plasma trapped by the strong magnetic field (with exception of a small part which precipitates into the ionosphere of Jupiter) is transported within the magnetosphere. The radial outflow of plasma is governed by diffusion and interchange motion.

The rotation of Jupiter provides the main source of energy for the magnetosphere and leads to the corotation pattern of the plasma convection. A mechanism to tap rotational energy is the field-aligned current system that transmits torque from Jupiter's ionosphere to the magnetospheric plasma (Balogh et al. 1992). Thus the radial current which enforces corotational flows in the equatorial plane and field-aligned currents close this current system through the ionosphere (see Figure 1.2). Large electric potentials associated with the field-aligned currents accelerate electrons into the ionosphere. This leads to the generation of the main auroral oval in the ionosphere. Conservation of angular momentum enforces an angular velocity decrease with distance, but the field-aligned current system opposes any corotation lag (Pontius 1997).

Where the ionosphere is not able to support sufficient angular momentum to the magnetosphere a break down of corotation occurs. Corotation of the magnetospheric plasma starts to decrease in a region beyond about 20 R_J. The angular plasma velocity lags corotation and the plasma which drags the frozen-in magnetic field field lines leading to a bent-back configuration as seen in Figure 1.3.

The swept-back configuration of the magnetic field implies the transfer of angular momentum from the planet to the equatorial plane. However, signatures of the swept-forward configuration have been also observed. That means the transfer of the momentum from a source in space to the planet's ionosphere (Dougherty et al. 1993).

Additionally the so called "region 2" current system (which is similar to the terrestrial one) was observed by Galileo. It consists of the partial ring current closed by a field-aligned current system (see Figure 1.4 Khurana 2001). The interpretation of the origin of this current system is still under discussion. Either this current system is generated by internal sources (Vasyliūnas 1983) or by the solar wind (Khurana 2001).

In the inner magnetosphere the plasma β (plasma pressure divided by magnetic pressure) is low (< 0.2) and plasma effects on the magnetic field are minor. The magnetic field switches the configuration at about 10 to 17 R_J from dipolar to non-dipolar (Tomás

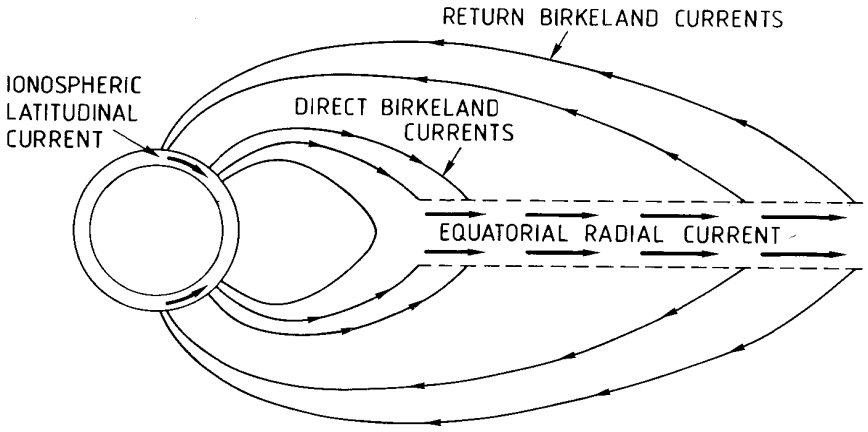

Figure 1.2: A sketch of the radially directed current enforced by corotational flows in the equatorial plane, from Vasyliūnas (1983).

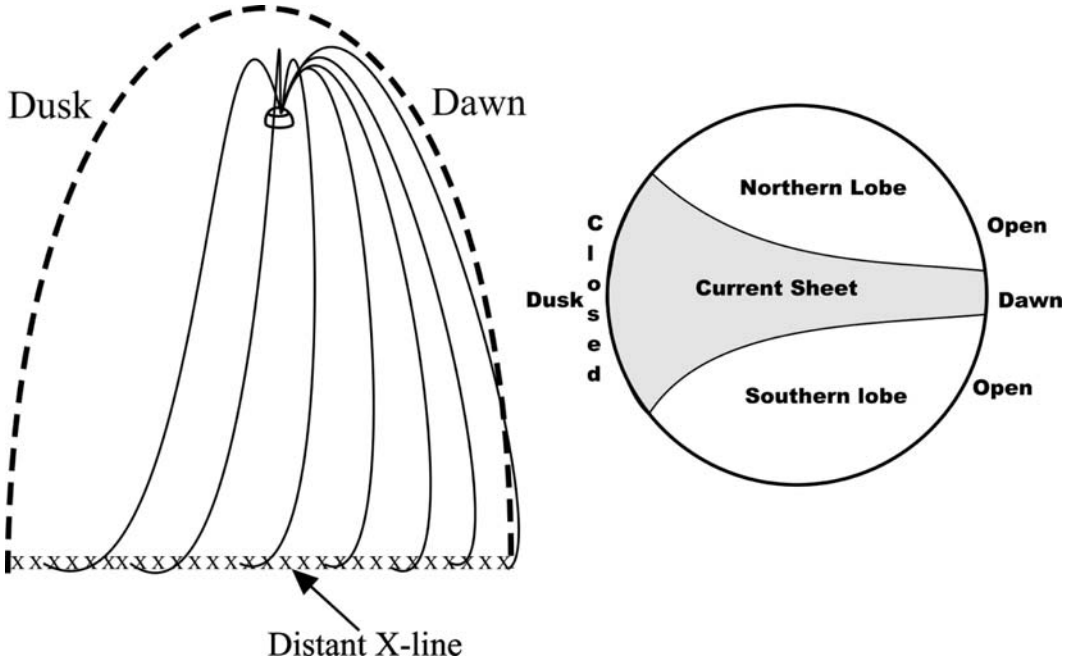

Figure 1.3: The configuration of the magnetotail Jovian is shown from above (left) and in a YZ cross section near X= 50 R_J (Khurana et al. 2004).

et al. 2004) and at a distance of about 24 R_J it becomes decidedly non-dipolar (Russell 2001). It has been suggested that the force balance in the middle magnetosphere is principally between the magnetic forces, centrifugal forces of the cold nearly corotating plasma and the pressure gradient of the hot plasma.

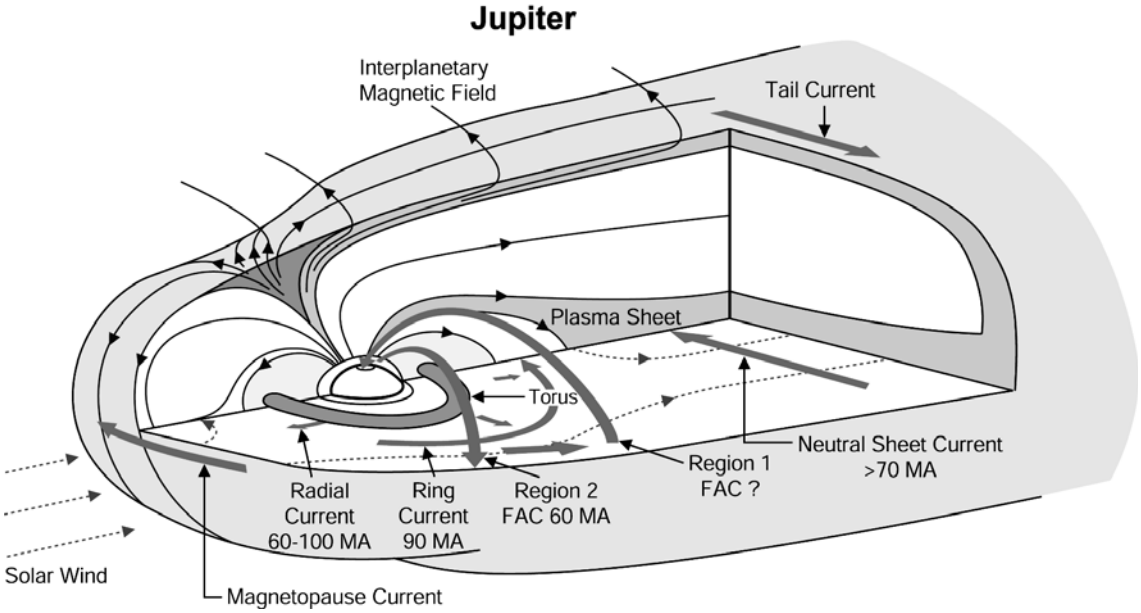

Figure 1.4: The current systems in Jupiter's magnetosphere. Adapted from Khurana (2001).

1.1.3 The outer magnetosphere: Internal and external influences

The plasma β in the outer magnetosphere is increasing to the order of unity in the current sheet. The magnetic field becomes strongly stretched in order to keep the plasma in balance with the centrifugal and thermal pressure forces. These forces together with the solar wind dynamic pressure define the location, structure and thickness of the current sheet.

The azimuthal plasma flow velocity becomes slower than corotation with increasing distance and levels off at an approximately constant speed of $\sim$ 200 km s^{-1} to $\sim$ 400 km s^{-1} depending on local distance beyond 20 to 40 R_J, (see Figure 1.5 Krupp et al. 2001). The connection of the magnetodisc currents to the magnetopause currents as a consequence of the magnetotail current system (tail current closed via neutral sheet current) further stretches the magnetic field lines to a long magnetotail which sometimes extends to the orbit of Saturn (Khurana et al. 2004). The current sheet at large distances (r $>$ 60 R_J) orients itself more and more parallel to the solar wind flow (Khurana 1992).

The study of Kivelson and Khurana (2002) deduced from the local time variations of the meridional magnetic field component B_θ shows that the magnetic field lines are less stretched on the dusk side than on the dawn side. The current sheet thickness is thinner on the dawn side than on the dusk side. This is sketched in Figure 1.3 (Khurana et al. 2004).

1.1.4 The dynamics of the magnetotail

As the dynamical behavior of the Jovian magnetotail is the main topic of this work the evolution of the understanding of the governing processes will be discussed chronologically.

Already before spacecraft missions reached Jupiter, Vasyliūnas in 1976 developed a

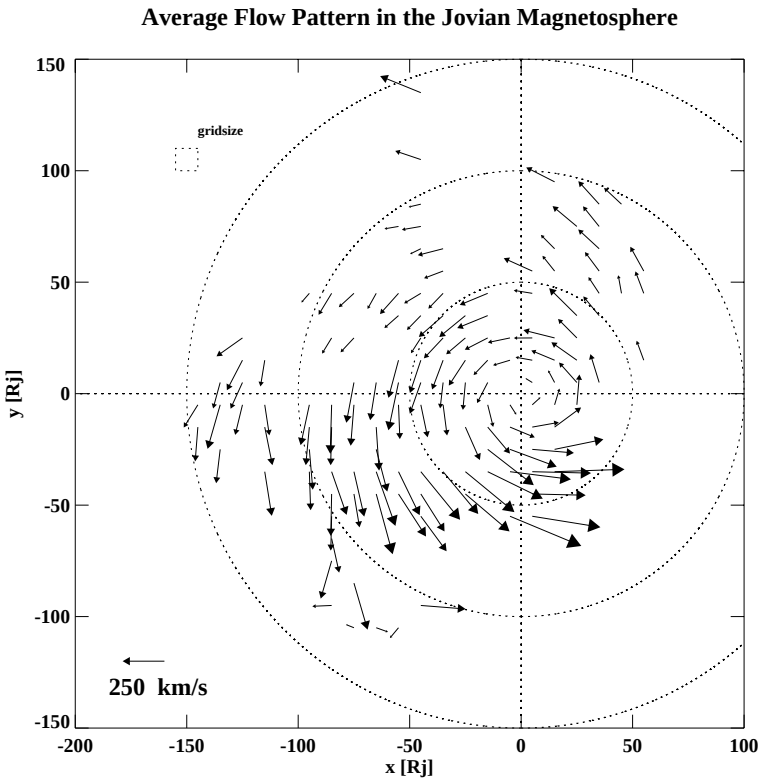

Figure 1.5: Average flow pattern in the Jovian magnetosphere, from Woch et al. (2004).

conceptual model for the middle and outer Jovian magnetosphere which was first published in 1983. The sketch of this model is presented in Figure 1.6. Vasyliūnas described the force balance associated with the corotational motion of the plasma including centrifugal effects. The dynamics of the Jovian magnetotail was represented as an internally driven reconnection scenario. The rigidly rotating magnetic flux tubes are filled with additional plasma and consequently the centrifugal force increases. This increases the outward directed force and leads to a stretching of the magnetic field lines. The increased centrifugal force can be balanced by magnetic stress only up to a limited distance. Beyond this distance force balance is no longer possible. This leads to changes in the magnetic field topology and the formation of an x-line and o-line at the limiting distance and a continuous development of plasmoids[1]. The plasmoids can move nearly free outward into interplanetary space. This centrifugally driven reconnection process proposed by Vasyliūnas (1983) is a continuous steady state process inherent to the Jovian magnetotail.

The first spacecraft missions which investigated the dynamics and flow pattern in the distant Jovian magnetotail were Voyager 1 and 2. Plasma discontinuities in the tail regime at about 55 to 60 R_J have been discovered and the plasma flow changes its direction from corotational to radially outward at about 130 to 150 R_J. Krimigis et al. (1980) detected the radially outward ion flow burst outside the Jovian plasma boundary (in the magnetosheath) at 150 R_J which lasts for about four hours and mainly consisted of heavy ions with Jovian origin. This event provided a dramatic example of the dynamics of the

[1] See Section 1.2 for details.

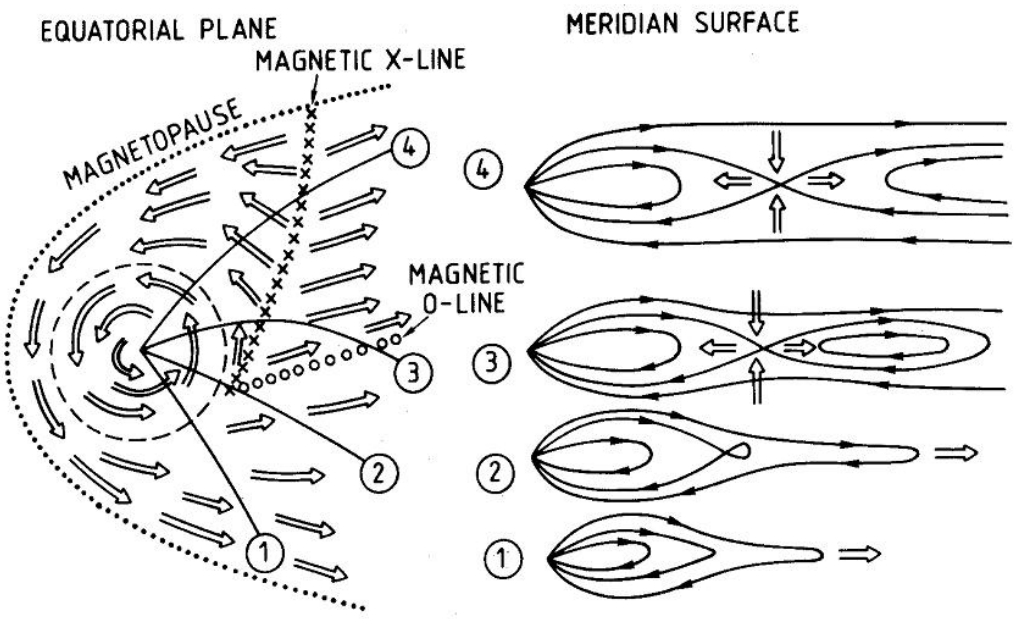

Figure 1.6: Qualitative presentation of the plasma flow in the equatorial cross-section (left) and of the associated magnetic field and plasma flow in the meridian surfaces (right), (adapted from Vasyliūnas 1983).

Jovian magnetosphere.

Magnetometers onboard Voyager 1 and 2 detected signatures of reconnection[2] in the Jovian magnetodisc. Anti-sunward streaming particle events associated with northward field inclinations were observed beyond about 80 R_J. They were interpreted as the need to adjust the length of the extended nightside field lines to the dimension of the dayside magnetosphere which leads to the separation of the tip of the flux tubes by reconnection (Nishida 1983). Since the events showed considerable variability they were suggested not to be due to a steady-state process as in Vasyliūnas model. The observed field component across the neutral sheet exceeded the dipole field strength, which was proposed to be the result of the tearing mode.

Zimbardo (1993) using a self-consistent axisymmetric magnetic field model based on the Voyager data found that the distended magnetic field at night side ($\sim 60\mathrm{R}_J$) of Jupiter can cause a tearing instability which leads to the change of the magnetic field topology. It is shown that observations of particle streaming, auroral emissions and radio bursts support the growth of the tearing instability in Jupiter's magnetosphere as a frequent and widespread phenomenon.

Further evidence for transient magnetic field reconnection across the current sheet beyond 50 R_J was found in the Galileo magnetometer data (Russell et al. 1998) with an example shown in Figure 1.7. Localized regions of strong northward and southward magnetic field components were attributed to episodic reconnection of confined patches of the near Jovian magnetotail. These disturbances appear to be spatially large but not of

[2]Details on reconnection process see Section 1.2

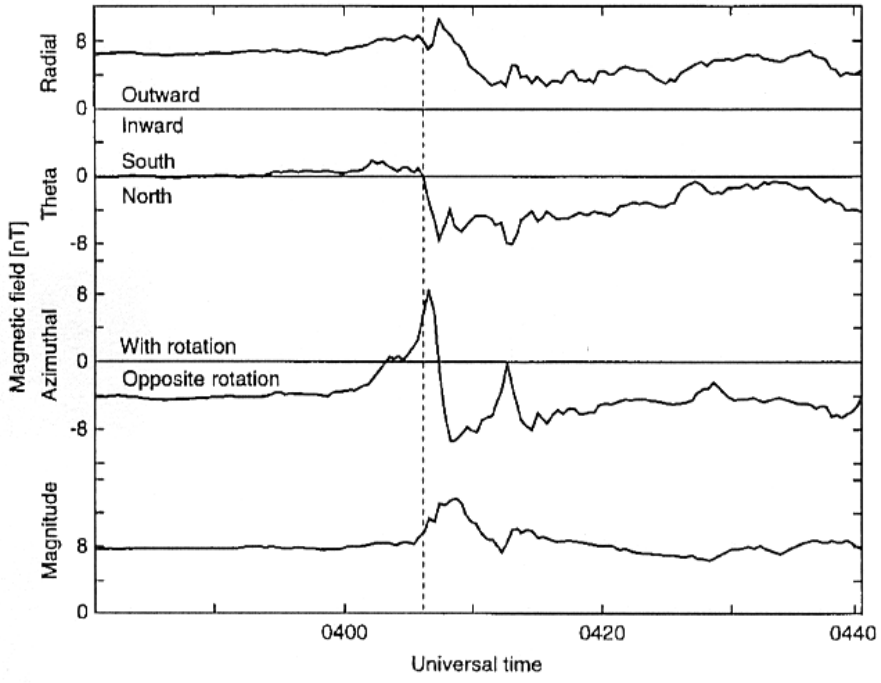

Figure 1.7: An example of explosive reconnection as observed by Galileo on DOY (Day of Year) 165, 1997. Taken from Russell et al. (1998).

a global nature, with the patches having a size of about 25 R_J, in radial and azimuthal direction. The events clearly indicate that the fast rotation of the Jovian magnetosphere produces important differences compared to Earth's magnetotail. At Jupiter angular momentum conservation leads to predictable perturbations in the azimuthal component of the magnetic field, because the magnetized plasma is convected either inward or outward by the reconnection process.

Based on Galileo Energetic Particles Detector (EPD) data Krupp et al. (1998) reported that energetic particle bursts frequently occurring in the Jovian magnetotail. They discovered a quasi-periodical occurrence of these events. The typical reoccurrence period on the Galileo orbit G2, studied by Krupp et al. (1998), was 2 to 3 days. This example of the variable dynamical behavior of the plasma flows in the predawn region of the Jovian magnetotail is presented in Figure 1.8. There the first order anisotropy vectors[3] in the equatorial plane are shown along the orbital track. Under the assumption that the first order anisotropy is due to plasma flow the particle bursts mainly consist of radially outward flowing ions embedded in a corotational flow sometimes followed by short intervals of inward flowing ions.

Woch et al. (1998) using the Galileo EPD data set noted that the middle magnetotail of Jupiter is also affected by quasi-periodic modulations of several parameters of the plasma sheet particle population and found a very similar periodicity of about 3 days. Most remarkably the particle energy spectra gradual softened within 2 days followed by an abrupt hardening within 1 day. It was suggested that these modulations correspond

[3]The details how the first order anisotropy vector have been derived are presented in the Section 2.7.1

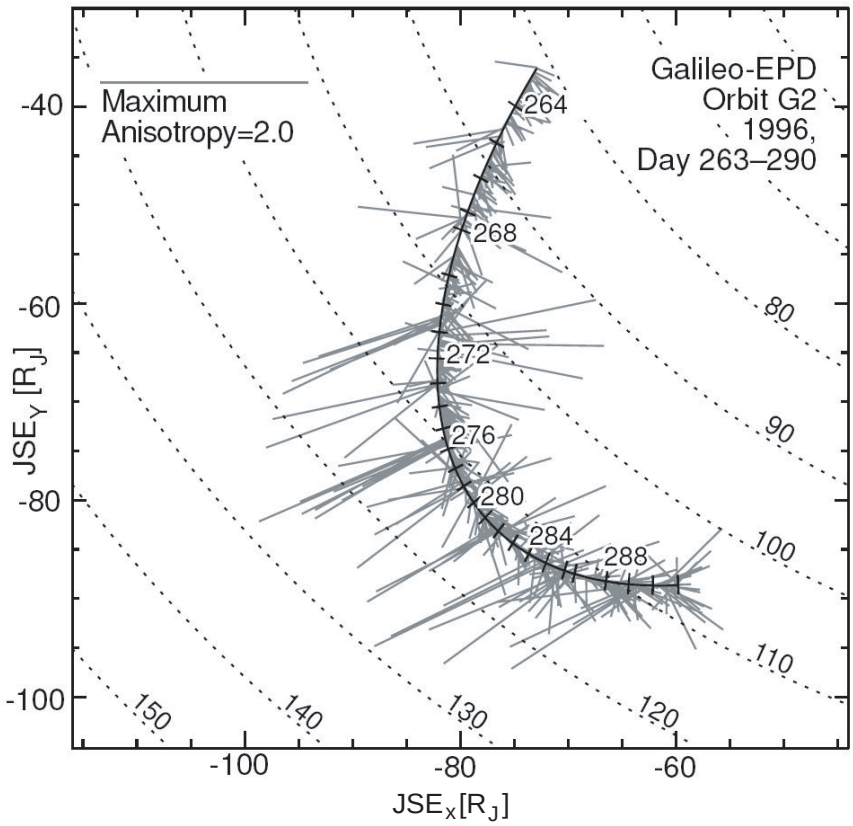

Figure 1.8: One hour averaged the first order anisotropy vectors of protons (80-220 keV) projected into the equatorial plane along G2 orbit. The lengths of the vectors are given by the first order anisotropy amplitude relative to the isotropic component. The radial and azimuthal directions are perpendicular and tangential to concentric circles, (Krupp et al. 1998).

to a quasi-periodic transition between two basic states of the Jovian magnetotail. One state is characterized by the plasma flow dominated in the corotational direction, a thick plasma sheet with high intensities of energetic particles and a hard energy spectrum. The other state is associated with tailward/sunward plasma flow, a thin plasma sheet with low intensities of energetic particles and considerably softer energy spectra.

Louarn et al. (1998) using observations of the Galileo PWS instrument found that intensification of auroral emissions and creation of new radiation sources in the outer regions of the Io torus recurrently appear with a periodicity of 2 to 3 days. They occur simultaneously with modifications of the plasma sheet structure in the Jovian magnetotail and could be linked to large-scale instabilities of the Jovian magnetotail.

Also, in other studies of the Jovian magnetosphere periodic processes were reported as well though with different periodicities. Based on measurements of keV electrons by Galileo Vasyliūnas et al. (1997) showed that the plasma sheet configuration as described by its thickness, the hinging distance, and/or its meridional motion undergoes time variations with a period of 5 to 7 days. Prangé et al. (2001), analyzing FUV auroral spectra (Hubble observations) from the Jovian magnetosphere, identified a variability of the au-

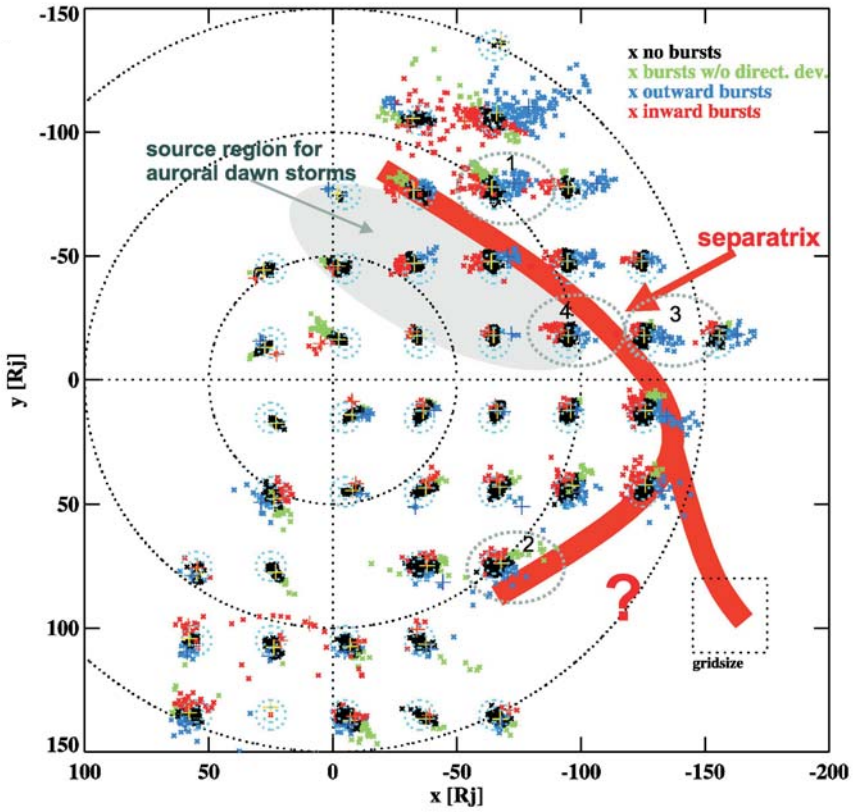

Figure 1.9: The x-line location, adapted from Woch et al. (2002).

roral activity index on time scales of 5 to 10 days, which was well correlated with disturbances of the magnetic field measured by the magnetometer on board of Galileo. The auroral activity obviously builds-up and decreases during a couple of days.

A single case study of a prominent particle burst event was carried out by Woch et al. (1999) by combining energetic particles, magnetic field and plasma wave data. It was suggested that this event represented a global configurational instability and in that sense the Jovian counterpart of a terrestrial substorm. This event was interpreted as a dynamical process where the Jovian magnetotail becomes unstable due to mass loading of magnetic flux tubes leading to reconnection. Likewise, Russell et al. (2000a) referred to magnetic field disturbances attributed to irregular transient reconnection events as Jovian substorms. Woch et al. (2002) deduced the most probable location of a near-Jupiter neutral line from a statistical study of particle flow bursts directions, (see Figure 1.9). It was shown that reconnection in the Jovian magnetotail is rather a transient than a continuous, steady state process.

At Earth the direction of the interplanetary magnetic field (IMF) is critical in the control of the circulation. At Jupiter the plasma circulation is dominated by the corotational electric field. The mass loading at Io triggers a gradual outflow of plasma. Eventually beyond about 50 R_J in the post midnight sector reconnection empties the magnetic field lines creating magnetized islands that flow down the Jovian tail and empty flux tubes that return to the inner magnetosphere. These flux tubes appear to be both small and fast

moving in order to return the required magnetic flux to the inner magnetosphere (Russell 2001).

1.1.5 The Jovian aurora and equatorial plasma flow

Aurora is the emission of light produced by the impact of any external particles on a planet's upper atmosphere (Chamberlain and Hunten 1987). The aurora provides a projection of magnetospheric processes. This allows to study magnetospheric processes which are not directly visible. Thus the association of dynamical processes in the Jovian magnetosphere and in particulary in the Jovian magnetotail with the corresponding main characteristic of the Jovian auroral emission will significantly enhance the understanding of many magnetospheric processes.

First we will consider the theoretical aspects of the Jovian aurora and then discuss the observations.

According to Cowley et al. (2003) the Jovian equatorial plasma flow in the steady state situation consists of three components, (see Figure 1.10). The first component of the Jovian flow is the sub-corotating "Hill region", which comprises the main part of the Jovian middle magnetosphere, extending in the equatorial plane to distances of several tens of R_J. It is associated with the breakdown of rigid corotation in the middle magnetosphere (see Section 1.1.2). This region is then surrounded by a second region where the flow is still driven by planetary rotation, in which current sheet dynamics and reconnection play an important role in the loss process of iogenic plasma downtail in a way first discussed by Vasyliūnas (1983), see Section 1.1.4. In Figure 1.10 this is shown as a steady-state process associated with a reconnection line marked by the dashes and X's denote the "Vasyliūnas-cycle tail X-line". By an "O" the O-type line of the plasmoid is marked (see also the sketch of Vasyliūnas in Figure 1.6). The outer edge of the plasmoid is shown by the dot-dashed line marked "P".

The third region contains the flow associated with the solar wind interaction and the Dungey-cycle (Dungey 1961). This process is initiated by magnetopause reconnection with the interplanetary magnetic field which presumably takes place over wide regions of the dayside boundary. This is indicated in Figure 1.10 by the dashed line with X's and the notation "Dungey-cycle magnetopause X-line". It is proposed that the reconnection site associated with the solar wind driven process will be confined to the dawn sector, as shown by the dashed line and X's labelled "Dungey-cycle tail X-line". The flux tubes closed at the "Dungey-cycle tail X-line" are transported back towards the dayside magnetopause (denoted as the "Dungey-cycle return flow") to complete the cycle.

The Dungey- and Vasyliūnas-cycle tail reconnection sites are associated with the mass-release processes in the Jovian magnetosphere. The ionospheric plasma flows which correspond to the equatorial plasma flows considered above are sketched in Figure 1.11. A sketch of plasma flows in the northern Jovian ionosphere is transformed to a frame where the planetary dipole is at rest, so that the flow pattern does not vary with time. The three corresponding ionospheric plasma flow components from lower to higher magnetic latitudes are as follows. First is the sub-corotating "Hill region". The "Hill region" is presumably directly related to the main auroral oval as consequence of the upward Birke-

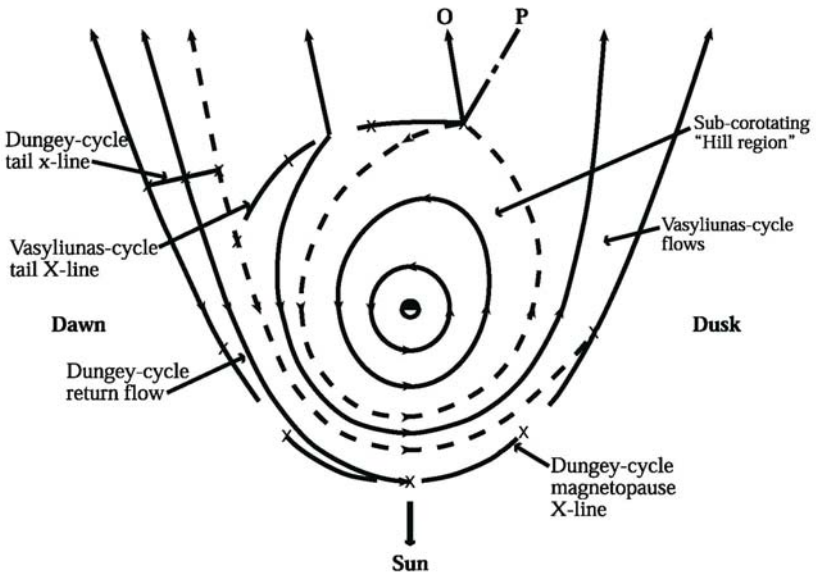

Figure 1.10: Sketch of the flows in the Jupiter's equatorial plane, from Cowley et al. (2003).

land current[4] (depicted by the circled dots) that enforces partial corotation of the outward moving iogenic plasma. Secondly, the Vasyliūnas cycle flow region which correspond to a (sub) corotating region where iogenic plasma is lost down tail. Empty flux tubes which initially carried the detached plasmoid return to near corotation in a narrow sector in the dawn region. The third region is occupied by Dungey-cycle flows. It consists of a region of open magnetic flux and anti-sunward flow, shown hatched in Figure 1.11 and a region of closed flux and return sunward flow taking place only on the dawnside of the region of open flux. This occurs presumably due to the magnetospheric asymmetry imposed by the Vasyliūnas cycle, especially by the outflow of iogenic plasma down the dusk and midnight tail. The dayside reconnection associated with the solar wind interaction is roughly symmetrically with respect to noon. It is represented as the Dungey cycle magnetopause X-line.

According to observations the structure of the Jovian auroral emission is usually divided into several major components: the footprints from Io, Europa and Ganymede; the main oval associated to the breakdown of rigid corotation with brightness ~ 50 to ~ 500 kiloRayleighs[5] (kR); a discrete belt of emissions equatorward of the main auroral oval - the secondary oval; and the polar emissions which appear poleward of the main oval with rapid temporal variations (Grodent et al. 2003a,b). These components are presented in Figure 1.12 which shows an image of the northern auroral region observed by the Space Telescope Imaging Spectrograph (STIS) onboard the Hubble Space Telescope (HST).

Grodent et al. (2003b) suggested to distinguish the polar emissions into three regions

[4] See the sketch 1.2 in Section 1.1.2.

[5] 1 kRayleigh = 10^9 photons $^{s-1}$ from a 1 cm^2 column of the atmosphere radiated into 4π steradians.

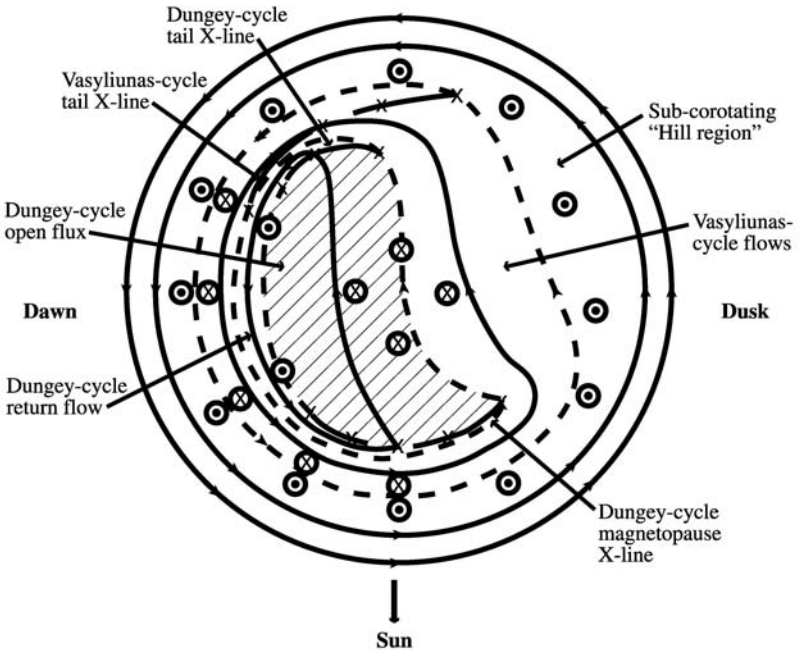

Figure 1.11: Sketch of the different flow regimes in the Jupiter's northern ionosphere, from Cowley et al. (2003).

fixed in magnetic local time (MLT)[6]: the dark region, the swirl region and the active region. These polar emissions contribute about 30 % to the total auroral emission in the northern hemisphere and show emission bursts lasting for approximately 100 s.

The dark polar region - an ionospheric crescent-shaped region at dawn void of auroral emissions (< 10 kR) (Stallard et al. 2001, Grodent et al. 2003b) - is postulated to be connected to the return flow of emptied flux tubes (Cowley et al. 2003) from the Vasyliūnas' x-line or Dungey cycle. The dark region continues duskward with a region of faint emission (tens of kR) which may be interpreted as the duskside part of the Vasyliūnas cycle flows where previously emptied flux tubes are gradually mass loaded by plasma from Io (Grodent et al. 2003b).

The swirl region is a region of faint patchy emission features (< 200 kR) occurring near the magnetic pole, with a residence time of $\sim$ 5 - 10 days, and possibly associated with the region of open flux tubes in the tail lobes (the solar wind-driven Dungey cycle hatched in the sketch 1.11).

The active region is confined to the noon to dusk side (between the swirl region and the main oval). The polar flares (brightness increase up to 400 kR) belong to this region. It is feasibly connected with the site of dayside magnetic reconnection of the Jovian magnetic field lines with the IMF, (see Dungey-cycle magnetopause X-line in sketch 1.11).

In addition auroral dawn storms (Clarke et al. 1998) or multiple dawn arcs (Grodent et al. 2003a) are observed in the Jovian aurora. They are characterized by a strong and

[6]MLT is the system of reference connected with the magnetic pole. As the globe rotates, all points on the same magnetic longitude have a certain magnetic local time. At MLT=12 a point faces in the "upwind" direction, and at MLT=24 or 0 in the "downwind" direction.

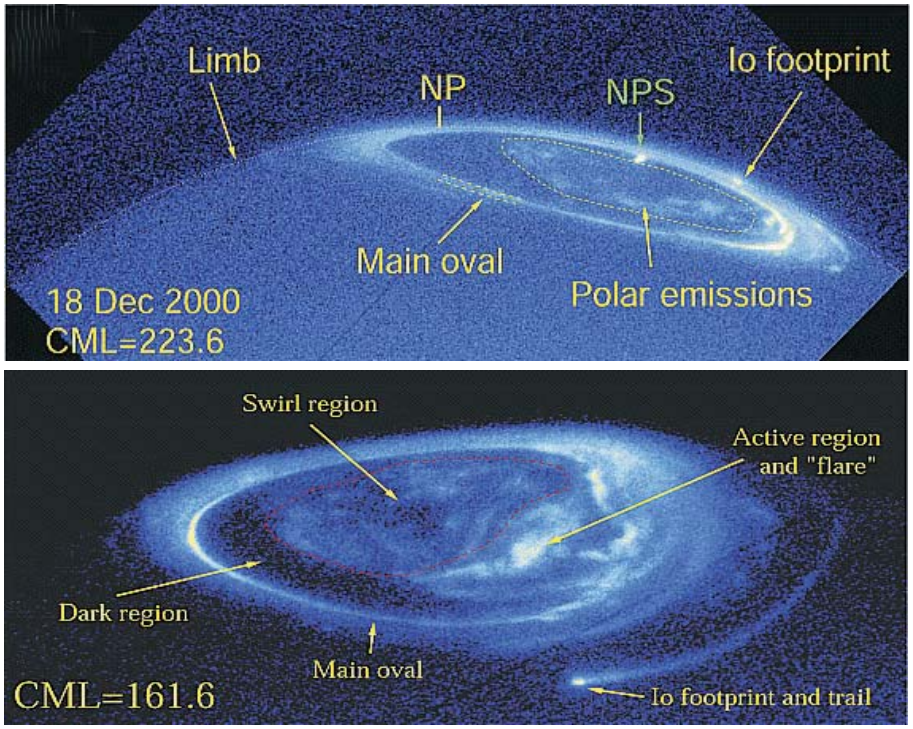

Figure 1.12: HST-STIS images of the northern polar region of Jupiter. Top image shows the main oval, the secondary oval, the polar emissions and nightside polar spots (NPS) (Grodent et al. 2004). Bottom image presents the features of the polar emissions: the swirl region, the dark region and active region with "flare" (Grodent et al. 2003b).

localized (in the dawn sector of the main oval) brightening (in excess of 1 MR). Those can be interpreted as follows: an upward current is necessarily associated with the break of the fast return flow in the high-pressure subcorotational regime in the middle magnetosphere and this could lead to intensive emissions. It was also suggested by Woch et al. (2002) and Cowley et al. (2003) that dawn storms may be associated with magnetic reconnection events in the Jovian magnetosphere.

Another morphological feature of the polar emissions is the so-called 'Nightside Polar Spots' (Grodent et al. 2004) - isolated auroral spots frequently observed poleward of the main auroral oval. The duration of these auroral spots is between 5 minutes and 1 hour with a reoccurrence period of about $\sim$ 1 to 2 days. 'Nightside Polar Spots' may be the auroral imprints of the transient reconnection events in the magnetotail. According to Khurana's "1997-model" these spots map roughly to the pre-midnight region of the magnetosphere beyond 100 R_J ($\sim$ 21:00 LT - local time). The apparent magnetic conjugacy of the two phenomena and their compatible duration corroborates such a relation.

1.2 Substorm or substorm-like processes at Earth and Jupiter

The dynamics of the Jovian magnetotail show some similar features and signatures as the Earth's magnetotail during substorms.

One of the outstanding problems in magnetospheric substorms is why the magnetotail is stable most of the time, and why do substorms occur just when they do (Huang et al. 2003)? Can substorms have some specific periodicity?

The key physical process in a terrestrial substorm is a reconnection process by which energy is added to the system and transformed to thermal and kinetic energy. Figure 1.13 presents a scheme of possible magnetic field and plasma flow configurations for steady state reconnection. Plasma and the frozen-in magnetic field flows from the ideal[7] region into the diffusion region. Due to the resistivity in this region the magnetic field is not frozen into the plasma anymore and the connectivity of the magnetic field lines change. Magnetic energy transforms into kinetic and thermal energy during this process. The outflowing plasma has (in the simplest, 2D-incompressible models) Alfvén speed.

Magnetic reconnection occurs at the dayside magnetopause when the interplanetary magnetic field and the Earth's field lines are antiparallel. Magnetic flux is added to the magnetosphere which leads to a stretching of the magnetotail and a thin current sheet formation. Current driven micro instabilities produce resistivity on hydrodynamic scales and magnetic reconnection occurs in this near Earth ($\sim$ 10 to 30 R_E) non-ideal MHD region. The whole process is called a substorm.

The substorm process is divided into three phases: growth phase, expansion phase and recovery phase, (see schematic representation in Figure 1.14). The most widely accepted model of the substorm process is named the Near Earth Neutral Line (NENL) model. The substorm onset leads to plasma sheet thinning and a NENL formation. After reconnection the plasma sheet field lines form a plasmoid (closed field lines) which move tailward. The plasmoid forms between this near Earth neutral line and a distant neutral line. During the reconnection process magnetic energy is transformed into kinetic energy. This leads to acceleration of the plasmoid which is expelled into the interplanetary space. A small amount of plasma is accelerated along the magnetic field lines toward the Earth and causes auroral emissions. In the substorm recovery phase the configuration returns to the initial state.

Let us consider the main substorm phases in detail.

- Growth phase

  The substorm process starts from the growth phase, which lasts around one hour. Substorms require the loading of energy prior to its unloading (Baker et al. 1999). The solar wind energy is transferred to the magnetosphere through reconnection between interplanetary and magnetospheric field lines. The energy loading leads to the magnetic field increase in the tail lobe and as consequence compression of the plasma sheet. The increase of the cross-tail current drives a tailward stretching of

[7] Ideal means ideal Magneto Hydro Dynamics (MHD), which is defined by ideal Ohm's law $\mathbf{E}+\mathbf{V}\times\mathbf{B} = 0$. The diffusion region has a term on the right side which is usually small, e. g. ($\eta\mathbf{j}$).

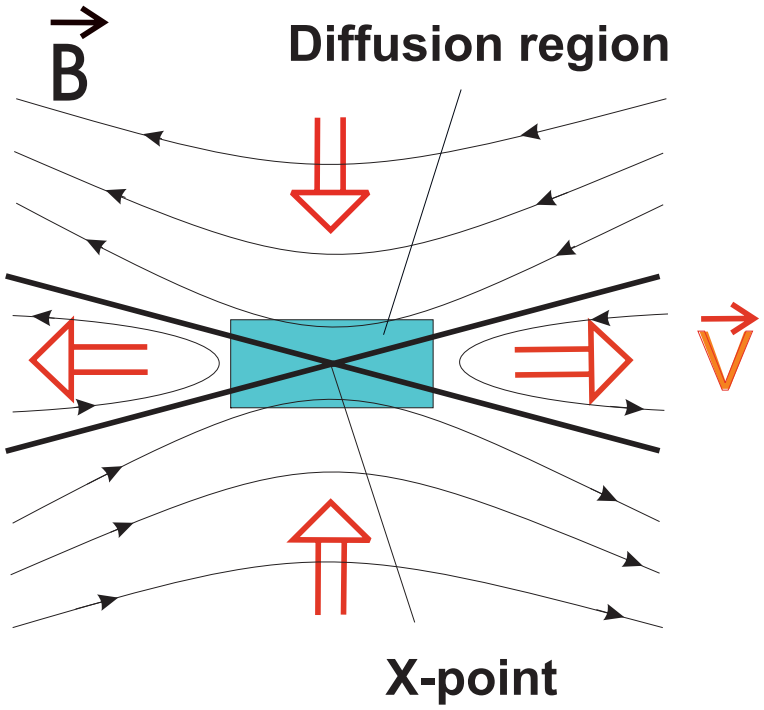

Figure 1.13: A schematic representation of the steady-state magnetic reconnection process. Plasma flows into the diffusion region carrying the frozen-in magnetic field. The connectivity of the magnetic field lines changes at the X-point. By this process magnetic energy is transformed into kinetic and thermal energy.

the near-Earth tail field lines. A current sheet becomes thin tailward of the dipole-like field lines (6-15 R_E[8]).

The thinning of the current sheet is associated with flux dropouts (decrease of the flux of energetic particles at a given location). The flux dropouts for both electrons and ions are observed together with noticeable increase in the magnetic field strength during $\sim$ 1 hour and abrupt enhancements occur as the magnetic field rapidly decreases. This field variations are consistent with intensification of the cross-tail current during growth phase (Lopez et al. 1989) and followed by current disruption and magnetic field relaxation during the expansion phase.

- Expansion phase

  The explosive part of the substorm process is associated with the expansion phase and the start of this phase is called the onset of the substorm. Stored energy is released.

  The typical duration of this phase is about 30 min with variations from 10 minutes to 2 hours. How substorm onsets are triggered is still not fully known. Several models are currently discussed. For example the current disruption model suggests that the process initiates in the near-geostationary region (Lui 1996), the neutral

[8]The Earth radius R_E is 6378 km

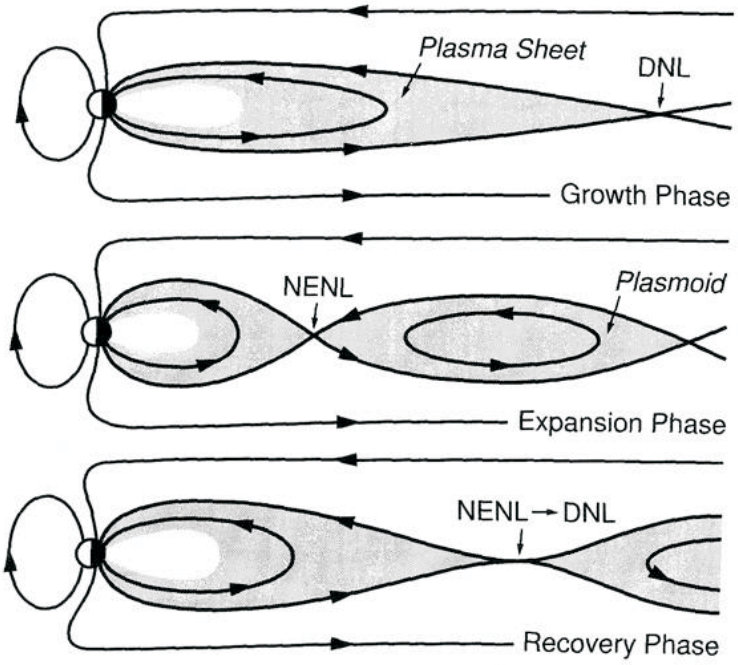

Figure 1.14: Schematic presentation of the plasma sheet evolution during substorm. DNL is a Distant Neutral Line, NENL is a Near Earth Neutral Line. Adapted from (Baumjohann 1991).

line model suggests that magnetic reconnection in the midtail releases the energy stored in the tail lobes (Baker et al. 1996), the role of the solar wind variations as initiation process was considered by Lyons (1996), the role of the ionosphere by Kan and Sun (1996). The phase is characterized by earthward and tailward high speed plasma flows. The plasmoid-associated ion bursts will be considered below in further detail. Part of the cross-tail current in the near-Earth disappears. The current disruption leads to closure of the interrupted current lines through the ionospheric current system and the creation of a substorm current wedge. This is accompanied by dipolarization of the magnetic field. Magnetic field oscillations with low frequency are often seen during and after the onset. Sketch 1.15 illustrates the substorm current wedge relationship to near-Earth current disruption and magnetic field line changes during the expansion phase. The most intense discrete aurorae occur due to electron acceleration down into the ionosphere by field-aligned electric potential drops during substorms. The observations established that reconnection occurs in the tail region around 25 R_E away from the Earth.

- Recovery phase

  In the recovery phase the plasma sheet and magnetic field return into the pre-substorm state within typically one hour.

Observations and numerical models show that terrestrial substorms are a global, coherent set of processes within the magnetosphere and ionosphere (Baker et al. 1999). The

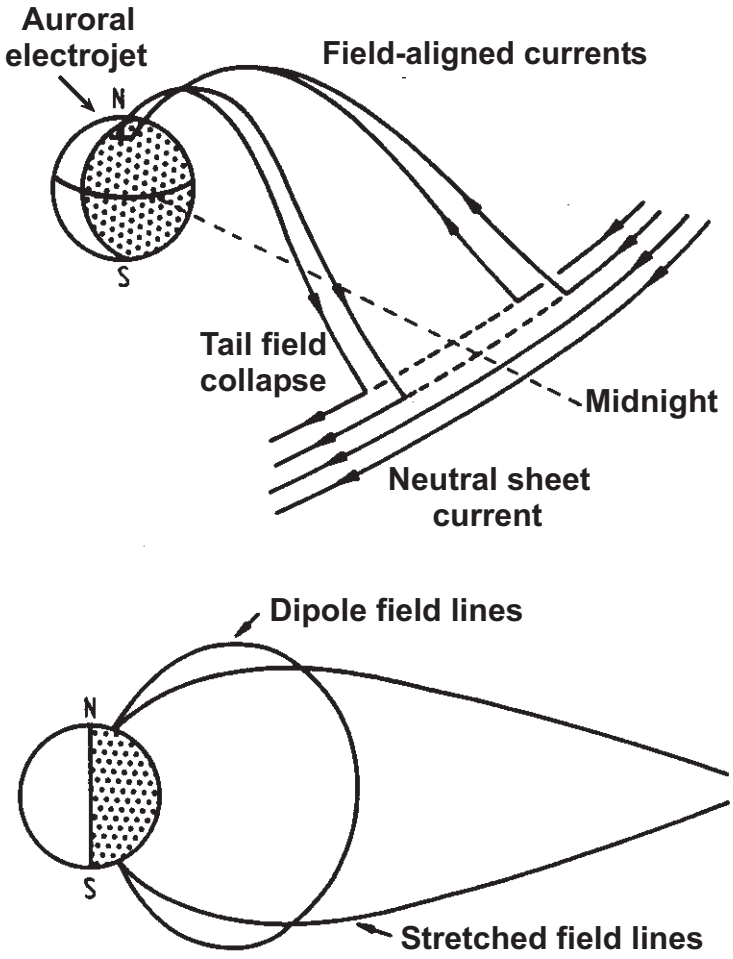

Figure 1.15: The substorm current wedge and reconfiguration of the nightside magnetosphere during substorms (Russell and McPherron 1973).

magnetosphere extracts energy from the solar wind flow, the energy is stored in the magnetotail, an extremely thin plasma sheet forms in the magnetotail, leading eventually to the explosive disruption of the current sheet at a geocentric distance of $\sim 25R_E$ in the nightside magnetotail. The details of the plasma physics may be different from case to case, but the magnetospheric system almost always passes through this loading-unloading cycle so that it can be considered as a "configurational" instability: The energy-loaded magnetosphere develops a magnetic stress state until the entire system collapses and the global reconfiguration leads back to a lower energy state. The loaded magnetosphere almost always develops rapidly to the same basic reconnection reconfiguration independently of the details of the localized initiation mechanism. The explosive disruption is associated with a catastrophic collapse comparable to a sand dune that has reached a very unstable configuration. Any small local perturbation can lead to a large-scale collapse irrespective of the nature of perturbations.

The fact that the magnetosphere behaves in a self-organized and coherent way lead to the description of the global system by a "state" vector (Vassiliadis et al. 1995). The

system evolution can be described in terms of a "bifurcation" diagram (Schröer et al. 1994). The magnetotail collapses catastrophically and the highly stressed reconfiguration changes by the relaxed, dipolar state.

1.2.1 The release process at Earth - plasmoid-associated energetic ion bursts

The plasmoids are formed after substorm onset, either due to a tailward retreat of the neutral line and further pinching off or due to formation of loops within the postplasmoid plasma sheet. The plasmoid-associated ion burst signatures were divided by Richardson et al. (1987) using the data from the ISEE 3 spacecraft into four different phases:

Phase 1 is the initial period associated with strongly tailward streaming energetic ions in a "tail lobe" region. The bursts constitute a major component of a "plasma sheet boundary layer" region surrounding the plasmoid/plasma sheet.

Phase 2 is the plasmoid phase with signatures of depressed magnetic field and the strong north and thereafter south field tilts. The energetic ions show high intensities with a broadened angular distribution.

Phase 3 is the postplasmoid plasma sheet. It is characterized by a depressed and usually continuously southward directed magnetic field. The ion intensities often slowly decrease and the angular distributions are getting narrow.

Phase 4 is a return into a plasma sheet boundary layer region lasting for a few minutes which has characteristics similar as Phase 1, before exiting into the tail lobe where much lower energetic ion intensities are residing.

The observations from Richardson et al. (1987) may be interpreted using the "neutral line" model of substorm behavior (Hones 1979, Richardson and Cowley 1985). Sketches of plasmoid formation and propagation in a meridional cross sections through the geomagnetic tail are presented in Figure 1.16. Solid lines represent magnetic field lines, the hatched areas show the regions of plasmoid (PM) and postplasmoid plasma sheet (PPPS) occupied by the hot thermal plasma. The dotted regions between the plasma sheet boundary and the magnetic field separatrix connected with the neutral lines represent the plasma sheet boundary layers (PSBL). The first panel presents the geomagnetic tail after substorm onset, where rapid reconnection of the magnetic field lines within the near-Earth plasma sheet forms closed loops of magnetic flux (the plasmoid). In the second panel the disconnected plasmoid starts to move tailward. Open tail lobe flux reconnects at the near-Earth neutral line and the interplanetary field surrounds topologically the plasmoid. In the third panel the plasmoid is accelerated downtail by the tension of interplanetary field lines and by dynamic pressure. During substorm recovery, the near-Earth neutral line moves downtail and the reconnection rate drops, until quiet time conditions will again dominate.

1.2.2 Periodic substorms

Whereas mostly the terrestrial substorms occur randomly and more or less as singular events, observations have shown that "periodical substorms" occur in the Earth’s magnetosphere, i. e. a sequence of substorms with quasi periodical repetition time. Huang et al. (2004) reported about the proton particle fluxes which exhibit a well-defined "sawtooth" profile with gradual decreases (flux dropouts) followed by rapid increases (injections).

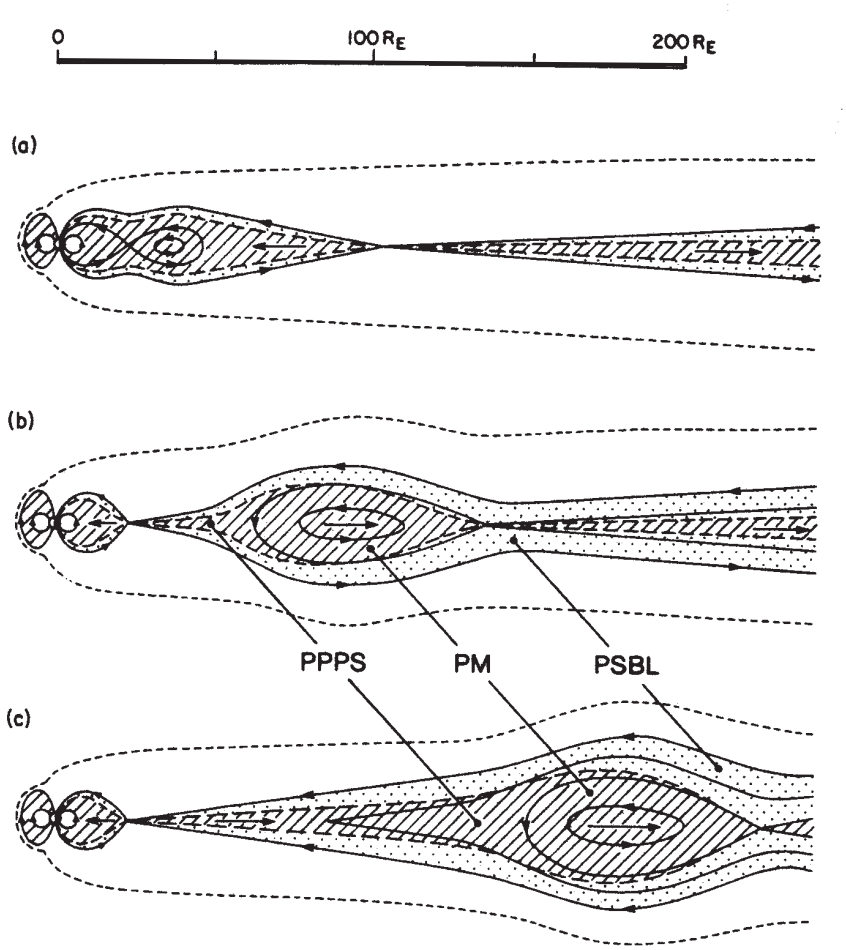

Figure 1.16: Sketch of the formation and propagation of plasmoids according to the NENL model. Magnetic field lines are denoted by solid lines, the hatched areas surrounded by dashed lines show plasma sheet regions as the plasmoid and postplasmoid plasma sheet. The dotted regions located between the plasma sheet boundary (bounded by dashed lines) and the field separatrices mapping to the x-line are the plasma sheet boundary layers containing energetic particles flow. The phase (a) shows the state briefly after substorm onset. The rapid near-Earth reconnection leads to the formation of the plasmoid within the quiet time plasma sheet. The phases (b,c) presents the plasmoid tailward motion after its disconnection from Earth. The plasmoid is topologically surrounded by interplanetary field lines formed by near-Earth reconnection of open tail lobe field lines. The contraction of the reconnected lines accelerate the lobe plasma from the neutral line, this leads to development of a wedge-shaped region Earthward of the tailward moving plasmoid called "postplasmoid plasma sheet" (Richardson et al. 1987).

These sawtooth injections coincided well with the AE index[9] increases, a southward turn-

[9]The Auroral Electrojet Index, AE, provides a global, quantitative measure of auroral zone magnetic activity which results from enhanced ionospheric currents flowing below and within the auroral oval. It is the total range of deviation at an instant of time from quiet day measurements of the horizontal magnetic field around the auroral oval.

ing of the meridional magnetic field component, an enhancement of energetic neutral atom emission in the ring current, and an intensification in the auroral emissions. The periodic magnetospheric substorms have an intrinsic cycle time of 2 to 3 hours (Huang et al. 2003). The sawtooth events occur at all local times also on the day side and the injections are dispersionless (Clauer and Cai 2005). Ganushkina et al. (2005) associated the tail current enhancements with growth phases of the sawtooth events and decrease of the tail currents with dipolarization. They found no signatures of an external driver for the sawtooth events.

The periodic substorms occurred after a solar wind pressure impulse has acted on the magnetosphere during magnetic storms. However, the solar wind did not show periodic variations with a repetition period of the sawtooth injections. The solar wind pressure oscillations or impulses can excite the periodic substorms, but the period of the substorms is determined by the magnetosphere itself. Isolated substorms can also occur when there is no obvious triggering from the solar wind. They occur during stable IMF as well as during fluctuating IMF (Huang 2002, Huang et al. 2003).

The observations provide evidence that the magnetosphere needs about 2 to 3 hours after a substorm onset to become again unstable for the next substorm. If the magnetospheric state is stable towards the respective plasma instability considered to be responsible for substorm onset, substorms will not occur, regardless whether the solar wind suddenly changes its direction or not. On the other hand, if the magnetosphere has reached the unstable state, an internal plasma instability can trigger substorm onsets, even if there is no external triggering condition of the solar wind. The investigations of Huang et al. (2004) show that the period of substorms is also not defined by the amount of solar wind energy transferred into the magnetosphere.

The near-tail reconnection (e.g., Ieda et al. 1998) and the current disruption (e.g., Lui 1996) are identified as possible mechanisms responsible for the generation of the periodic substorms. The "minimal substorm" model of Freeman and Morley (2004) based on three principles propose a statistical and physical description of the timing of substorm onsets in the Earth's magnetosphere and suggests that the substorm cycle may be intrinsically simple on a global scale and that the complicated pattern of substorm occurrence arose from the complexity of the solar wind driver.

The solar wind power P drives the substorm and leads to the accumulation of energy E in the magnetotail at a rate of

$$\frac{dE}{dt} = P \tag{1.1}$$

At any given time, the solar wind boundary condition define an energy state F that the magnetotail would like to exist in:

$$F = C - DP \tag{1.2}$$

where the constant C is a critical energy threshold and the constant D is related to the substorm periodicity. The magnetotail is constrained by its magnetic configuration from adopting the energy state F until it becomes sufficiently stressed with an energy C and then the magnetotail moves to the lower energy state:

$$E \rightarrow F \text{ when } E \geq C. \tag{1.3}$$

This transition is associated with the substorm onset and the expansion phase.

This model can simulate periodic substorms driven by a steady solar wind. For real solar wind conditions this model gives distribution of a waiting time between pairs of adjacent substorms onsets in an agreement with the observations.

1.2.3 Possible drivers for reconfiguration processes in the Jovian magnetotail

The dynamics of the Jovian magnetotail described in Section 1.1.4 lead to the discussion which physical processes can enforce reconfiguration processes associated with reconnection and mass-release in the Jovian magnetosphere.

It is most natural to associate the dynamical processes revealed in the Jovian magnetosphere with terrestrial substorms[10]. However, before doing that it seems necessary to clarify our notion of a substorm. In order to avoid misunderstanding due to different conceptions of the term substorm.

Nishida (1983), Russell et al. (2000a), Woch et al. (1999), Louarn et al. (1998) suggested that *substorm-like processes in the sense of a global configurational instability* of the magnetotail or even the whole magnetospheric-ionospheric system occur also in the Jovian magnetosphere. The overall observational signatures of a substorm process in the Jovian magnetosphere appear at first sight very much similar to the terrestrial one. The onset of auroral wave emissions, outward and inward flows of plasma, magnetic field distortions resembling plasmoid structures have all been reported (Louarn et al. 1998, Woch et al. 1999). Potential auroral signatures of these magnetospheric phenomena have recently been identified (Grodent et al. 2004). However, in application to Earth the term "substorm" often inherently comprises the loading of the magnetosphere by solar wind – magnetosphere interaction.

For Jupiter there exist different points of view regarding the driving mechanism of such dynamical disturbances. Can reconnection with the IMF produce the substorm processes as at Earth? Or are the dynamical disturbances internally driven?

In contrast to the "classical" substorms at Earth which under favorable conditions happen randomly under suitable conditions, substorm-like disturbances at Jupiter seem to reoccur with a characteristic time constant of several days (Woch et al. 1998, Louarn et al. 2000, Krupp et al. 1998). This intrinsic periodicity has led to the suggestion that the Jovian substorms are not driven by solar wind - magnetosphere interactions but by an internally driven process.

At Earth, in the classical externally driven case driven by addition of magnetic flux in the tail, reconnection of tail flux tubes are the prime relaxation process of a substorm. At Jupiter, the driving mechanism is believed to be the centrifugal force on rapidly rotating, mass-loaded flux tubes which lead to a thinning of the plasma sheet which enables spontaneous reconnection. This centrifugally driven reconnection process was first proposed by Vasyliūnas (1983) as a steady state process inherent to the Jovian magnetotail (see Section 1.1.4).

The plasma dynamics are principally driven by rotational forces rather than by interaction with the solar wind (Pontius 1997). This is explained by the strong magnetic field and the fast rotation of Jupiter and additionally by the weaker solar wind flux at Jupiter's

[10] See Section 1.2 in details.

orbit. Another evidence that reconnection with IMF is less effective at Jupiter than at Earth is obtained from the study of the flux transfer events at the Jovian magnetopause (Walker and Russell 1985). They were typically smaller and less frequent than at Earth. In fact, reconnection is less efficient for high plasma β conditions (Scurry et al. 1994). High plasma β conditions occur behind the Jovian bow shock and lead to lower efficiency of the reconnection process in comparison with the terrestrial case. The dynamics of the Earth's magnetosphere are very much affected by the product of the solar wind velocity and the component of the magnetic field perpendicular to the solar wind flow. At Jupiter, the mechanical energy flux in the solar wind intercepted by the huge magnetosphere would be small compared to the energy flux into the Jovian magnetosphere associated with the mass release from Io. Thus the reconnection driven by solar wind energy appears to be minor at Jupiter and would not affect the rapidly rotation plasma of the magnetosphere whose corotational electric field is much than that of the solar wind (Russell 2001).

Grodent et al. (2004) associated the Night Side Polar emissions with the "Jovian mass ejection". An overloading by thermal and rotational energy occurs due to iogenic mass loading. This excess mass and energy is released by a process analogous to solar coronal mass ejections.

Russell et al. (1998) has estimated the magnetic flux of reconnection events and corresponding magnetic flux that is mass-loaded at Io and came to the conclusion that the reconnection processes and the mass loading process are approximately in balance. The magnetic flux tubes that has been convected radially outward mass-loaded by the iogenic plasma can be returned to the inner magnetosphere as emptied magnetic flux tubes. The emptied magnetic flux tubes in the vicinity of Io were discussed by Kivelson et al. (1997), Russell et al. (2000b).

Louarn et al. (2000) suggested that enhancements in the various auroral radio emissions, with the creation of new sources of radiation in the Io torus and corresponding large fluctuations in the magnetodisc density are related to an instability developing in the external part of the Io torus or in the close to the Io torus magnetodisc. This instability leads to sporadic injections of new plasma populations into the magnetotail.

Slightly aside of the conventional points of view is the idea that the observed quasi-periodic fluxes of the energetic ion populations occur due to the existence of a low-dimensional and chaotic mechanism corresponding to the internal magnetosphere dynamics of Jupiter (Pavlos et al. 2004).

In order to investigate the importance of the IMF, Fukazawa et al. (2005) simulated the interaction between the Jovian magnetosphere and the solar wind using a time dependent three-dimensional global magnetohydrodynamical code. The simulations show that periodical plasmoid injections with a repetition period of 32-37 hours can be driven during long lasting periods of the northward IMF turn (185 hours). The magnetic flux feeds the magnetosphere and the convective flow determines the period of plasmoid emissions. However, the time to respond to changes in the IMF is very long (Walker and Ogino 2003) and the solar wind variations are usually on shorter time scales. Thus this mechanism cannot explain the commonly observed periodicities in the Jovian magnetosphere.

Also considering the solar wind as driving mechanism, Southwood and Kivelson (2001) pointed out the influence of compression and rarefaction of the Jovian magnetosphere induced by solar wind shocks on the stability of the Jovian plasma disc. They suggested that specifically during times of rapid expansion forces on mass-loaded flux

tubes will lead to the formation of detached plasma "blobs" breaking off at the outer edge of the middle magnetosphere and lead to subsequent outward transport of plasma.

Galopeau and Boudjada (2005) using the combination of Galileo/PWS and Wind/-WAVES observations found that the Jovian hectometric emissions (HOM) and the solar wind parameters have quasi-similar variations when a time lag of about 153 days is taken into consideration. They claim changes in the solar wind cause the observed hectometric emissions and/or injection events investigated by Louarn et al. (1998).

Based on Cassini and Galileo data, Gurnett et al. (2002) reported that HOM and extreme ultraviolet auroral emissions from Jupiter are triggered by interplanetary shocks propagating outward from the Sun, leading to similar processes that occur during geomagnetic storms at Earth.

1.3 Open Questions

The understanding of the dynamics of the Jovian magnetosphere has improved substantially in the past decade. However, some questions still remain unanswered, among these are.

- What is the nature of the observed radially outward and inward ion bursts / reconfiguration events in the Jovian magnetotail?
- Do substorm-like processes occur in the Jovian magnetosphere? What are the similarities and what are the differences to terrestrial substorms?
- What is the role of the solar wind and the interplanetary magnetic field in driving substorm-like processes at Jupiter?
- Why do these release processes occur periodically? Which mechanism is responsible for the release of plasma into the interplanetary space?
- Are there fundamental commonalities with substorms and periodical substorms occurring at Earth?

These questions will be investigated in this work. The main task of the thesis is to study in detail the dynamical processes in the Jovian magnetotail and their driving mechanisms.

The study is organized as follows. The instruments and tools used to investigate reconfiguration processes are described in Chapter 2. In Chapter 3 reconfiguration processes are studied using observations. First the single reconfiguration events are analyzed in detail and then summarized statistically. The quasi-periodical nature of the reconfiguration events is presented and compared with the periodical terrestrial substorms. To quantify the characteristics of the reconfiguration events and to compare them with the characteristics of terrestrial substorms a statistical study of the ion flow bursts is provided. The general characteristics of the reconfiguration events derived from the presented study are summarized after that. To explain the intrinsic time constant of the Jovian reconfiguration process a simple conceptual model is developed and presented in Chapter 4. Finally the summary of the main results is given in Chapter 5.

2 Instrumentation and Data Analysis Methods

2.1 Exploration of the Jovian magnetosphere

Seven spacecraft have explored the Jovian magnetosphere so far. Six of these were flyby missions which spent only a few days in the magnetosphere.

Pioneer 10 in 1973, was the first spacecraft to pass by Jupiter on a low inclination trajectory (SIII[1] latitude $< 15°$) at a distance within 1.8 R_J of its cloud tops. Pioneer 10 provided a reasonably accurate measurement of the magnetic dipole moment and magnetic field strength. The azimuthal asymmetry in the structure of the Jovian magnetosphere was detected.

A year after, Pioneer 11 flew by Jupiter in December 1974, on a highly inclined trajectory (maximum SIII latitude 52°) at a distance within 0.6R_J of Jupiter's cloud tops. Pioneer 11 observations have confirmed the earlier Pioneer 10 observations of the large size and extreme variability of the outer magnetosphere. Both Pioneers observed the dynamic interaction of the Jovian magnetosphere with the solar wind.

Voyager 1 made extensive measurements of the Jovian system in early 1979 on a nearly equatorial trajectory. Scientific studies of the Jovian magnetosphere focused on the source of the Jovian radio emissions, the dynamical properties of the magnetospheric plasma, aurora, and satellite-magnetosphere interactions.

Evidence was found for a transition of the magnetic field lines from a dipolar ($\leq$ 25 R_J) to a current sheet like configuration. The plasma flow was detected to be in corotational direction throughout the magnetosphere to distances of 130 to 150 R_J. At this distance the plasma flow direction changes to a persistent antisunward flow. It was discovered that the Io torus is populated by heavy ions. Voyager 2 started substantive Jovian measurements on 25 April 1979, as Voyager 1, on a nearly equatorial trajectory. The configuration of the equatorial current sheet was studied in detail.

Ulysses passed by Jupiter in February 1992 on a mid to high latitude trajectory. The spacecraft investigated the dusk high latitude region of the Jovian magnetosphere. It was revealed that the size of the Jovian magnetosphere changes dramatically in response to different dynamic conditions.

Galileo was the first spacecraft which orbited around Jupiter and will be described in Section 2.2 in detail. This spacecraft covered the Jovian magnetotail particularly well.

Finally, Cassini briefly passed the dusk boundary region in December 2000, providing the unique opportunity of simultaneous observations with Galileo and ground-based

[1] See Section 2.6 for details.

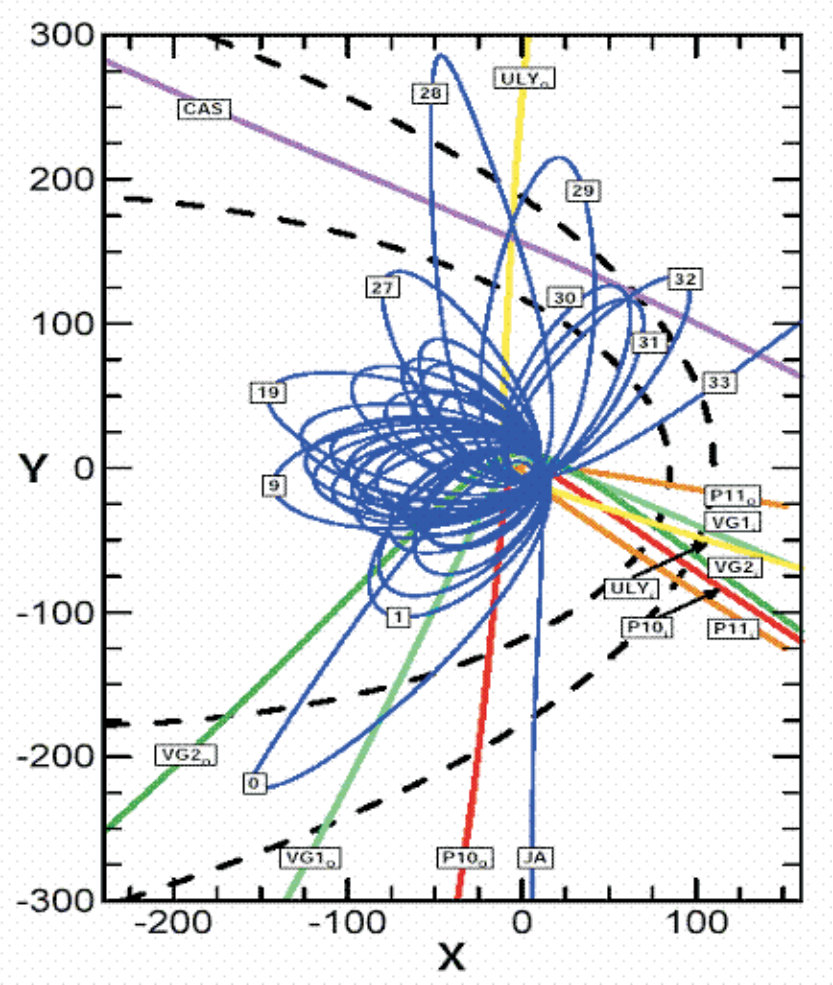

Figure 2.1: The trajectories of the different missions to Jupiter, projected onto the equatorial plane (x - y plane of the Jupiter Solar Ecliptic (JSE) coordinate system). Pioneer 10 and 11 fly-bys are presented in red and orange (respectively), Voyager 1 and 2 are shown in green, Ulysses is presented in yellow, Cassini in violet and Galileo orbits in blue. The Sun is located to the right of the Figure. Dashed lines show nominal bow shock (outer line) and magnetopause (inner line) locations.

observations of the near Jovian system.

2.2 The Galileo mission

The unrevealed questions about Jupiter which appeared after the flyby missions of the Pioneers, Voyagers and Ulysses spacecraft led to the development of Galileo as the first Jupiter orbiting mission.

The NASA mission was named in honor of Galileo Galilei who first made telescope observations of Jupiter and discovered four satellites (Io, Europa, Ganymede and Callisto, now known as the Galilean satellites) which suggested to him that the Copernican system

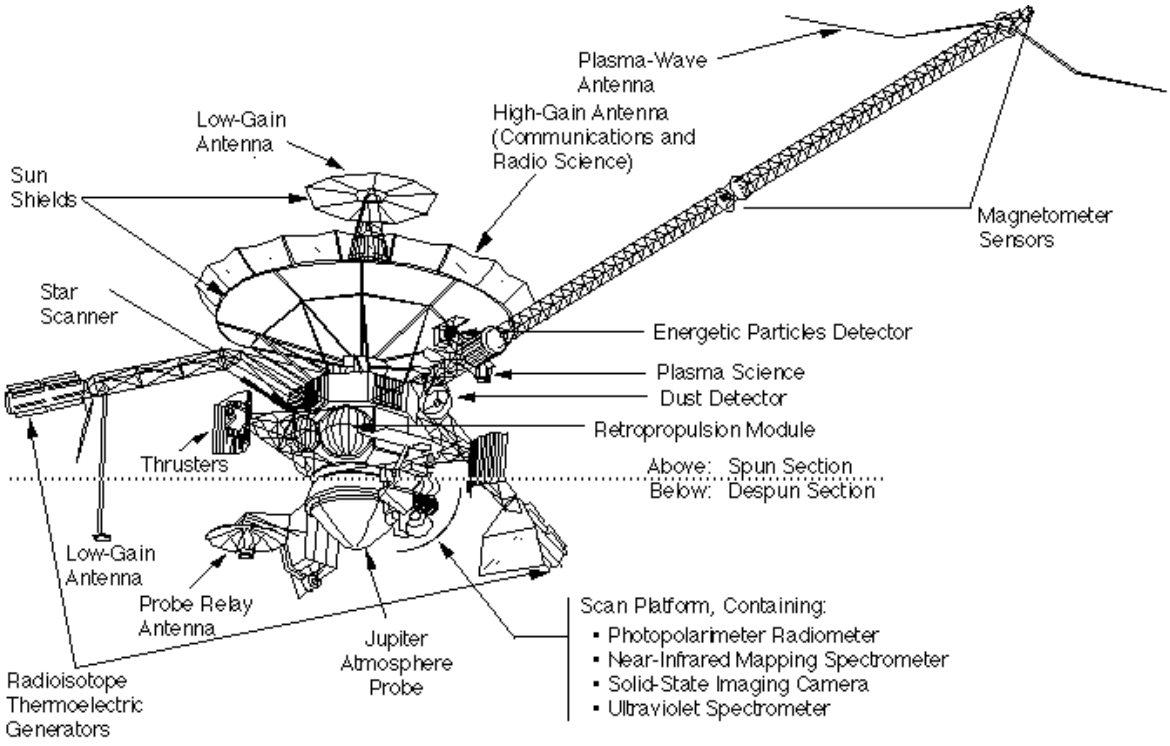

Figure 2.2: A sketch of the Galileo orbiter. Credit: JPL/NASA.

with the Sun in the center of the solar system could be correct.

The mission was planed and developed in 12 years. Galileo was initially scheduled to be launched in 1982 but it was postponed because of difficulties in both the Shuttle and the Centaur upper stage. Galileo was launched on October 18, 1989 aboard the space shuttle Atlantis. Its travel through the interplanetary space took 6 years. The spacecraft reached its orbit around Jupiter on December 7, 1995. It transferred data from the Jovian system for 8 years. The mission ended on September 21, 2003, when Galileo was intentionally steered into Jupiter's dense atmosphere. The interplanetary travel of the spacecraft followed the trajectory named VEEGA (Venus-Earth-Earth Gravity Assist), this allowed Galileo to get sufficient speed to reach Jupiter. The travel of the spacecraft from launch to impact was 4,631,778,000 km. On the way to the giant planet Galileo's scientific payload was used to investigate Venus, Earth, the Moon, the asteroid belt, with close look at the asteroids Gaspra and Ida, and Dactyl the moon of an asteroid. Galileo observed the collision of the comet Shoemaker – Levy 9 with Jupiter. Even the interplanetary cruise itself was fruitful, for example with recording the most intense dust storm ever detected by a spacecraft.

The Galileo mission included two spacecraft: the Galileo orbiter and the Galileo probe, the latter for in situ studies of the Jovian atmosphere. A sketch of the orbiter is presented in Figure 2.2.

The Galileo orbiter is the combination of a spinning spacecraft as the Pioneers, and Ulysses and of a three-axis stabilized spacecraft as the Voyagers. An innovative "dual-spin" design provided conditions favourable for instruments which require rotation e. g. to measure fields and particles, as well as for remote sensing experiments which demand

steady pointing. The Galileo orbiter had 12 scientific experiments.

The instruments and their area of investigation are shown in Table 2.1.

Table 2.1: Scientific experiments on board of the Galileo orbiter.

Name of an instrument	Field of investigation
Remote-sensing instruments	
Solid-State Imaging Camera (SSI)	satellite study including small satellites, the Jovian atmosphere, auroral phenomena, rings
Near-Infrared Mapping Spectrometer (NIMS)	surfaces of the satellites of Jupiter, the Jovian atmosphere
Photopolarimeter/Radiometer (PPR)	the intensity and polarization of sunlight
Ultraviolet Spectrometer/ Extreme Ultraviolet Spectrometer (UVS/EUS)	atmospheres of the Jupiter and Galilean satellites, aurora, satellites surfaces
Fields and Particles Instruments	
Magnetometer (MAG)	the strength and direction of the magnetospheric magnetic field
Plasma Wave Subsystem (PWS)	the properties of varying electric and magnetic fields
Energetic Particles Detector (EPD)	the energies and flux of ions and electrons
Plasma Instrument (PLS)	the energies, directions of ions and electrons, defining of the ion composition by mass-spectrometer, in the energy range (9 eV - 52 keV)
Dust Detector Subsystem (DDS)	measurements of dust (10^{-6} - 10^{-7}) particles mass, electric charge, velocity
Engineering Experiment	
Heavy Ion Counter (HIC)	measurements and monitoring of the very high-energy heavy ions, hitting spacecraft
Radio Science	
Celestial Mechanics	detection of small changes in the trajectory of the spacecraft
Radio Propagation	ionospheres of the Galilean satellites and Jupiter, Jupiter's neutral atmosphere

The main scientific goals of the Galileo orbiter mission are:

- study the circulation and dynamics of Jupiter's atmosphere;
- investigate the Jovian upper atmosphere and ionosphere;

- reveal the morphology, geology and physical state of the Galilean satellites;
- study the composition and distribution of surface minerals on the Galilean moons;
- determine dynamic properties, the gravitational and magnetic fields of the Galilean satellites;
- study the interaction of the Jovian magnetosphere with the Galilean satellites;
- characterize the vector magnetic field, the energy spectra, composition, and angular distribution of energetic particles and plasma.

The orbits of Galileo have encounters with the Galilean moons. Each orbit is denoted by the initial of the respective satellite and the sequential number of the orbit. Thus the G2 orbit is the second orbit, and has an encounter with Ganymede.

Galileo covered distances up to 150 R_J. The closest approach to Jupiter was at a distance of 2.5 R_J.

The present work uses data sets from the EPD and MAG instruments as well as the PWS instrument. These instruments will be described in the following sections.

2.3 The Energetic Particles Detector

The Energetic Particles Detector (EPD) is an instrument on board of the Galileo spacecraft designed to measure the characteristics of the charged particles population such as energies, intensities, composition and angular distribution to determine, in particular, dynamics and configuration of the Jovian magnetosphere. The Galileo EPD in comparison with the respective instruments on previous missions is more advanced in terms of possibilities to measure the time and spatial variations of the energetic particles. The advantages of the EPD instrument are the 4π steradian angular coverage for Jovian energetic particles and the extended coverage of particle energies. The EPD instrument was built in a joint effort of the Johns Hopkins University Applied Physics Laboratory (JHU/APL), Max-Planck-Institut für Aeronomie (MPAE) (nowadays The Max-Planck-Institut für Sonnensystemforschung (MPS)), and the National Oceanic and Atmospheric Administration Space Enviroment Laboratory (NOAA/SEL). For a complete description of the EPD instrument see Williams et al. (1992). The mass of the EPD instrument is 10.5 kg, its size is 19.5 cm $\times$ 27 cm $\times$ 36.1 cm, the power requirement is 4 W for heaters and 6 W for electronics.

A scheme of EPD is given in Figure 2.3. The EPD consists of two double-headed detector telescopes: the Low Energy Magnetospheric Measurement System (LEMMS) and the Composition Measurement System (CMS). These detectors will be considered in more detail below.

The rotation of the detector heads, which are mounted on a platform, by a stepper motor in combination with the satellite spin provides the almost 4π steradian angular coverage with exception of a small solid angle ($\leq$ 0.1 sr) along the spin axis which is blocked to avoid direct sun light into the detector. A sketch of the stepper motor positions (view point from above) on EPD is shown in Figure 2.4. After a full spacecraft rotation the stepper motor moves by 30°. The 4π coverage is achieved after 7 spacecraft spins

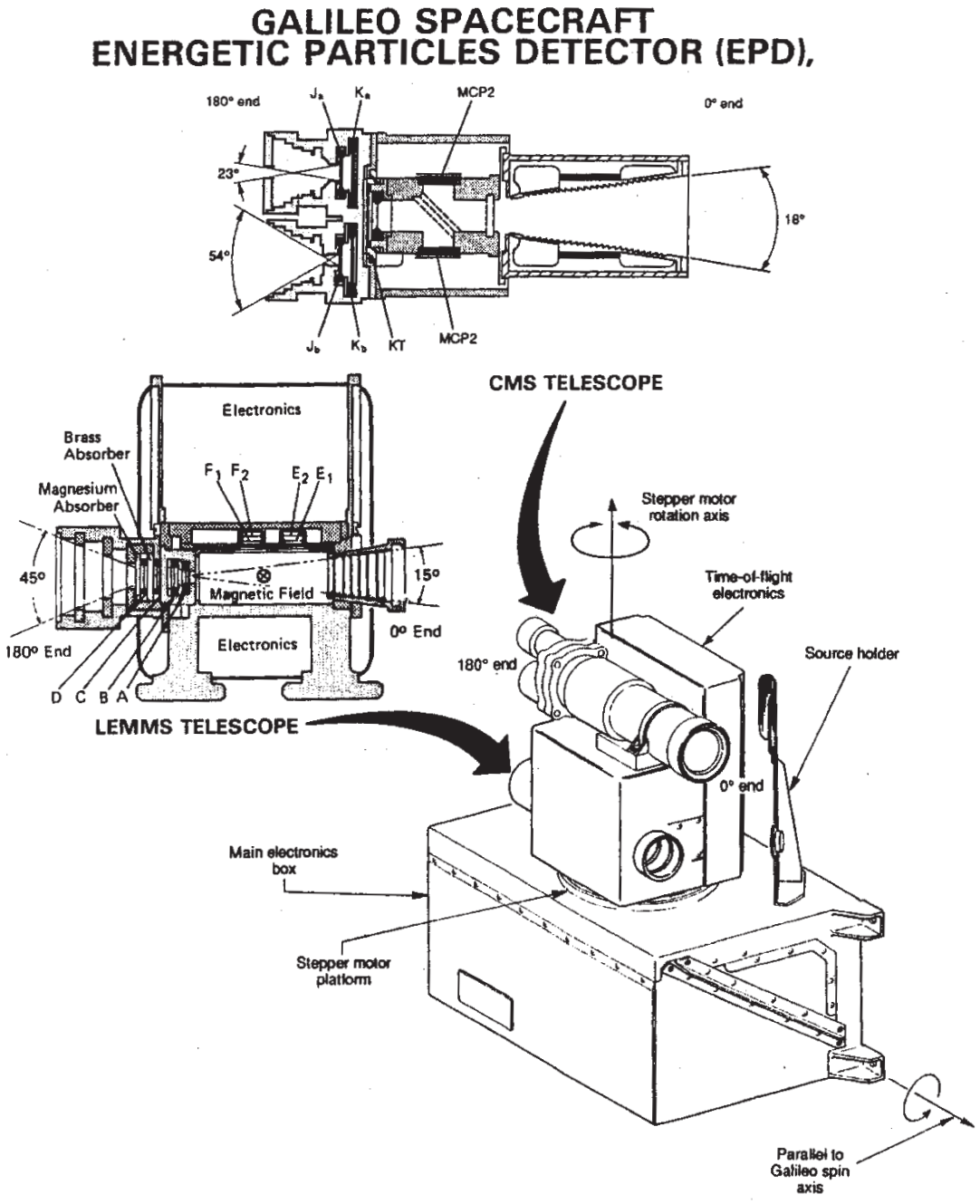

Figure 2.3: A sketch of the Energetic Particles Detector, from Williams et al. (1992).

($\sim$ 140 seconds), when the motor stepped through positions 1-7. Position 0 is used for calibration purposes. The stepper motor moves during the rotation through 8 positions, separated by 30° and in case of the position 0 and 1, by 45°.

It was planned that the Galileo spacecraft will transmit data with two different rates: from a high gain antenna at a rate of 134 kbps, and low resolution data at a rate of 160

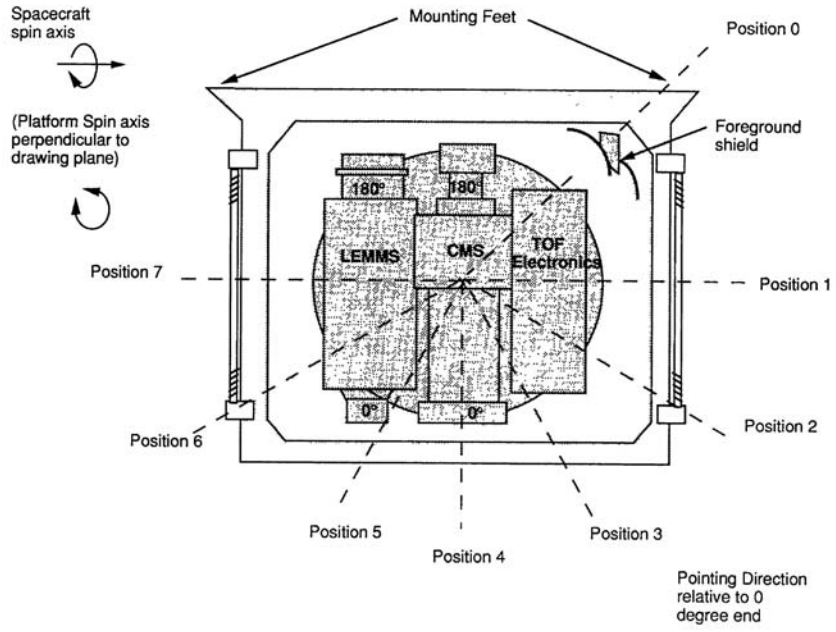

Figure 2.4: The stepper motor positions if looked on EPD from the top. The spin axis of the spacecraft is parallel to the position 1 to 7 line, from Williams et al. (1992).

bps. But because of technical problems with the high gain antenna the data had to be transmitted by the low gain antenna only. The transmission was rearranged in two different modes, real time mode and record mode. In this work the real time data were used, which are available during almost the whole mission. In real time mode the available bit rate is 5 to 40 bps, in this mode the unit sphere is divided into 16 angle sectors (see Figure 2.5) and scanned with a time resolution of 3 to 11 minutes depending on the transmission rate to Earth.

2.3.1 Low Energy Magnetospheric Measurement System (LEMMS)

The intention of the LEMMS telescopes is the measurement of ions in the energy range from 22 keV to 55 MeV and electrons from 15 keV to 11 MeV with high angular ($< 20°$) and temporal (1/3 to 4/3 s) resolution. The energy ranges are split into the 32 rate channels. The LEMMS instrument is a double-ended telescope consisting of 8 strongly shielded silicon solid state detectors with a totally depleted barrier surface. A sketch of the instrument is shown in Figure 2.6.

To separate ions and electrons in the A, E and F channels LEMMS uses a baffled collimator and a magnetic field deflection method.

The separation of the ions and electrons in A, E and F channels of LEMMS is done as follows: the charged particles entering the telescope at the $0°$ end are parallelized by the collimator and then deflected by the magnetic field. Due to the action of the Lorentz force ions and electrons will be separated in opposite directions and deflected from the original direction with an angle depending on the initial energy and charge of the particle, and be registered by different detectors. Ions are registered by detectors A and B in 12 energy

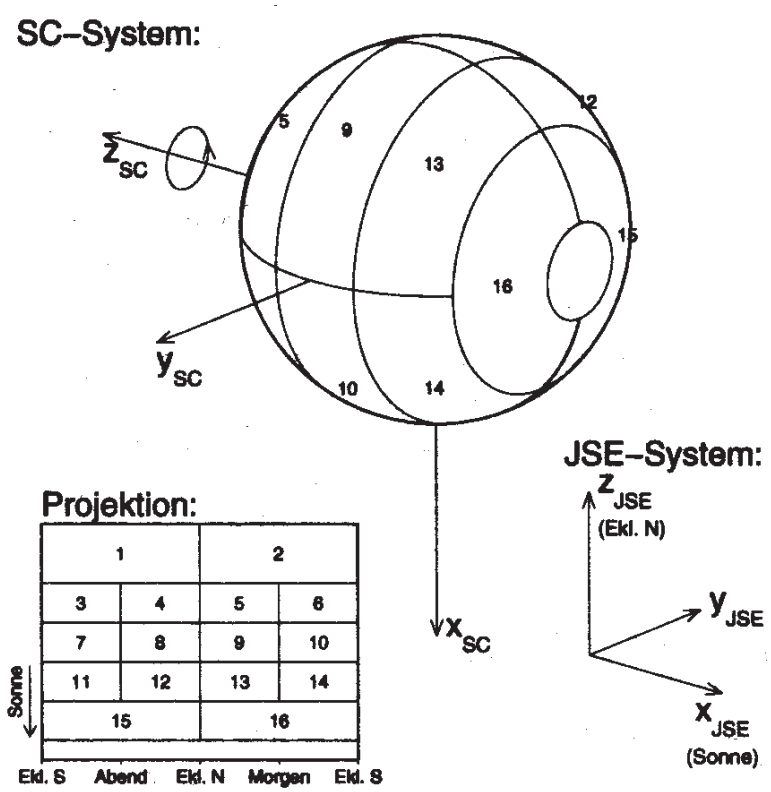

Figure 2.5: The sectorization of the real-time data, from Lagg (1998).

Table 2.2: LEMMS rate channels.

Ions		Electrons	
Channel	Energy range (keV)	Channel	Energy range (keV)
A0	22-42	E0	15-29
A1	42-65	E1	29-42
A2	65-120	E2	42-55
A3	120-280	E3	55-93
A4	280-515	F0	93-188
A5	515-825	F1	174-304
A6	825-1680	F2	304-527
A7	1680-3200	F3	527-884
DC0	1450-3350		

channels from 22 keV to 100 MeV. In this study the channels presented in the Table 2.2 will be used. Electrons are counted by the detectors E and F, divided in 8 energy channels, with an energy range between 15 keV and 884 keV. The ions and electrons with a higher energy range are measured by the double absorber detector telescope, mounted on $180°$.

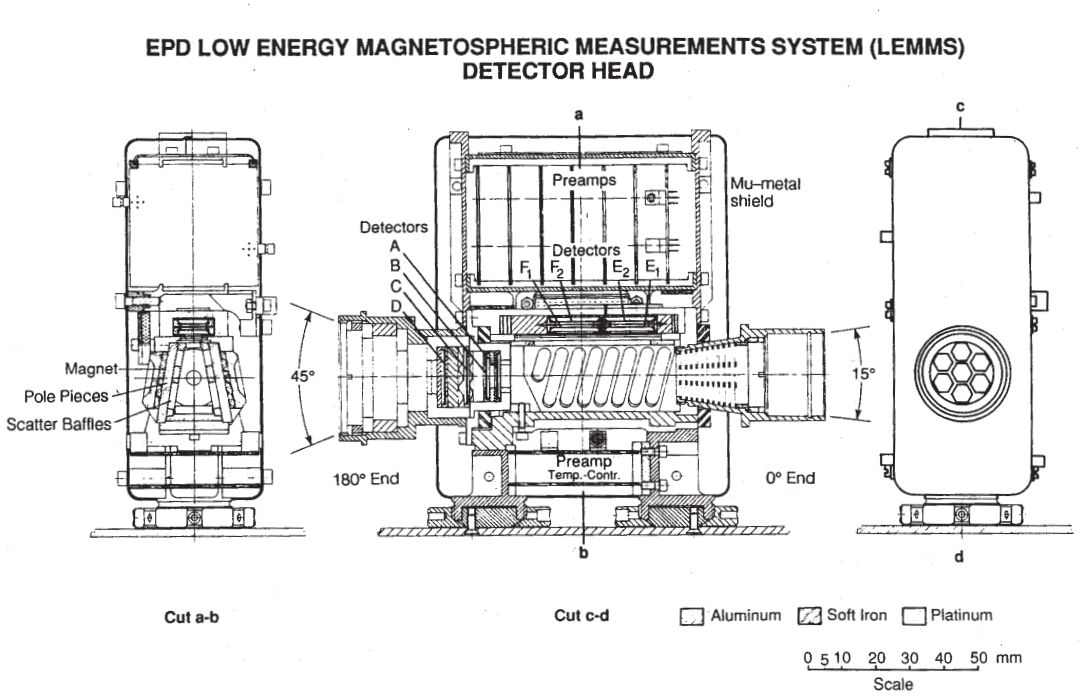

Figure 2.6: The EPD LEMMS telescope, from Williams et al. (1992).

There are two detectors C and D. Ions are measured in an energy range from 14.5 MeV to 100 MeV, electrons in two integrated channels ≥ 2 MeV and ≥ 11 MeV.

The detectors provide measurements in count rate (counts s^{-1}) which is converted to the differential, directional particle flux I $[cm^{-2}s^{-1}sr^{-1}keV^{-1}]$. The flux describes the trapped radiation intensities, energies and directionality of particles.

The conversion from count rate to differential, directional flux requires the knowledge of the geometric factor of the telescope, the energy bandwidth of the channels and the efficiency of the detectors. The detector efficiency is assumed to be unity, the energy bandwidth of the channels is known from pre-launch calibration measurements and simulations. Due to the magnetic deflection system the geometric factor of the telescope is a function of energy. The computation of the geometric factor for these channels therefore requires the knowledge of the energy dependence of the particle distribution. A power law spectrum $I(E) \propto E^{-\gamma}$ is a good approximation for most of the particle fluxes measured.

The spectral index γ is a priori unknown. The geometric factor and the spectral index can be iteratively calculated by the following procedure: for any value of γ the geometrical factor is defined and from the measured count rates the energy distribution is computed. From this energy distribution the new γ is obtained and then the procedure is repeating until the γ will not change anymore.

Low-energy ions: detectors A and B

The detectors A and B measure the low energy ion population (from 22 keV to 100 MeV). Ions enter the 15° full angle collimator, pass eleven baffle plates defining seven hexagonal entrance aperture channels and converging towards the detector A. The detec-

tor A has 8 different rate channels to detect ions (Z $\geq$ 1) in the energy range between 22 keV and 3.2 MeV and the detector B discriminates three outputs for high energy (Z $\geq$ 2) ions as well as high-energy electrons using coincidence logic between A and B. To minimize the background contamination, the LEMMS instrument uses coincidence/anti-coincidence conditions between the detectors and is protected by platinum-iridium shielding. Electrons ($\leq$ 22 MeV) are deflected from detector A and entering the detectors E and F.

Low-energy electrons: detectors E1, E2, F1, F2

The deflected electrons are entering the magnetic deflection region – an inhomogeneous magnetic field generated by permanent magnets with a maximum center line strength of 650 G. There are two detectors recording the incoming electrons: E1 in the energy range ($\geq$ 15 to 200 keV) and F1 ($\sim$ 100 to 1000 keV). The outputs of detectors E1 and F1 are separated into 8 rate channels (see Table 2.2). The detectors E2 and F2 are operated in anticoincidence to reduce background effects.

High Energy Electrons and Ions: detectors C and D

Detectors C and D are used to measure high energy ions and electrons. Both detectors have two thresholds, of $>$ 2 MeV and $>$ 11 MeV for electrons, and of 14.5 MeV and 51 MeV for ions, in detectors C and D respectively.

2.3.2 The Composition Measurement System (CMS)

Whereas LEMMS cannot separate ion species, the CMS is an instrument to measure the composition of ions in the Jovian magnetosphere. Measurements are performed in the energy range of $\simeq$ 2 keV nuc^{-1} to $>$ 10 MeV nuc^{-1}. The CMS consists of two different particle telescopes: the time-of-flight (TOF) and the ΔE $\times$ E solid state detectors, which are schematized in Figure 2.7. The data from the ΔE $\times$ E detector are not used in this work.

CMS TOF telescopes

The TOF telescope is orientated in the 0° direction while the Δ E $\times$ E solid state detector which covers higher energies looks in the 180 ° direction. The CMS TOF telescope consists of a collimator with a sweeping magnet followed by a thin parylene front foil, and a solid state detector, at the rear of the time-of-flight path. After entering the telescope the ions hit a front foil causing the emission of secondary electrons from the inner surface of the foil. The electrons are accelerated by an electric field and travel to the microchannel plates (MCP). MCP's provide 'start' and 'stop' fast timing pulses for measurement of the ion time-of-flight between the front foil and K_T. The time-of-flight between the front foil and K_T as well the ion energy measurements by K_T allow to define the ion mass. The energy ranges and species registered by TOF telescope are presented in Table 2.3.

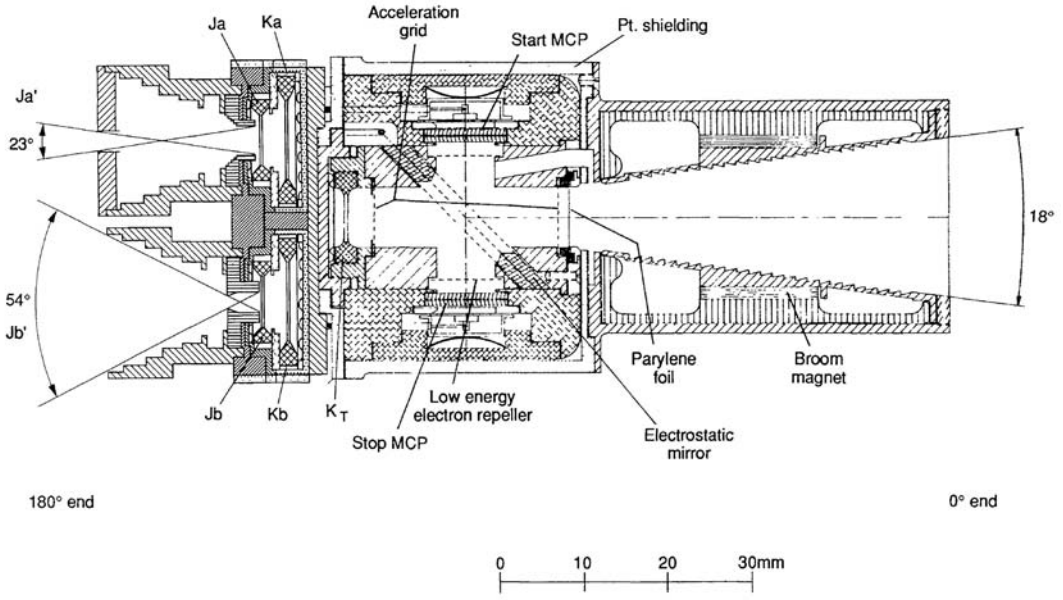

Figure 2.7: EPD CMS detector head, from Williams et al. (1992).

Table 2.3: CMS TOF channel description.

Species	Channel name	Energy range(MeV $nucl^{-1}$)
Protons	TP1	0.08-0.22
	TP2	0.22-0.54
	TP3	0.54-1.25
Alphas	TA1	0.027-0.155
	TA2	0.155-1.00
Oxygen	TO1	0.012-0.026
(Medium	TO2	0.026-0.051
Nuclei)	TO3	0.051-0.112
	TO4	0.112-0.562
Sulfur	TS1	0.016-0.030
(Intermediate	TS2	0.030-0.062
Nuclei)	TS3	0.062-0.31
Heavy Nuclei (Fe)	TH1	0.02-0.20

2.4 Magnetometer

The magnetometer (MAG) had two sets of triaxial fluxgate magnetometers, where each set covers a different range of magnetic field strength. To avoid the influence of the Galileo spacecraft on the measurements of the magnetic field, the sensors were located on long booms (11.03 m and 6.87 m from the spin axis of the spacecraft, respectively). The

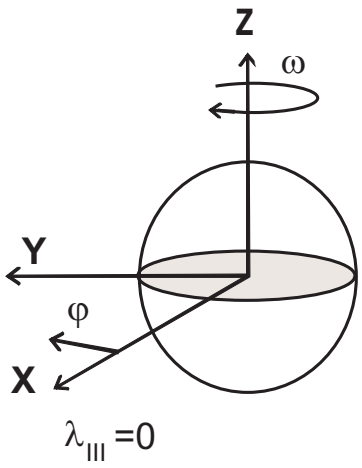

Figure 2.8: Jovian System III.

magnetometer instrument measures magnetic field vectors in three different sensitivity ranges with the sampling frequency dictated by the available downlink (Kivelson et al. 1992). During the intervals used in this work, the MAG sensor on the tip of the boom was in the $\pm$ 512 nT range with a resolution of 0.25 nT and a temporal resolution of 24s. The orientation of the sensor is known with an accuracy better than 0.1°. The magnetic field data will be presented in the SIII -coordinate system.

2.5 The Plasma Wave Spectrometer (PWS)

The purpose of the Plasma Wave spectrometer is to measure the varying electric and magnetic fields characteristics in the frequency range 5 Hz to 5.6 MHz and 5Hz to 160 kHz, respectively, for the identification of plasma waves. An electric dipole antenna was mounted at the tip of the magnetometer boom to study the electric field. The measurements of the magnetic field were provided by two search coil magnetic antennas, which were mounted on the high-gain antenna feed. The electric and magnetic fields were measured almost simultaneously which allows to distinguish between electrostatic waves and electromagnetic waves.

2.6 Coordinate system

The scheme of the Jovian System III (1965) (SIII -coordinate system) is shown in Figure 2.8. The Jovian system III is a left-handed Jupiter-centered system which rotates with the planet. The z-axis of the system is defined as the rotation axis of Jupiter with the positive direction oriented northward. The x-axis is fixed on the Jovian prime meridian, $\lambda_{III} = 0^{\circ}$, as defined by the International Astronomical Union in 1976. The longitude is measured clockwise from this prime meridian. For most of the studies the magnetic field data will be presented in this coordinate system. In this system the radial component of the magnetic field is positive in the outward direction, the azimuthal component is

positive in the direction of Jupiter's rotation and the south-north (meridional) component is positive southward.

2.7 Anisotropy, velocity and pressure calculations

From the measurements of the ion intensities by EPD the ion flow anisotropies, flow velocities and the ion pressure can be estimated.

2.7.1 Anisotropy

The angular distribution of convected ions at Jupiter can be interpreted in terms of low-order spherical harmonics as long as $2v_F/v_{ion} < 1$, where v_F is the convection velocity and v_{ion} is the ion speed.

Assuming that the particle intensity $I(E, \theta, \phi)$ can be described by a continuous function on a sphere, the spherical harmonic expansion can be written as

$$I(E, \theta, \phi) = I_{omni} \sum_{n=0}^{\infty} \sum_{m=-n}^{m=n} A_{nm}(E) Y_{nm}(\theta, \phi),$$

where E is the energy and the omnidirectional ion intensity is so that $A_{00} = 1$. I_{omni} is

$$I_{omni}(E) = I_0 \left(\frac{E}{E_0} \right)^{-\gamma},$$

where γ is a spectral index. The functions Y_{nm} are defined as

$$Y_{nm}(\theta, \phi) = P_{nm}(\cos\theta) \cos(m\phi) m > 0,$$

$$Y_{nm}(\theta, \phi) = P_{n|m|}(\cos\theta) \sin(|m|\phi) m < 0,$$

where P_{nm} are the normalized Legendre polynomials, the angles θ and ϕ are given by the motor position of EPD and the spin rotation of the spacecraft, respectively (Krupp et al. 2001). Details on this technique can be found in (Sanderson and Page 1974). The 16-sector measurements of ions are analyzed by using spherical harmonics. In this study only the vector of the first-order anisotropy $\mathbf{A_1} = (A_{1-1}, A_{10}, A_{11})$ will be considered.

The first-order anisotropy vector is generally composed of a combination of vectors such as ion convective flow $\mathbf{A_{flow}}$, field-aligned streaming, intensity gradient effects $\mathbf{A_{grad}}$ and other, usually small, components

$$\mathbf{A_1} = \mathbf{A_{flow}} + \mathbf{A_{grad}} + ...$$

Under the condition $2v_F/v_{ion} < 1$ the convective anisotropies of ions at Jupiter can be represented as

$$\mathbf{A_{flow}} = \frac{2(\gamma + 1)\mathbf{v_{flow}}}{v_{ion}} \tag{2.1}$$

where $\mathbf{v_{flow}}$ is the convection velocity, v_{ion} is the ion speed (Krupp et al. 2001). A first approximation for the intensity gradient anisotropy $\mathbf{A_{grad}}$ is

$$\mathbf{A_{grad}} = \frac{m v_{ion}}{q B^2} \left(\mathbf{B} \times \frac{\nabla I}{I_{omni}} \right), \tag{2.2}$$

where m and q is the mass and the charge of the ion, B is the magnetic field. However, no evidence was found of large contributions from the intensity gradient in the analysis of EPD data. In a first approximation the flow component appears to dominate the first-order anisotropy (Krupp et al. 2001).

2.7.2 Velocity

From expression (2.1) for the flow anisotropy it is possible to estimate the total convection velocity (flow velocity)

$$\mathbf{v_{flow}} = \frac{\mathbf{A_{flow}} v_{ion}}{2(\gamma + 1)}.$$

The derived flow velocity is sensitive to the accuracy of the determination of energy spectral slope γ. In this study the omnidirectionally averaged γ values are used. v_{ion} is determined from the geometric mean energy of the respective ion channel.

The transverse component of $\mathbf{v_{flow}}$ in Expression 2.1 is dominated by the drift velocity

$$\mathbf{v}_{\perp} = \frac{\mathbf{E} \times \mathbf{B}}{B^2},$$

which is independent of the properties of the energetic ions (mass, charge, energy). When $\mathbf{A_{grad}} \sim 0$ in 2.2 and when the field-aligned flows are also species-independent then all ion velocities are the same (Krupp et al. 2001).

2.7.3 Pressure

An estimate of the plasma pressure is important for understanding the dynamics within the plasma sheet. Therefore a tool to calculate a proxy for the plasma pressure from the EPD measurements was developed. A relationship between the pressure P and the particle energy E is given by:

$$P = \frac{2}{3} nE, \tag{2.3}$$

with n being the particle number density. The quantity nE is the energy density of the particles and can be expressed as the second integral moment of the velocity distribution:

$$nE = m \int f(\mathbf{v}) v^2 d^3\mathbf{v}, \tag{2.4}$$

where f is a distribution function, m is the particle mass and v the particle velocity. To determine the particle pressure it is necessary to know the velocity distribution $f(\mathbf{v})$ of each ion species populating the Jovian magnetosphere. Instead of the velocity distribution the Galileo EPD measurements allow to determine the energy distribution for the individual ion species, which can easily be converted to the velocity distribution.

Determination of particle distribution from EPD measurements

To define the energy distribution of hot ions the so-called kappa distribution (a Maxwellian core with a power law tail) is often used to characterize particle spectra in a

planetary magnetosphere. The kappa-distribution expressed through the ion energy can be written as follows

$$I = \frac{C}{2} E \cdot [E + kT(1+\gamma)]^{-1-\gamma}. \tag{2.5}$$

where I is the differential intensity $[\mathrm{cm}^{-2}\mathrm{s}^{-1}\mathrm{sr}^{-1}\ \mathrm{keV}^{-1}]$, E is the measured energy [keV], C is the fitting parameter, kT is the core Maxwellian temperature and γ is the kappa distribution power law spectral index (Mauk et al. 2004).

The energy spectra of S, O, H and He are assumed to be represented by Equation 2.5. So the best parameters for these distributions in order to fit the all-ion channels (LEMMS instrument) as well as the species-discriminated CMS/TOF-channels are searched. Thus to derive the spectra of every single species it is required to determine the fitting parameters C, kT and γ for these distributions. All reliable ion channels (a1 – a7, tp1 – tp3, to2 – to4, ts1 – ts3, ta1 and ta2) were used for these calculations. The detectors that provide these channels also allow the measurement of angular distributions, but due to the poor statistics of the count rates in the magnetotail angle-averaged rates have been used for this study.

The task now is to find the values of the energy spectra parameters. First an initial set of distribution parameters is guessed, then the parameters are calculated by using a Pikaia[2] algorithm (Charbonneau 1995) to fit a kappa distribution to all used ion channels.

Figure 2.9 shows an example of the energy distributions obtained by this fitting algorithm at the current sheet crossing in the middle magnetosphere at 24 R_J during a 11.5 min time interval. The top panel shows ion channel rates measured by EPD (small symbols connected by the solid lines) and the count rates computed by integrating the optimized analytic spectra over the channel's energy bandwidth (big symbols connected by the dashed lines) for the ions of H, He, O and S. Table 2.7.3 contains information about the presented data and the optimized parameters of these analytic spectra. The bottom panel of Figure 2.9 shows the best energy spectra for the given count rate distribution of ion species. The goodness of fit ("fitness") is derived from converting energy distributions back to count rates and then calculating the least square differences between the experimental and analytical rates "sigma" and the value of the "fitness" (see values of "fitness" and "sigma" in Figure 2.9, the top panel).

Figure 2.10 presents derived sample spectra for the magnetotail region at 80.6 R_J using this technique.

In general the obtained spectral fits are not perfect. The dynamical processes in the Jovian magnetotail do not always follow the spectral law given in Equation (2.5), which leads to additional systematic errors. The problems of some energy channels, e. g. a0, a8, dc0, dc1, introduce uncertainties in the shapes of the spectra. An error propagation calculation was performed taking into account the statistical effects of low count rates. An example of the statistical error for the sulfur intensity is shown in Figure 2.9 by dashed

[2]The Pikaia fit is a method which finds the single parameter set that minimizes the difference between the model's predictions and the given data set. The algorithm is as follows: (1) Evaluate the goodness of fit ("fitness") of each number of the dataset (through a chi square measure with the data). (2) Select pairs of solutions from the dataset, with the probability of a given solution being selected made proportional to that solution's fitness. (3) Breed the two solutions selected in (2) and produce two new solutions ("offspring"). (4) Repeat steps (2)-(3) until the number of offspring produced equals the dataset. (5) Use the new dataset of offspring to replace the old dataset. (6) Repeat steps (1) through (5) until some termination criterion is satisfied.

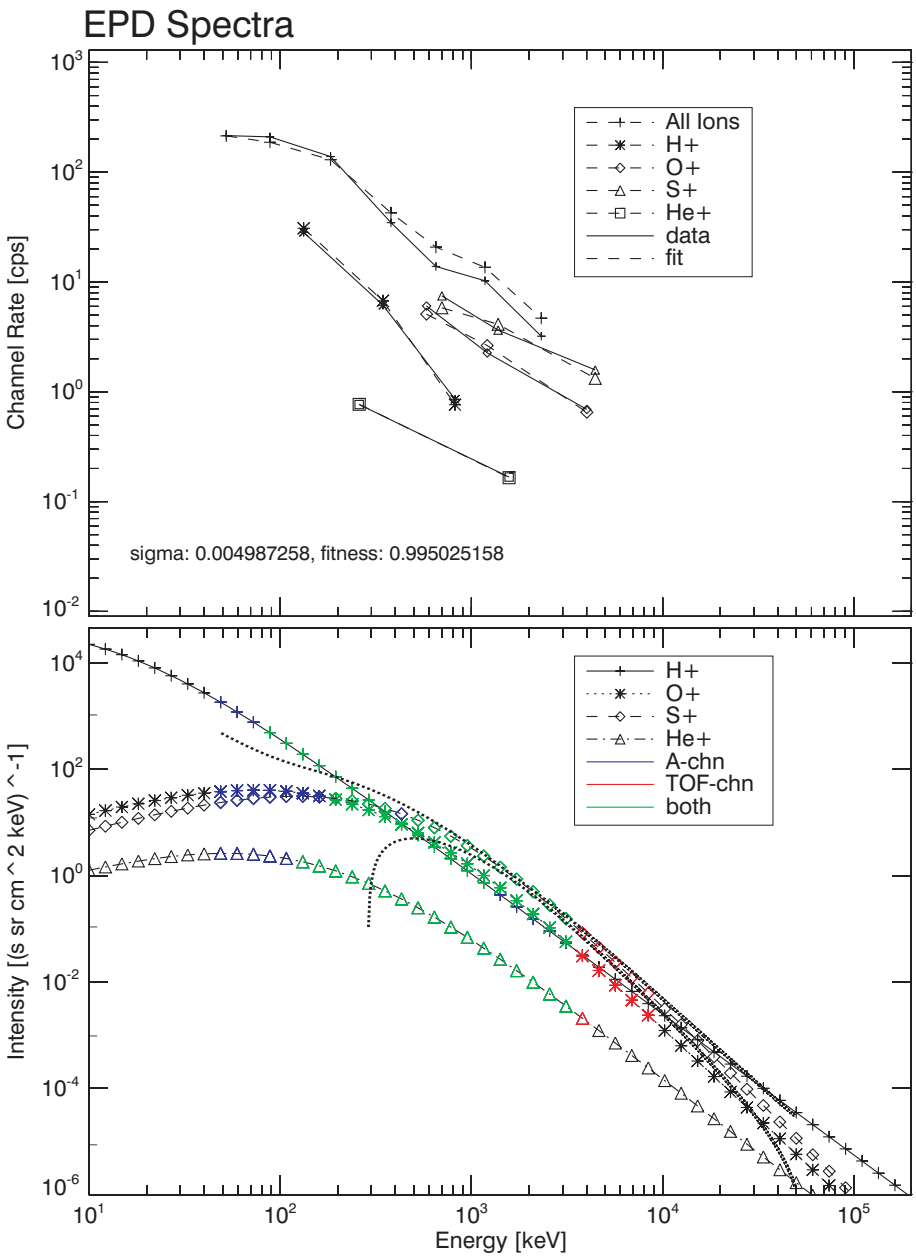

Figure 2.9: Top: An example showing ion channel rates measured by EPD, and rates obtained with analytic spectra for the ions of H, He, O and S at 24 R_J. Bottom: The ion energy spectra obtained by optimization of the EPD ion channel rates. The color-coding defines the energy ranges which covered by EPD measurements: blue by the all-ion channels from LEMMS instrument, red by CMS/TOF channels and green by both channels. The statistical error of spectra for the sulfur is show by dashed lines.

lines. This estimation is based on the variations observed in the energy spectra calculations when the input count rates were randomly varied according of the Poisson distribution.

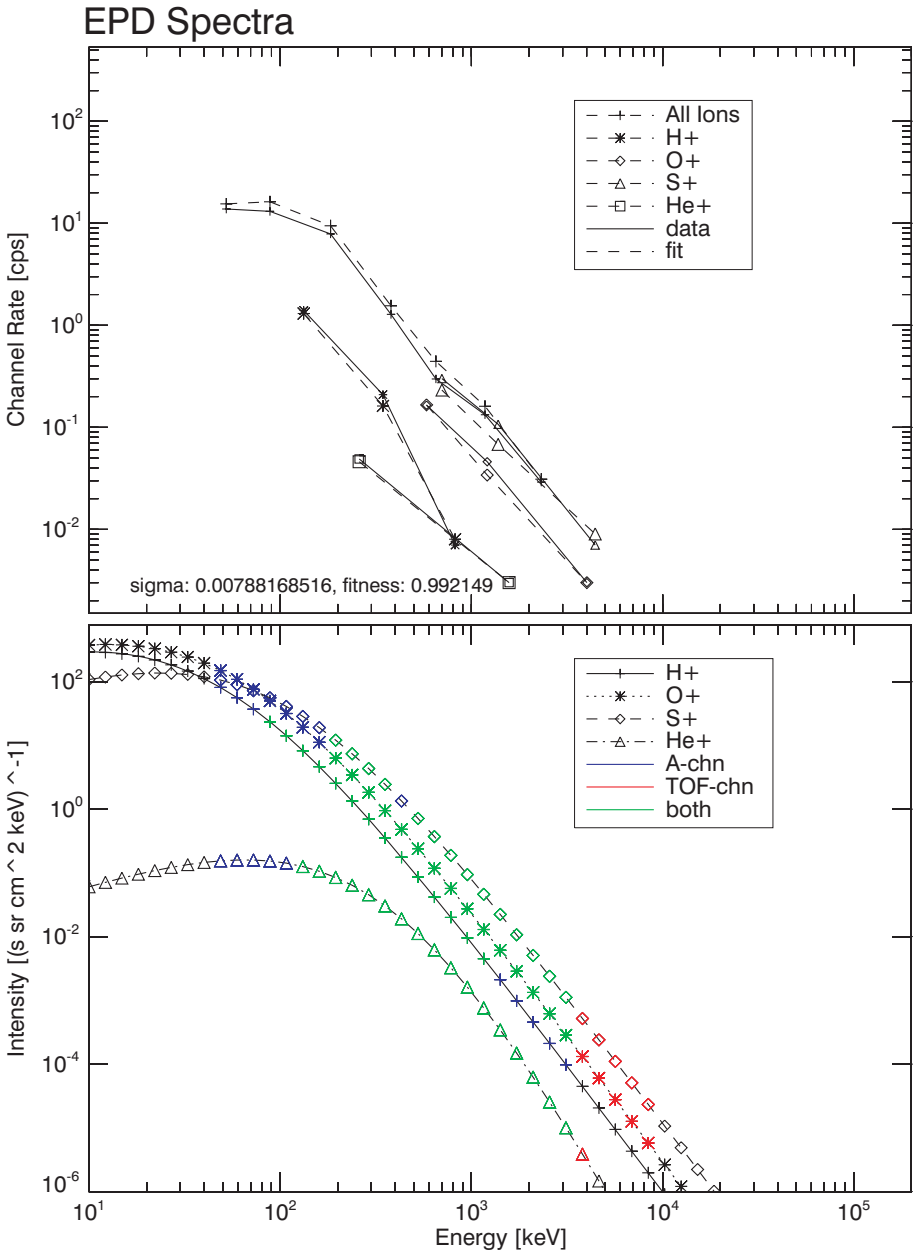

Figure 2.10: Same format as Figure 2.9. Spectra are measured in the magnetotail at 80.6 R_J.

Pressure calculations

With this knowledge of the ion spectra the pressure can be found as the second velocity moment of the ion velocity distribution or as the second integral moment of the ion spectra. Under the assumption of the isotropic angular distributions of ions in the convected frame and of nonrelativistic speeds of ions ($E = mv^2/2$), meaning that $E^{1/2} \propto v$, $(I/E) \propto f(\mathbf{v})$, and $(E^{1/2}dE) \propto d^3\mathbf{v}$, Equation 2.4 can be transformed to the following

Table 2.4: Ion spectral parameters derived from the fit to the measured distributions for the ion energy range from 50 keV to 50 MeV.

	C	kT, [keV]	γ
C9, 1997 180 04:30 UT, 24 R_J, LT=19:18			
H	2.23	2.4	2.65
O	8.2	58	3.44
S	36.08	95	3.63
He	0.2	30	2.81
C9, 1997 188 17:15 UT, 80.57 R_J, LT=22:55			
H	0.019	8	3.97
O	0.058	9.9	3.99
S	0.245	18.5	4
He	0.019	55	5.4

expression:

$$P(\text{dynes cm}^{-2}) = A \int (E^{1/2})^2 (I/E)(E^{1/2} dE), \tag{2.6}$$

where $A = 2 \cdot 4\pi (m/2)^{1/2}/3$, m is the ion mass [g], E is the energy [erg]. The ion pressure is derived from the analytic spectral fits by numerically integrating over the energy range between 50 keV and 50 MeV (the range is chosen as in paper of Mauk et al. (2004) to compare the results).

Unfortunately the determination of the ion pressure has some severe limitations. For instance, the spacecraft is in the actual center of the current sheet only for short periods of time ($\sim$ 10 minutes), which is even shorter than the measurement interval needed for the pressure derivation. Another limitation is that in order to investigate the dynamics of the plasma pressure the 68 consequent current sheet crossings were selected over a wide radial interval from 24 R_J to 114 R_J of the C9 orbit. The spectral fit for every data point in the ion pressure estimations was calculated automatically. Thus the same set of weighting factors (weight of each ion channel in the fitting process) and the same ranges of the fitting parameters were used for every current sheet crossing, independent of the radial distance. Generally (in the case of smaller number of current sheet crossings) the pressure would be better defined by searching the best set of parameters individually for every single current sheet crossing. Even if the estimated quantities are roughly defined, the qualitative dynamical trend can still be investigated. The statistical error for the pressure determination is about $\pm 16\%$ at 24 R_J, about $\pm 45\%$ at 80 R_J and about $\pm 185\%$ from 97.8 to 112 R_J. Therefore the statistical error increases with the radial distance due to the decrease of the count rates per second with distance.

An example of the pressure calculation is shown in Figure 2.11. Our pressure calculations and the results of Mauk et al. (2004), Kane et al. (1999) and Frank et al. (2002) are in reasonable agreement.

The thermal plasma pressure was measured with the PLS instrument over the range of

0.9 eV to 52 keV and the partial energetic particle pressure was calculated from 50 keV to 5 MeV. Mauk et al. (2004) estimated that the hot particle pressure dominates the thermal pressure closer to the planet. In the middle magnetosphere the ratio of the averaged thermal plasma and the partial energetic particle pressure (on the C9 orbit) is about unity which agrees with the result obtained by Mauk et al. (2004). In the Jupiter's magnetotail the ratio of the partial energetic particle pressure (on the C9 orbit) to the averaged thermal plasma pressure is about 0.5 which means that cold pressure is dominating.

An important parameter to characterize the plasma confinement is the plasma β, which is defined as the ratio of plasma to magnetic pressure

$$\beta = \frac{2\mu_0 P}{B^2}, \tag{2.7}$$

where μ_0 is magnetic permittivity. The estimations show that the plasma β in the Jovian magnetotail is high in the current sheet center (high plasma pressure and low magnetic filed) with $\beta \simeq 10$ and low in the lobe region (low plasma pressure and high magnetic filed) plasma with $\beta \simeq 0.01$, as expected.

In order to follow the evolution of the pressure balance between magnetic field and hot ion plasma it is necessary to consider the relation of the plasma pressure in the current sheet center to the magnetic pressure in the lobe region. Unfortunately current sheet encounters take place in average only every 5 hours. That gives some restrictions for the investigation of the plasma pressure dynamics. In contrast to the ion pressure the magnetic pressure can be determined rather reliably. The magnetic pressure is calculated when the spacecraft is located in the lobe region. Lobe encounters last usually around 4 hours, which is rather long compared to the current sheet crossings. The bottom panel in Figure 2.11 shows the calculated pressure balance. As expected, the average value is a bit lower than unity.

Regrettably, the thermal plasma pressure was impossible to include in the plasma pressure calculations due to inaccessibility of the data.

It would be very interesting to check the changing dynamics and relation between the plasma pressure perpendicular to the current sheet $P_\perp$ and the parallel plasma pressure $P_\parallel$ to investigate the triggering processes in the Jovian magnetosphere but unfortunately the statistics does not allow it.

In summary, the EPD measurements in the tail region are not fully sufficient to monitor the evolution of the ion pressure in the magnetotail, especially not in a quantitative manner. The conclusions that can be drawn on the plasma pressure estimations are therefore limited.

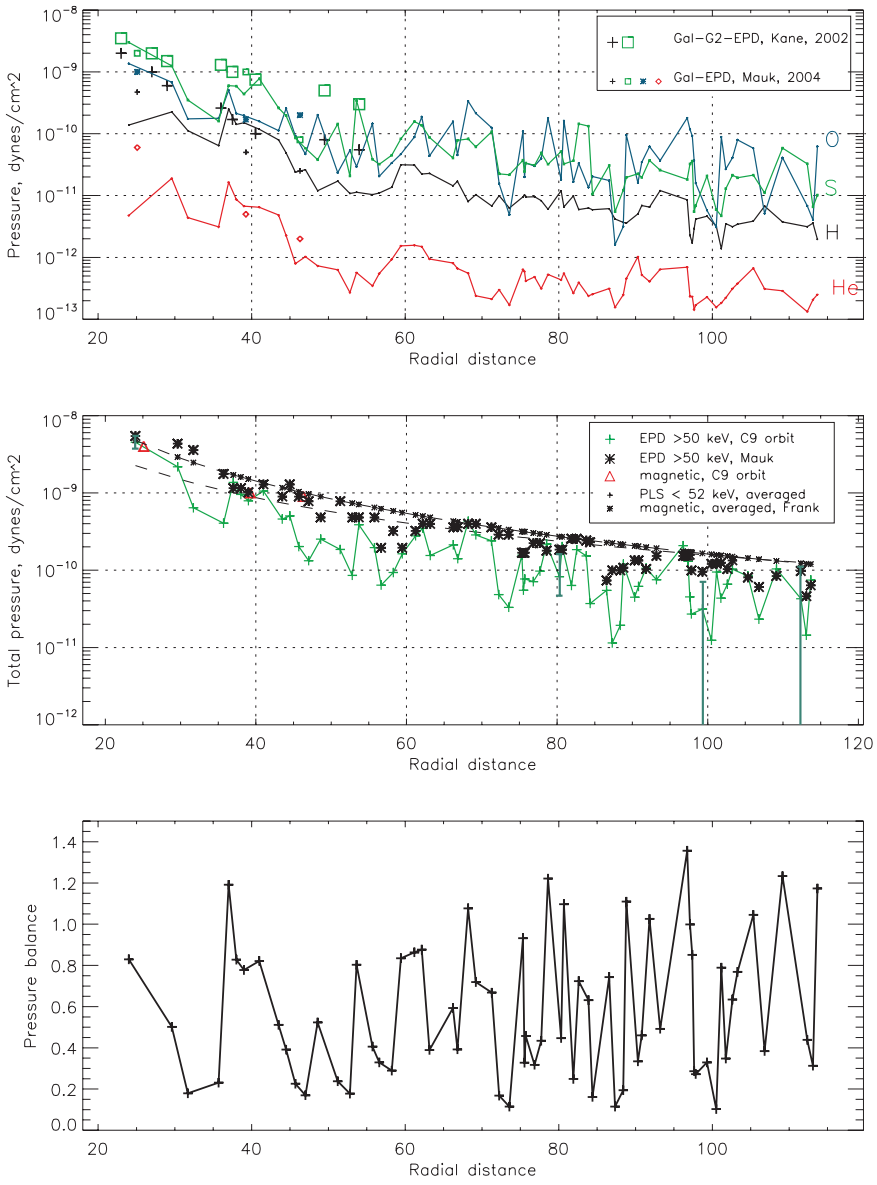

Figure 2.11: Comparison of the pressure estimations with the results obtained in previous studies to verify the method and its extension to the distant magnetotail. The time period from DOY 180 04:30 to 197 16:30 in 1997 is displayed. Top: The partial ion pressures (from 50 keV to 5 MeV) close to the current sheet center plotted as a function of radial distance for different ion species (O, S, H and He ions). The different symbols denote the results of Mauk et al. (2004) and Kane et al. (1999), for the individual species.
Middle: The sum of partial pressure for O, S, H and He versus radial distance presented by the green line with crosses. The statistical error of the EPD pressure is shown by the vertical thick green lines. The asterisk symbols present the magnetic pressure in the lobe regions which proceeded or followed the corresponding current sheet crossing. For comparison the variations of the thermal plasma pressure from the Galileo PLS instrument, obtained by Frank et al. (2002) and the magnetic pressure during DOY 1997 is shown. The total energetic ion pressure calculated by Mauk et al. (2004) is denoted by red triangles.
Bottom: The partial pressure balance as function of the radial distance.

3 Reconfiguration processes in the Jovian magnetosphere

To extend the knowledge about the dynamical processes in the Jovian magnetotail the EPD data set from Galileo orbits G2, E6, G7, G8, C9, C10 and E16 was scanned for the occurrence of particle flow burst events, i.e., intervals with significant deviation of the particle flow from the usual corotational direction. These events are the most prominent observable signature of substorm-like processes (Woch et al. 1999). From the set of flow burst events the 34 most prominent events were selected for further analysis.

The 34 periods with flow bursts are usually associated with considerable structural changes of the plasma sheet / current sheet, which indicate a general and global configuration change of the Jovian magnetotail. These events are referred as "reconfiguration events". The wobble of the Jovian magnetodisc provides the possibility for a latitudinal scan through the entire plasma sheet / lobe region twice each 10-hour rotations. Since a magnetotail reconfiguration process generally lasts for several planetary rotation (see below) it is possible to monitor the evolution of the plasma and magnetic field properties in all key regions of the magnetotail throughout the process.

Figure 3.1 shows the consequences of the magnetodisc wobbling for the observed energetic particles and the magnetic field. When Galileo encounters the current sheet we observe the highest ion intensities and the lowest magnetic field. During lobe encounters the inverse situation takes place: we observe a maximum in the magnetic field and a minimum in the ion intensities. The flat magnetodisc is well seen from the short duration of the current sheet crossings (~ 1) hour and by the long lobe encounters of ~ 4 hours. Figure 3.1 exemplifies the "background" quiet time variations observed by a spacecraft in the equatorial plane. The significant changes to this pattern introduced by the reconfiguration events will be discussed in the following sections.

3.1 Reconfiguration events – single event studies

To give an impression on properties common to the majority of reconfiguration events and also to show interesting signatures of individual events we will present 3 typical examples of reconfiguration events in the Jovian magnetotail.

3.1.1 Event I

Figure 3.2 shows data for the time interval of Galileo's orbit G7 from DOY 269, 05:00 to DOY 272, 05:00. Galileo was in the predawn sector of the magnetotail (02:30 LT) at

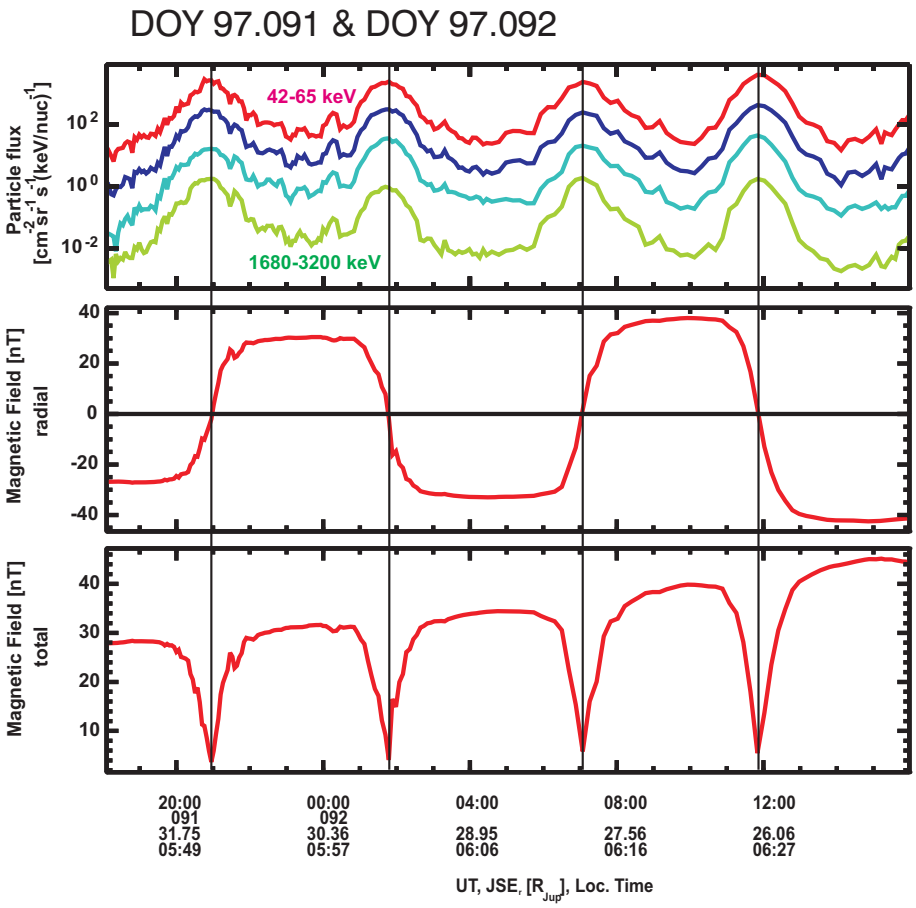

Figure 3.1: Omnidirectional ion intensities (42 - 3200 keV) (first panel); and the radial and total magnetic field component (second and third panel respectively) on Galileo orbit G7 from DOY 091, 18:00 to DOY 092, 16:00 in 1997. The plot illustrates the "quiet time" changes of the ion intensities and magnetic field data due to the periodical magnetodisc modulations with a period of ~ 10 hours.

around 103 R_J. The first panel shows omnidirectional ion intensities in 7 energy channels covering the energy range from 42 keV to 3.2 MeV. The second panel displays the radial and azimuthal components of the ion directional flow anisotropy. The next four panels show the magnetic field magnitude and its components in the SIII-system. The time resolution of the particle measurements is 11 min. The magnetic field is displayed with a time resolution of 24 s. The event was presented in Kronberg et al. (2005). The description below is following the one given in their paper.

Over the whole displayed interval the large amplitude periodic fluctuations in the magnitude of the magnetic field and its direction (primarily visible in the radial component) are observed. As discussed above these fluctuations are caused by the wobble of the flattened Jovian magnetosphere and its current sheet topology (Dessler 1983), see also Figure 3.1. Simultaneously, changes of the ion intensities are seen, with the largest intensities around the current sheet center and decreasing intensities when the spacecraft is moving towards the lobe region.

At the beginning of the displayed interval from 05:00 UT on day 269 up to 09:00 UT on day 270 the ion intensities vary gradually in response to the changing relative position of the spacecraft and plasma sheet center imposed by the planetary rotation. No distinct plasma sheet / lobe boundaries are encountered. During the first two rotations Galileo is south of the plasma sheet center with the exception of a brief dip through the current sheet at 10:00 on day 269, as evidenced by the polarity change of the radial magnetic field component. Thus the plasma sheet is displaced northward from its nominal position. Except for times of close proximity to the current sheet the magnetic field shows a persistent and significant southward tilt. The azimuthal component of the ion directional flow anisotropy is dominating throughout this interval. It indicates that the plasma flow can be estimated to be in the corotational direction. The average flow speed is about 300 km s^{-1}. The magnetic field is consistently in the expected swept-back[1] orientation (anticorrelation between azimuthal and radial component).

This initial phase can be characterized in many aspects as a quiet, undisturbed period, with a plasma sheet being in a stable configuration. The lack of plasma heating, particle beams or flow bursts, and transient magnetic field distortions support this view. The plasma sheet is possibly also rather extended in latitude with a magnetic field showing a significant southward tilt i.e., a residual dipole component.

Possibly triggered by a change of the relative position of Galileo with respect to the current sheet, the spacecraft crosses the current sheet at around 04:00 UT on day 270, and Galileo is for the first time substantially above the current sheet engulfed in the northern plasma sheet. During this period the azimuthal flow anisotropy component rises gradually, indicating faster corotational flows and at the current sheet encounters an increase in the particle intensity is seen to values higher than those seen before. At about 07:30 UT magnetic field oscillations are observed (see Figure 3.3 in detail). Shortly after these oscillations, the plasma sheet transits abruptly from a "quiet" into a disturbed state. The corotational flow breaks down. Instead, a large radial flow anisotropy component is observed together with a component in anti-corotational direction. The plasma is now streaming tailward. Simultaneously, ion intensities rise significantly. Right at the onset of the tailward streaming, the magnetic field, which has been primarily current sheet-like before, with a dominant radial and a small southward component, now shows short spike-like intensity increases by several nT, above values seen during the adjacent lobe encounters. The increases are primarily due to a significant bipolar excursion of the south-north component which indicates that the magnetic field is strongly tilted in the meridional plane for short periods of time. For about 20 min before the onset of the strong northward turn the magnetic field is in a swept-forward configuration, see Figure 3.3, since the azimuthal and radial component show the same polarities (Dougherty et al. 1993). This period shows all characteristic signatures of a plasmoid. From this time onwards, also a different topology of the plasma sheet is observed.

Instead of ion intensities gradually decreasing towards higher latitudes now distinct boundary layers between the plasma sheet and the lobes have developed. The core plasma sheet appears to be thin and strongly collimated at the current sheet position. The boundary layers consist of high intensity beams of tailward streaming ions and electrons. Whereas during the "quiet" time interval, ion intensities have peaked at the current sheet center,

[1] See explanation in Section 1.1.2

highest intensities are now observed in the boundary layers (see bursts labelled D1, D2, and D3).

Until 20:00 UT on day 270 the strong tailward anisotropy (flow) persists. During this period a further spike in the magnetic field intensity is seen. This time the spike is primarily produced by a substantial component in the northward direction. During the spike the magnetic field becomes swept forward out of the meridian plane.

Between 20:00 and 22:00 UT on day 270 the particle flow anisotropy has reversed its direction. A large radial inward component with a significant corotational component is observed during the subsequent plasma sheet crossings, which indicates a sunward moving plasma. The first plasma sheet crossing with inward motion shows the highest particle intensities encountered during the whole event and the strongest confinement of the plasma at the current sheet center (D4). At the subsequent crossings the plasma sheet widens and distinct boundary layers with inward streaming particle beams again become discernible (burst D5).

Around 17:00 on day 271, the plasma sheet has returned to its "quiet" topology. The ion intensity has dropped, the sheet has widened in latitude and the flow is back in corotational direction.

Figure 3.4 combines ion intensities and observations of the Galileo PWS experiment previously published by Louarn et al. (1998). It shows that the disturbed time interval is associated with the onset and intensification of broad kilometric emissions (bKOM). Intensifications of bKOM emissions are usually attributed to the onset of auroral activity (Ladreiter et al. 1994). It strongly indicates that the observed disturbances of the magnetic field and plasma population is not localized but part of a global process.

A striking feature of the presented time interval is that the magnetic field intensity measured in the lobe remains approximately constant throughout the event, in particular during the time period preceding the disturbance. From the "quiet" to the disturbed and back to the "quiet" condition the magnetic field remains approximately at the same level. In contrast, the ion intensities exhibit an increase shortly before the disturbed interval.

The last panel of Figure 3.2 shows for completeness the magnetic pressure and the partial pressure due to ions above 50 keV (in red). The magnetic pressure measured in the lobe regions remain roughly constant throughout the event. The values of the partial pressure in the current sheet center are denoted by asterisks. In this case during "quiet" period only three data points monitor the evolution of the plasma pressure and this is insufficient to make conclusions. However, there is an indication for a significant increase of the plasma pressure just prior to the onset of the disturbances. In the disturbed phase itself, the plasma pressure could not be calculated with the procedure described in Section 2.7.3. Due to the appearance of intense beams and strong temporal variations it is impossible to fit the ion population with the help of a kappa distribution.

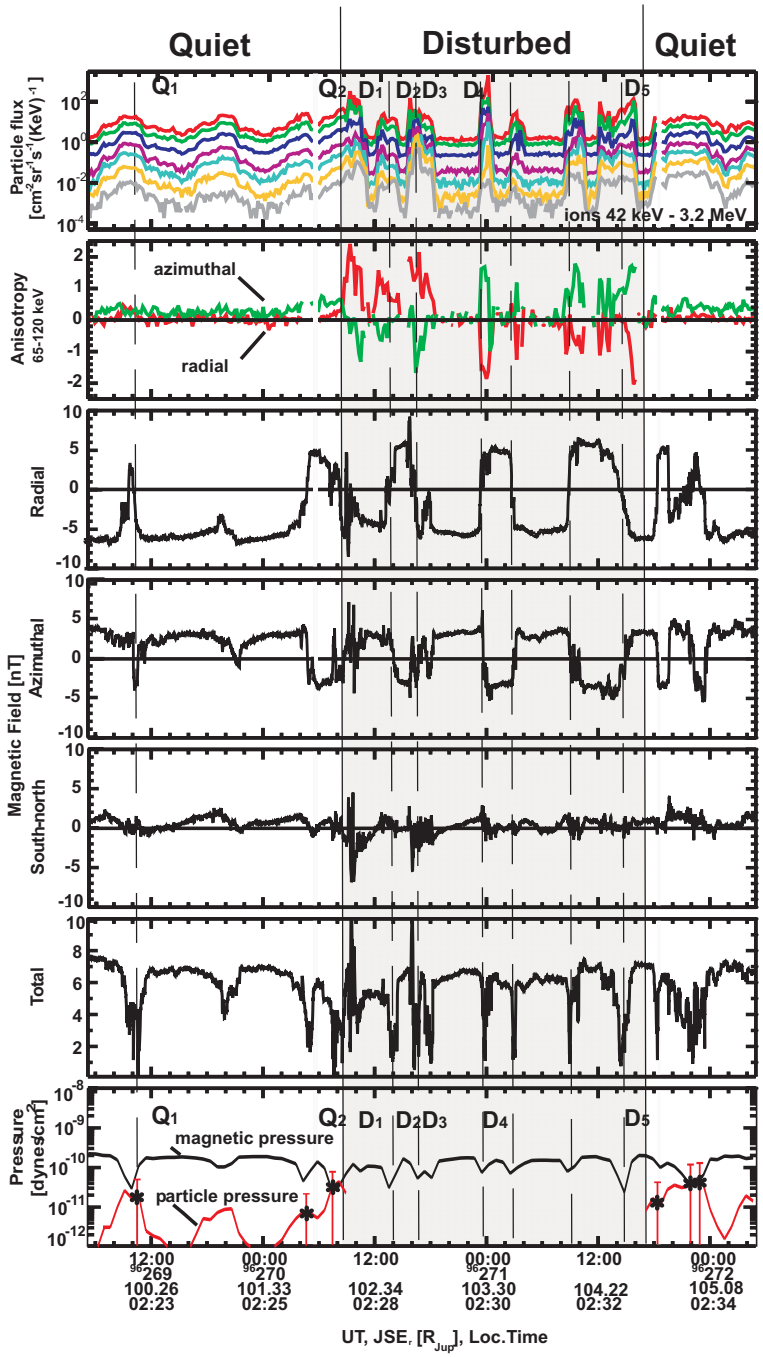

Figure 3.2: Energetic particle and magnetic field observations on Galileo orbit G2 from DOY 269, 05:00 to DOY 272, 05:00 in 1996. From top to bottom are displayed: omni-directional ion intensities (0.042-3.2 MeV) (first panel); first order ion anisotropies in the radial (positive is outward) and corotational direction (second panel); the magnetic field components (third to fifth panels) in SIII coordinates (the radial component is positive in the outward direction, the azimuthal component positive in the direction of Jupiter's rotation, the south-north component positive southward) and its magnitude (sixth panel); the partial ion pressure (from 50 keV to 5 MeV) (red lines) and the magnetic pressure (black line) (seventh panel); continuous vertical lines outline "quiet" and disturbed periods, dashed lines labelled Q and D refer to some representative current sheet crossings.

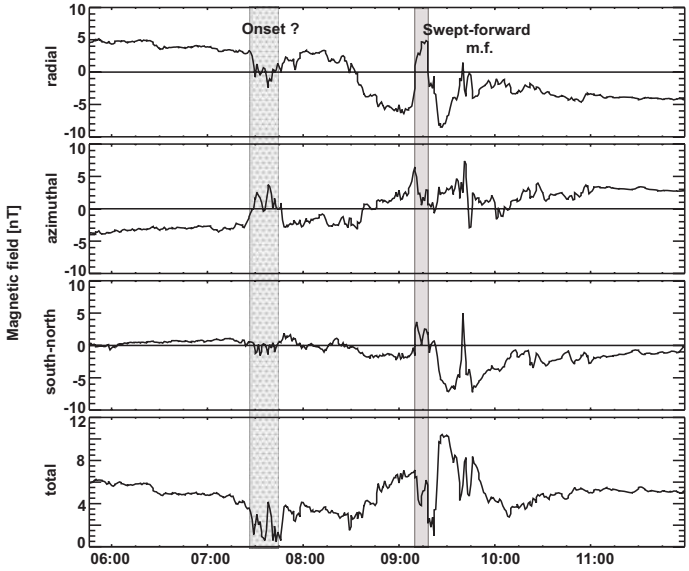

Figure 3.3: The magnetic field variations for the time period DOY 270 05:45 to DOY 270 12:00 in 1996. The first grey-shaded area marks the magnetic field oscillations which can be associated with the onset of the reconfiguration event, the second corresponds to the swept forward magnetic field configuration.

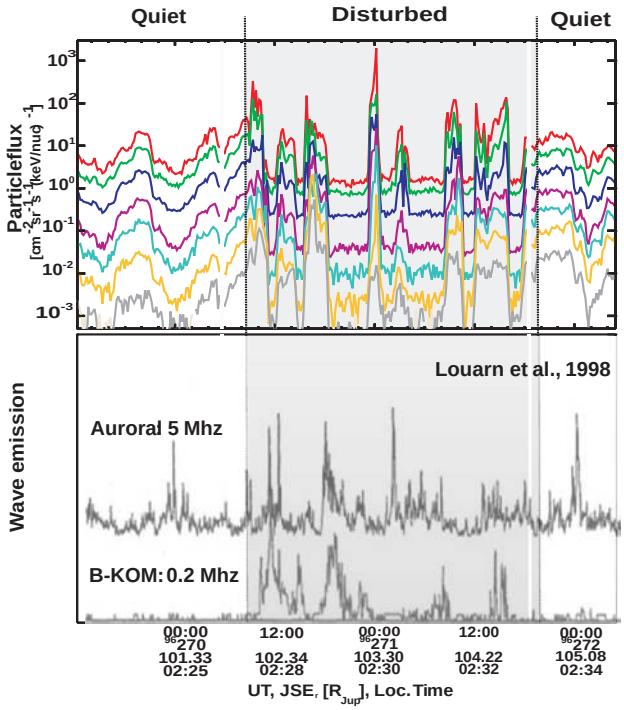

Figure 3.4: Ion intensities and auroral radio emission from Louarn et al. (1998) for the same time period as in Figure 1 (DOY 269, 12:00 to DOY 272, 05:00 in 1996).

3.1.2 Event II

In contrast to the previous event with a constant magnetic field intensity Figure 3.5 shows the most prominent example of a reconfiguration event with a magnetic pressure increase. During this event Galileo was in the tail region at roughly $95R_J$, in the predawn sector (02:00 LT). Figure 3.5 covers 4 days of observations from day 159 to day 163 in 1997.

Before day 159, 21:00 UT the magnetic field and the energetic particle population show regular variations imposed by the planet rotation. The magnetic field strength in the lobe regions is moderate and at a level usually seen at these distances. The plasma flow is in the corotational direction, as shown by the dominant azimuthal component of the ion anisotropy. The north-south component of the magnetic field is small and consistently southward as expected for an undisturbed Jovian magnetic field topology. The corotational flow velocity is about 300 to 500 km s^{-1}. All these observations suggest that the Jovian magnetotail is in a quiet, undisturbed state.

This situation changes after 21:00 on day 159. At the next lobe encounter the total magnetic field has increased by a factor of 1.5 and remains enhanced during the next lobe encounters. Likewise, there is an indication for a stronger confinement of the plasma sheet. However, there are no significant disturbances of the current sheet topology and the flow remains corotational. It takes about 20 hours to 20:00 on day 160 until clear indications for a disturbed state of the magnetotail are observed. The azimuthal component of the magnetic field starts to exhibit pronounced fluctuations. The magnetic field changes from an, in average, southward orientation to a slightly northward direction. At 00:00 UT on day 161 the breakdown of corotation and the first ion burst flow event is observed. Right in the center of the current sheet an ion intensity enhancement is seen simultaneously with a strong increase of the ion anisotropy in the radial outward direction, exceeding the co-rotational anisotropy by far.

The particle event is associated with bipolar fluctuations of the azimuthal and north-south components of the magnetic field. A second, less pronounced, particle flow burst event is seen at the following crossing, a third one at the crossing thereafter.

The latter is the most pronounced one in terms of ion intensity and radial anisotropy. It again has a radial outward direction, but the azimuthal component is in anticorotational direction, which indicates a tailward flow. At the same time a bipolar change of the north-south component of the magnetic field is seen. The ion intensities reach their highest values for the displayed interval. The particle burst has clear bulk flow properties in the sense that different species (protons, oxygen and sulfur) have the same velocity of up to 1800 km s^{-1}. These velocities exceed the rigid corotation velocity of 1200 km s^{-1}. A detailed view is presented in Figure 3.6. The ion intensities exhibit a sharp boundary towards the lobe and the strong confinement around the current sheet, indicating a thin plasma sheet. After the intense outward flow burst the magnetic field intensity in the lobe has dropped significantly to a level even below that of the undisturbed time period.

A fourth ion burst event is seen during the next plasma sheet encounter right at the northern lobe boundary. This time the burst is directed towards Jupiter. Following this last burst event the plasma flow is returning to the corotational direction. No further anisotropies or magnetic field disturbances are observed. The ion intensities return to the predisturbed level.

This event displays many significant features similar to terrestrial substorms. The

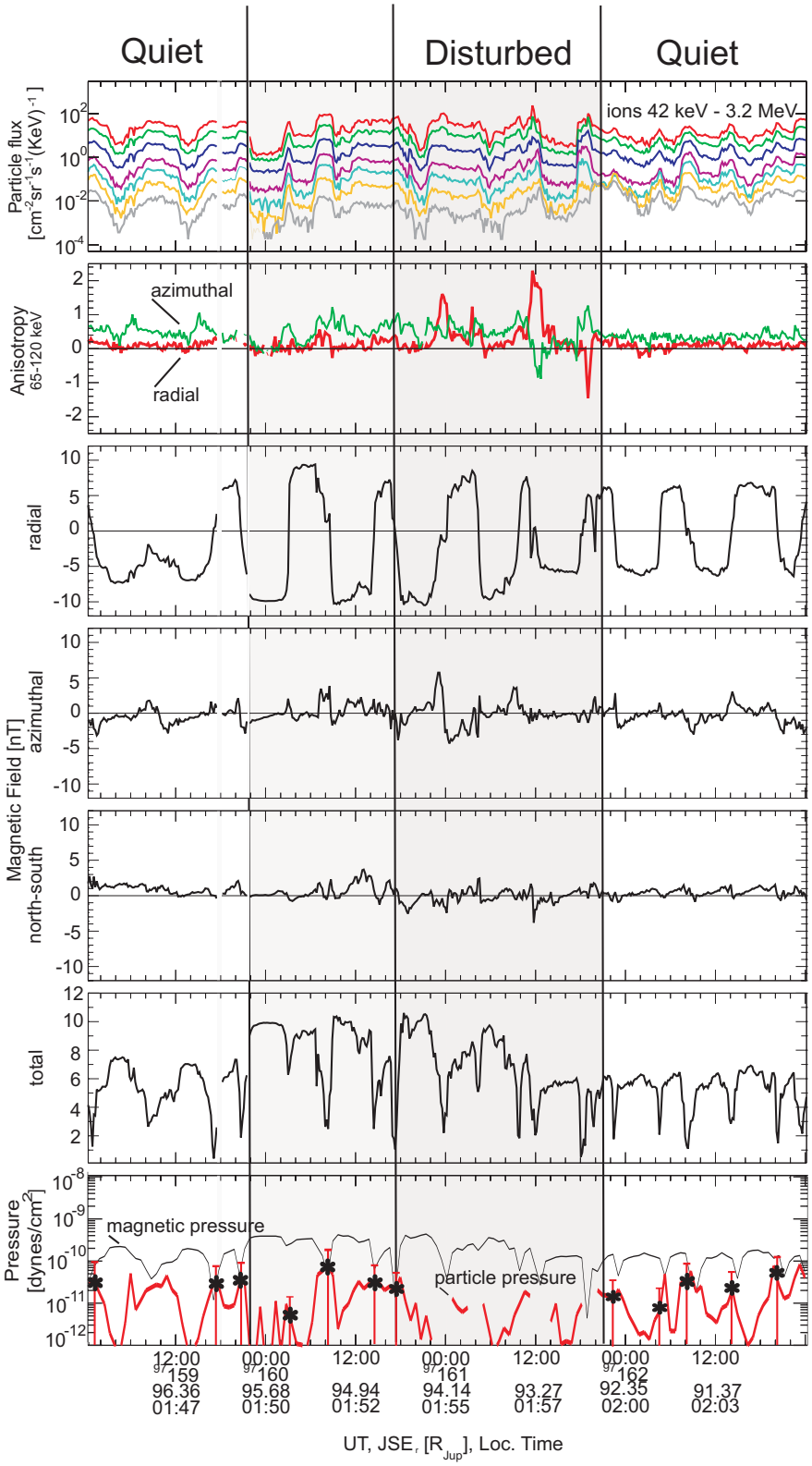

Figure 3.5: Same as Figure 3.2 but for the time interval DOY 159 to DOY 163 in 1997 on Galileo orbit G8.

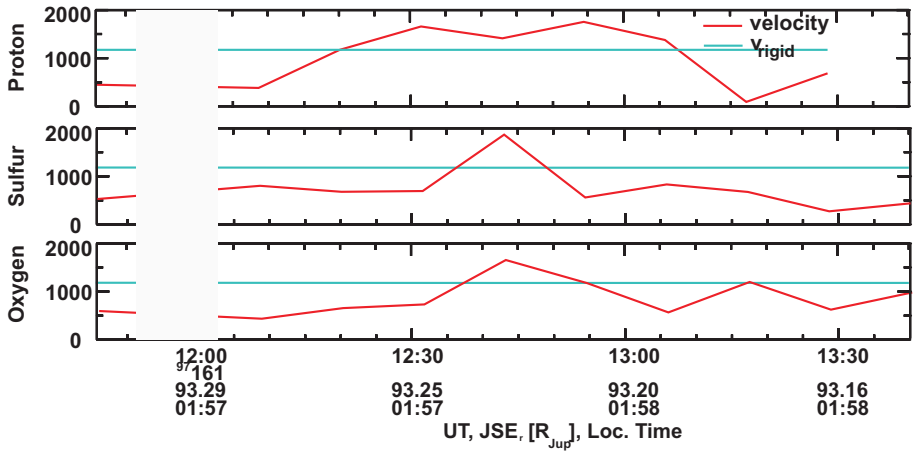

Figure 3.6: Flow velocities of the protons (top), sulfur (middle) and oxygen (bottom) for the time period DOY 161 11:45 to DOY 161 13:40 in 1997.

magnetic pressure increase preceding the disturbance might indicate that this event is solar wind driven.

The ion pressure in the current sheet crossings (denoted by asterisks in Figure 3.5) does not show a clear variation. Significant increase of the magnetic pressure does not correspond to the similar increase in the plasma pressure.

3.1.3 Event III

Another example for a substorm-like event is shown in Figure 3.7. During this event Galileo was in the tail region at roughly 112 R_J, in the predawn sector (03:10 LT). Figure 3.7 covers almost 3 days of observations from day 279 12:00 to day 282 07:00 of 1996. It exhibits the key features of the reconfiguration event, i. e. a change of the plasma flow direction and in the magnetic field topology. The particle flux evolution indicates the formation of a thin plasma sheet. The azimuthal component of the ion anisotropy shows a gradual increase during the "quiet" time period. This is followed by the breakdown of the corotational flow direction to a radially outward flow. Thereafter, the flow changes its direction from radially outward to radially inward. Bipolar fluctuations superimposed on a persistent northward tilt are observed in the south-north magnetic field component. The main reason for presenting this event is the possibility to observe the gradual increase of the plasma pressure in the center of the current sheet together with an increase of the magnetic pressure in the lobe region preceding the disturbance.

All presented cases are different in terms of the evolution of the magnetic pressure as far as possible to resolve the hot plasma pressure.

Summarizing this section it is concluded that the reconfiguration events are very similar to substorms at Earth. It is hard to derive which mechanism drives such reconfiguration events in the Jovian magnetosphere out of three examples. In order to get more insights in these processes a statistical study will be carried out.

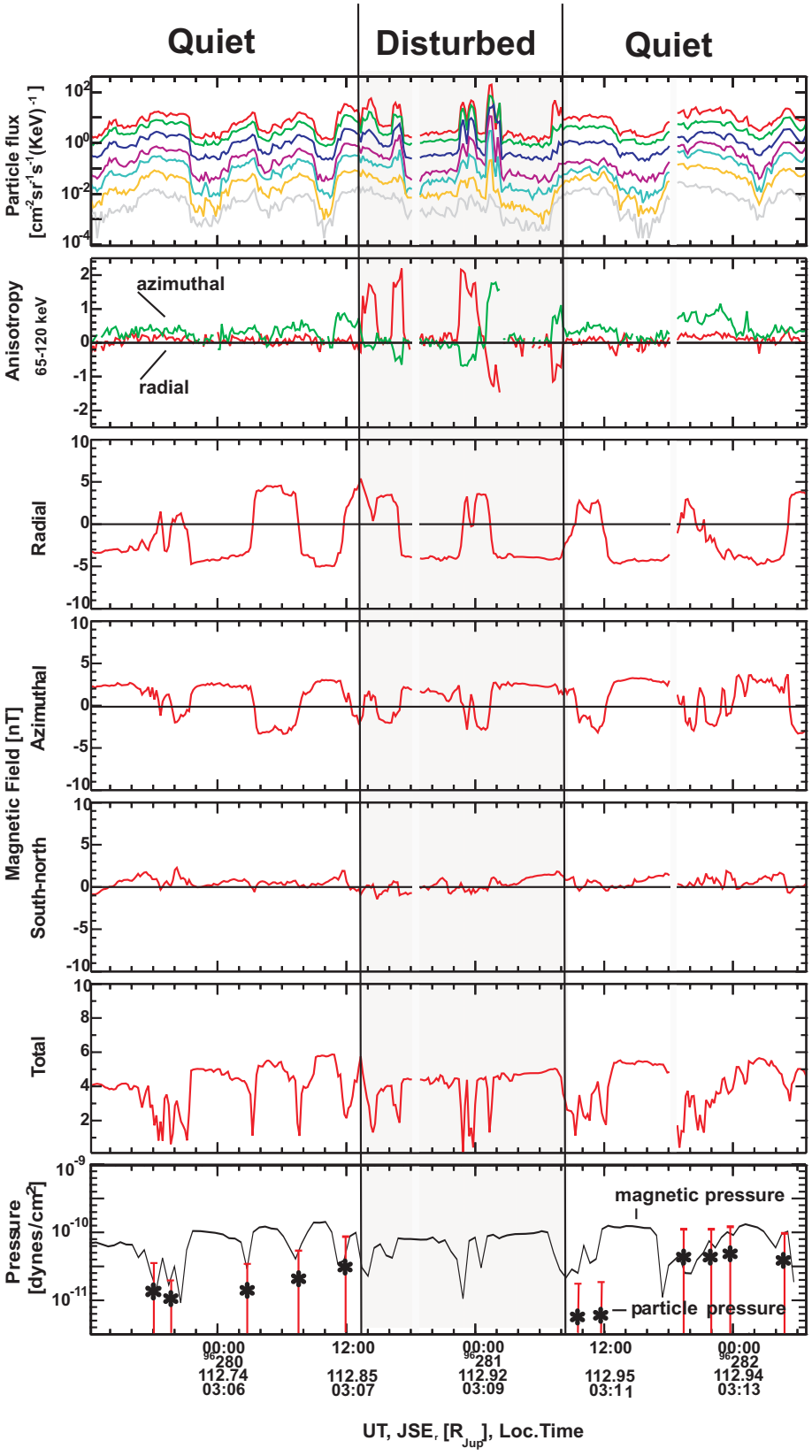

Figure 3.7: Same as Figure 1 but for the time interval DOY 279 12:00 to DOY 282 07:00 in 1996 on Galileo orbit G2.

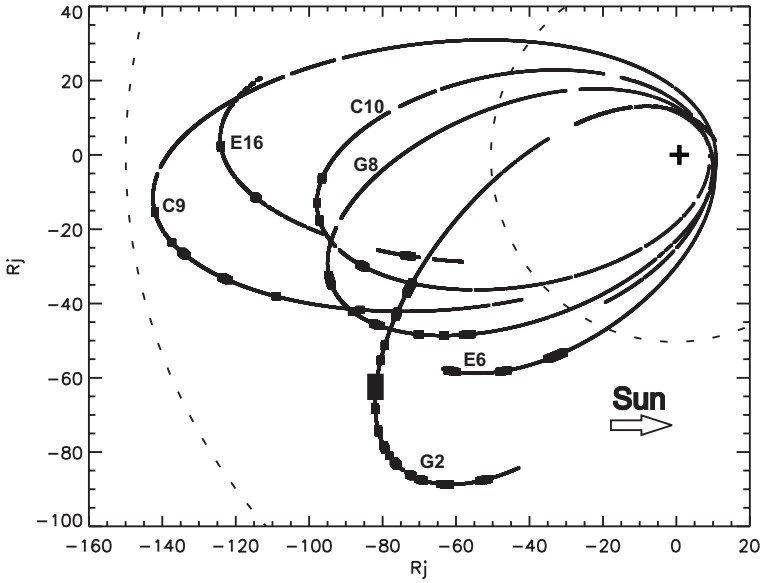

Figure 3.8: The G2, E6, G8, C9, C10 and E16 orbits of Galileo in Jupiter Solar Ecliptic coordinates. The locations of the detected reconfiguration events are marked by black signs.

3.2 Reconfiguration Events – statistical study

Overall 34 clear cases of reconfiguration events were identified in the data base used for this study. 3 characteristic examples of which were presented in the previous section. The events generally show a complex sequence of radially outward and inward bursts, associated with increasing particle intensity, thinning of the plasma sheet, bipolar fluctuations of the south-north magnetic field and a distortion of the azimuthal magnetic field. Some of the characteristic properties of the events (orbit, date, radial distance, local time, duration, flow direction and change of the total magnetic field at the pre-substorm phase in respect to the field of the corresponding preceding "quiet" period of the magnetotail) are summarized in Table 3.1. Figure 3.8 presents a map of the location of the 34 events. The reconfiguration events are mostly seen in the sector from midnight to dawn consistent with the location of the statistical x-line derived by Woch et al. (2002). This region is favored for the occurrence of reconfiguration events also in the Vasyliūnas model (see Section 1.1.4) due to the relatively thin plasma sheet.

In analogy to the "classical" terrestrial substorm (a solar wind driven process) it would be expected to observe a substantial increase of the magnetic flux in the magnetotail before the onset of substorm-like processes (Cheng 2004). In the case of an internally driven process this is not necessary.

Thus, of specific importance with respect to the physical processes behind the reconfiguration events is the behavior of the magnetic field. Out of the 34 selected reconfiguration events 15 events show no increase of the magnetic field intensity, some of them even a decrease. For one event which is included in this group it is hard to derive a value of the magnetic field change, but it will be in the range of less than 10%. For these events the magnetic field intensity stays essentially constant in the period prior to the disturbance

onset. An increase in the order of 1 nT to 2 nT (corresponding to a 10 to 20 % increase) was observed for 14 events. This increase was for the majority of events limited in time, essentially just affecting the last lobe encounter (or a fraction of it) before the disturbance onset. Such magnetic field increases are often associated with an increase of the plasma pressure in the plasma sheet during plasmoid formation. The gradual increase of the radial magnetic field component can be also associated with the stretching of the current sheet during the mass-loading process (see details below).

Only a small number of events, about 5 out of 34, show a distinctively different behavior of the magnetic field, namely a substantial, long-lasting increase of the magnetic field in the lobe regions prior to the disturbed time periods, (e. g. event II as discussed in Section 3.1.2).

If the reconfiguration events are internally driven it is expected to observe signs of the periodical mass-loading and mass release process.

An increase of the plasma pressure (especially the parallel component) in the pre-reconfiguration process period could be a possible signature of the stretching of mass-loaded flux tubes by the centrifugal force. The stretching of magnetic flux tubes can identified by meridional magnetic field component (see Section 4) and/or as was mention before, by an increase of the radial magnetic field component. These signatures are actually very similar to the signatures observed during the growth phase of a terrestrial substorms.

The investigation of the ion pressure evolution during the predisturbed phase were attempted for the 15 most promising events. However, it is essentially impossible to draw definitive conclusions regarding to the evolution of the plasma pressure based on the EPD data set due to the big statistical error for the plasma pressure in the distant magnetotail.

In order to show that the reconfiguration events are global disturbances, the time intervals of these events (as presented in Table 3.1) were compared with the time periods of the auroral intensity increases from Louarn et al. (2000)[2]. About 73 % of the reconfiguration events from the G2, G7 and G8 orbits coincide with enhancements in the flux of the various auroral radio emissions.

Thus, the statistical study of the Jovian reconfiguration events exemplifies that they are global disturbances which are very similar to terrestrial substorms. The difference is the absence of the substantial magnetic flux increase in the magnetotail before the onset of substorm-like process. Instead the observed slight increases in the magnetic field can be associated with an increase of the plasma pressure.

[2] See Section 1.1.4 in detail

Table 3.1: Reconfiguration / substorm-like events and their properties.

Orbit	Time interval, UT	Radial distance R_J	Local Time	Duration Hours	Direction i-inward, o-outward[1]	Increase/ Decrease, B_{tot}[2],%
G2	1996 26213-26308	79	01:40	19	i	0
G2	1996 2641230-2642230	88	01:58	10	o	30
G2	1996 26700 -26704	94	02:10	4	o	5
G2	1996 26807 -26810	97	02:17	3	o	-25
G2	1996 27008 -27117	103	02:30	33	oi	0
G2	1996 2721930-2730430	100	02:38	9	oi	15
G2	1996 27510 -27600	110	02:50	14	oi	-15
G2	1996 27716 -27812	112	03:00	20	o	10
G2	1996 27908 -27912	112	03:05	4	o	0
G2	1996 28012 -28108	113	03:09	20	oi	20
G2	1996 28312 -28403	112	03:30	15	o	-20
G2	1996 28500 -28518	111	03:28	18	oi	15
G2	1996 28800 -28904	109	03:40	28	oi	20
G2	1996 29208 -29306	101	03:57	20	oi	?[3]
E6	1997 07815 -07915	84	02:55	24	oi	0
E6	1997 08300 -08314	76	03:20	14	i	10
E6	1997 08601 -0862330	63	04:00	22.5	i	20
G8	1997 15207 -15322	100	01:20	39	oi	20
G8	1997 15804 -15809	97.5	01:43	5	o	20
G8	1997 16022 -16118	94	01:55	20	oi	50
G8	1997 16500 -16505	85.5	02:17	5	o	25
G8	1997 16620 -1662330	79.5	02:30	3.5	o	15
G8	1997 1680130-1681430	75	02:40	13	oi	5
C9	1997 22200 -2220730	142	00:23	7.5	o	5?
C9	1997 22808 -22812	139	00:39	4	o	10
C9	1997 23011 -23110	136	00:45	23	i	15?
C9	1997 23621 -23709	127	01:00	12	io	0?
C10	1997 28120 -28204	95	00:16	8	oi	10
C10	1997 28504 -28508	96	00:30	4	oi	25
C10	1997 28711 -28721	98	00:40	10	oi	5
C10	1997 29417 -29510	90	01:15	17	oi	25
E16	1998 23708 -2371830	124	23:00	10.5	oi	-10
E16	1998 24613 -24702	116	00:22	13	o	-20
E16	1998 25907 -2591630	78	01:20	9.5	oi	20

[1]Prime direction of the burst events relative to the planet (o: outward, i: inward).

[2]The increase of the total magnetic field at the pre-substorm phase is given with respect to the field of the corresponding preceding "quiet" period of the magnetotail.

[3]In this case it was hard to define the change of the magnetic field.

3.3 Quasi-periodicity of the Jovian reconfiguration events

Studies regarding the periodic behavior of different quantities in the Jovian magnetosphere on time scale of days were reviewed in Section 1.1.4.

To exemplify the periodical 2 to 3 day (i.e. 5 to 7 Jovian day) modulations in the Jovian magnetosphere a segment of orbit G2 in the distant predawn magnetotail is presented in Figure 3.9. It shows one of the clearest periodicities of the ion flow anisotropy (Woch et al. 1998, Krupp et al. 1998), the associated distortions of the south-north magnetic field component (Kronberg et al. 2005) and the auroral emissions together with the plasma sheet modulations (PWS data Louarn et al. 1998).

Figure 3.9 presents the azimuthal and radial components of the ion directional flow anisotropy (top panel); the south-north component of the magnetic field in high temporal resolution (second panel); and a highly smoothed time series (third panel); the average radial magnetic field values in the lobe regions (fourth panel); and a compressed view of wave spectra recorded every 36.7 s (152 frequency channels ranging from 5.6 Hz to 5.6 MHz, bottom panel). Above 500 kHz, the spectra show detected emissions of auroral origin. Between 500 kHz and 50 kHz, two kinds of radiation are observed: the b-KOM of auroral origin (Ladreiter et al. 1994) and the n-KOM characterized by a 10 hour recurrence. The n-KOM originates from a few distinct sources which corotate in the outermost part of the Io torus (Reiner et al. 1993). Below 10 kHz the continuum radiation is detected. The presence of this emission is discovered almost everywhere in the magnetospheric cavity (Louarn et al. 2000). It shows a very clear low-frequency cut-off close to the plasma frequency. This will be used to estimate the local plasma frequency. The 5-hour modulation of the continuum radiation is due to wobbling of the magnetodisc and indicates that the spacecraft regularly crosses the plasma sheet. The time interval from day 265 12:00 to day 280, 00:00 is displayed.

A pronounced 2 to 3 day modulation of the anisotropy and its magnitude is seen, indicating alternating times of corotational flow and outward/inward flow. Times of outward/inward flow are generally associated with transient bipolar south-north magnetic field distortions. The smoothed time series clearly shows quasi-periodic oscillations of the magnetotail magnetic field. The magnetic field changes its polarity from southward to northward just before the onset of the burst events. Then, after the disturbed period, the magnetic field gradually returns to a southward configuration and continues to increase until the next flow direction change. These magnetic field changes imply a change of the current sheet/plasma sheet topology from a thin postplasmoid type configuration to a "dipolarized" thicker structure (plasmoid-like). Magnetic field line reconnection occurs from the center of the forming plasmoid structure toward the planet and leads to mass release (see G2 orbit in Figure 3.12). The radial component of the magnetic field does not show any clear periodical modulations, in particular no substantial increases in predisturbed time periods. Slight decreases of the radial magnetic field component are seen during disturbed phases. The whole time interval can be divided in "quiet" phases ($\sim$ 2 days) associated with mass-loading of the Jovian magnetotail and disturbed phases ($\sim$ 1 day) which imply reconnection, the disruption of the tail and mass release (Kronberg

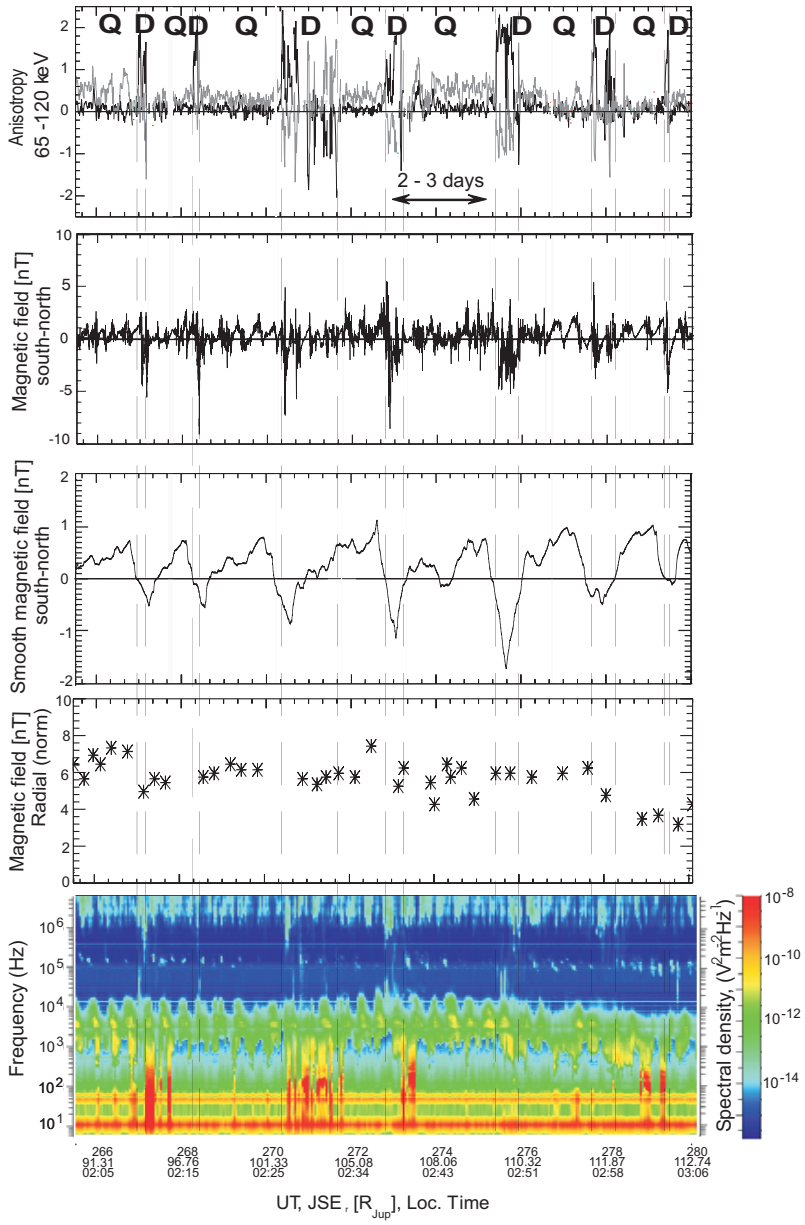

Figure 3.9: First order anisotropies in the radial (black, positive is outward) and corotational direction (gray) (first panel); the south-north component of the magnetic field (high-resolution: second panel; smoothed: third panel); the average absolute radial magnetic field values in the lobe regions (fourth panel); a time-frequency spectrogram from PWS observations: The observations have been taken in the time interval DOY 265, 12:00 to DOY 280, 00:00 in 1996 (Galileo orbit G2). The magnetic field data are presented in the SIII-coordinate system. Dashed vertical lines outline "quiet" and disturbed periods.

et al. 2005).

The intensification of the auroral radio emissions and the b-KOM activity together with the thinning of the plasma sheet (identified by the intensification of the continuum radiation) are clearly associated with ion bursts and bipolar fluctuations in the south-north

magnetic field.

Another example of periodic modulations in the Jovian magnetosphere is presented in Figure 3.10, as a segment of orbit E16. In this example Galileo was located in the distant midnight magnetotail in contrast to the close dawn region in the first example (see Figure 3.9). Usually in the distant midnight magnetotail region the particle burst events are not well developed, as shown in the statistical study of Woch et al. (2002). The plasma sheet is probably thicker in this region and reconnection occurrence is different from the dawn region. But even in this region one can observe periodic changes of the magnetotail topology with a repetition period of around 3 days. In this time period the spacecraft was located planetward to the region of the statistical neutral line formation derived by Woch et al. (2002). It is close to the local time sector where the x-line can be expected to develop according to the Vasyliūnas model, whereas the previous example was observed at a local time at which the plasmoid formation process is developing.

This example allows to follow the change of the current sheet morphology. As in the previous example the time period is divided in "quiet" phases and "disturbed" phases (Kronberg et al. 2005). The top panel presents the ion flow anisotropy (radial and azimuthal components) which shows recurrent disruptions of the ambient particle flow in the corotational direction by radially outward/inward flow bursts. The second panel shows the absolute value of the radial magnetic field component. To better visualize the evolution of the radial magnetic field component in the lobe regions maximum B_r data points are connected by a black line. The radial magnetic field component in the lobe regions exhibits pronounced increases during "quiet" periods. At the same time periods the south-north magnetic field component (third panel) shows an overall decrease. Such a behavior of the radial and the meridional magnetic field components is consistent with a gradual stretching of the plasma sheet configuration. The fourth panel presents the energy spectral index γ for sulfur. The spectra gradual softening (increasing γ) within 2 days followed by an abrupt hardening (decreasing γ) within 1 day. The increase of the spectral index is associated with the thinning of the plasma sheet. This will be considered in more detail in Section 3.3.3. The spectral periodicity is most obvious in the variation of the spectral index of sulfur (inner source). These type of ion spectral index variations are typical for the middle magnetosphere and the distant dusk to midnight tail region. The modulations can be explained by topological changes of the Jovian magnetosphere (Woch et al. 1998). The fifth panel shows the ratio of the south-north component of the magnetic field to the absolute value of the radial component. In order to calculate the ratio, values of the south-north magnetic field component closest to the current sheet center and the values of the radial magnetic field component in the lobe region were taken. These values and the corresponding ratio are presented in Table 3.3. Clear decreases of these ratios corresponds to a stretching of the magnetic field during "quiet" periods. To the end of the "quiet" periods the magnetic field is distended to such a degree that the condition for an onset of the tearing mode instability is satisfied. According to Zimbardo (1993) the threshold for the tearing mode instability is ($B_\theta/B_r = 0.025$). This value is denoted by a red line in Figure 3.10.

Table 3.2: The evolution of the magnetic field values during the "quiet" phases of the reconfiguration events during orbit E16. The absolute value of the radial magnetic field component in the lobe region and the south-north component in the current sheet center as well as the ratio of these are given.

Time, UT	$\|B_r\|$, (lobe), nT	B_θ (csc), nT	B_θ/B_r
1998 235 14:44	3.01		
1998 235 21:13		0.22	0.07
1998 236 00:04	3.92		
1998 236 06:55		0.11	0.028
1998 236 09:35	4.35		
1998 236 12:27		0.15	0.034
1998 236 19:25	4.35		
1998 236 22:28		0.04	0.0091
1998 239 01:24	3.39		
1998 239 02:09		1	0.29
1998 239 04:15	3.44		
1998 239 05:35		1.18	0.34
1998 239 08:04	3.81		
1998 239 10:32		1.22	0.32
1998 239 14:21		0.57	
1998 239 18:23	3.85		0.14
1998 240 04:04	4.78		
1998 240 08:26		0.15	0.031
1998 242 04:15	4.72		
1998 242 06:44		0.66	0.139
1998 242 23:06	5.5		
1998 243 01:46		0.068	0.012
1998 244 19:23	3.89		
1998 244 22:03		0.82	0.21
1998 245 05:40	5.39		
1998 245 10:03		1.22	0.22
1998 245 14:37	5.29		
1998 245 17:17		0.07	0.013
1998 247 04:43	3.4		
1998 247 09:06		0.61	0.17
1998 248 00:24	3.52		
1998 248 03:27		0.16	0.045
1998 248 12:48		0.09	
1998 248 15:06	4.81		0.018
1998 248 20:14	4.03		
1998 249 00:03		0.042	0.01

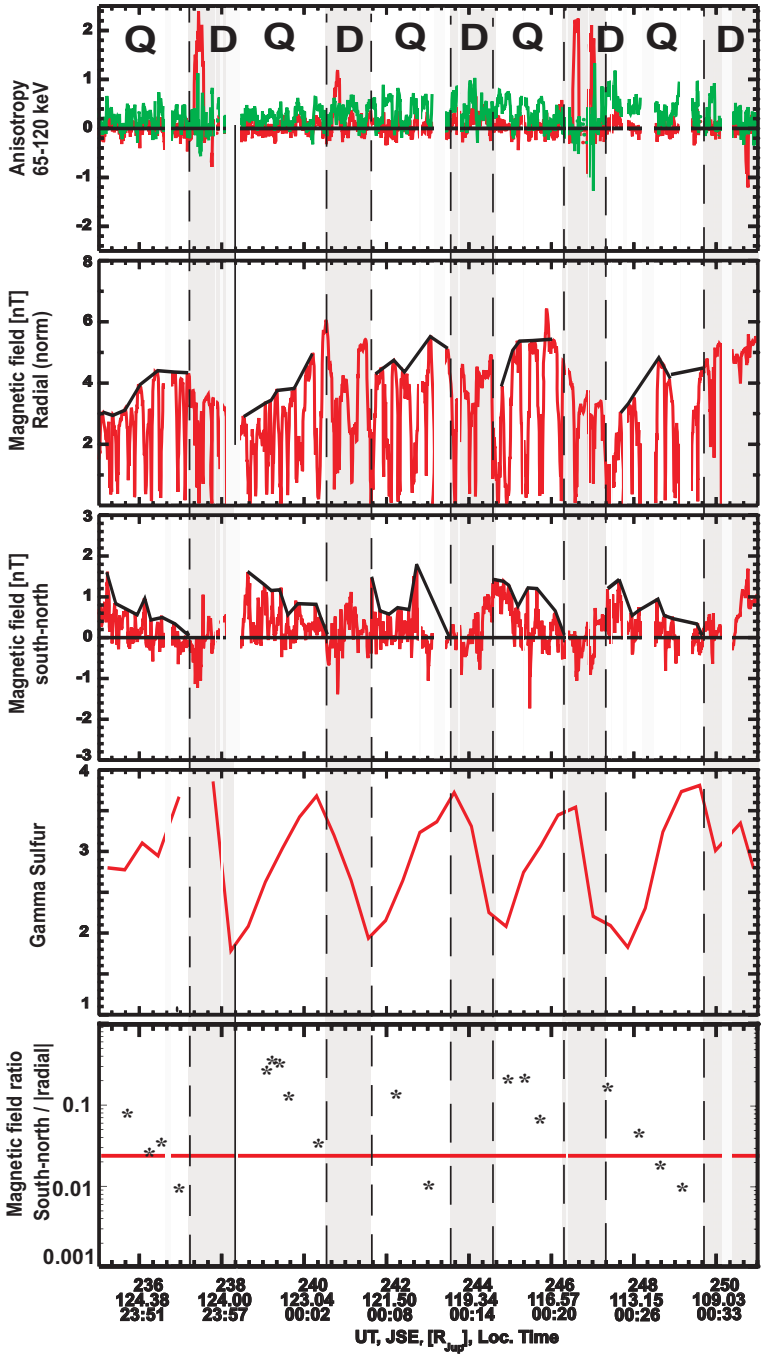

Figure 3.10: First order anisotropies in the radial (black, positive is outward) and corotational direction (grey) (first panel); the absolute value of the radial magnetic field component, the black line presents the rough envelope (transient events are neglected) (second panel); the south-north component of the magnetic field, the black lines show again the envelope (third panel); the sulfur energy spectral index γ, averages over 10-hour-averages (fourth panel); the ratio of the south-north magnetic field component in the current sheet crossing to the absolute value of the radial magnetic field component, the red line shows the threshold for the ion tearing instability (Zimbardo 1993) (fifth panel). The time interval DOY 235, 00:00 to DOY 251, 00:00 in 1998 (orbit E16) is shown. The dashed lines indicate times at which the Jovian magnetotail transits from a "quiet" to "disturbed" state or vice versa.

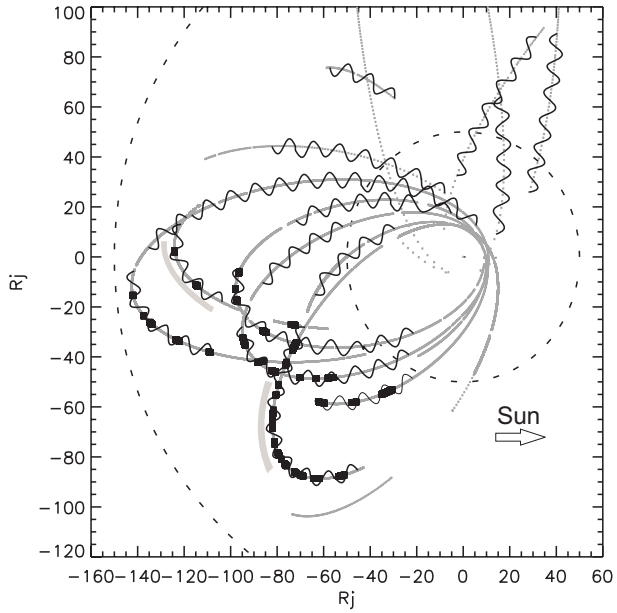

Figure 3.11: The G2 - Io33 orbits of Galileo in Jupiter Solar Ecliptic coordinates (excluding time periods with insufficient data coverage). Time periods with a periodical behavior of the ion spectral index γ are indicated by a wavy line. The locations of the reconfiguration events are marked by black dots. The grey marker close to midnight shows the time period presented in Figure 3.10. The grey marker in the predawn region corresponds to the time period presented in Figure 3.9

Orbital segments during which clear periodicities of the spectral index are observed are shown in Figure 3.11. The figure presents a summary map of observed spectral index periodicities in a range of approximately 1.5 to 6 days, which are shown by wavy lines (extended version of Figure 3.8). The figure covers the interval from mid-1996 to end of 2002 (Galileo orbits G1 to Io33), excluding orbital segments with insufficient data coverage. In most regions of the Jovian magnetosphere visited by the Galileo spacecraft periodic variations have been observed.

Based on this striking similarity of the modulation period for the burst events and the periodicities observed in the ion spectral shape it is suggestive to assume that the reconfiguration events in the magnetotail and the modulation of particle properties in the middle magnetosphere are inherently related and thus the whole Jovian magnetosphere is affected by the reconfiguration process.

3.3.1 Topological changes of the Jovian magnetotail

The presented two examples of periodical modulation in the Jovian magnetotail (Figure 3.9 and 3.10) show clearly a different periodical behavior of the south-north magnetic field component. The first example observed at predawn exhibits a gradual dipolarization of the plasma sheet during "quiet" time period. The second example observed close to midnight shows a gradual thinning of the plasma sheet. The increase in the south-north magnetic field component during the "quiet" mass-loading phases observed during the

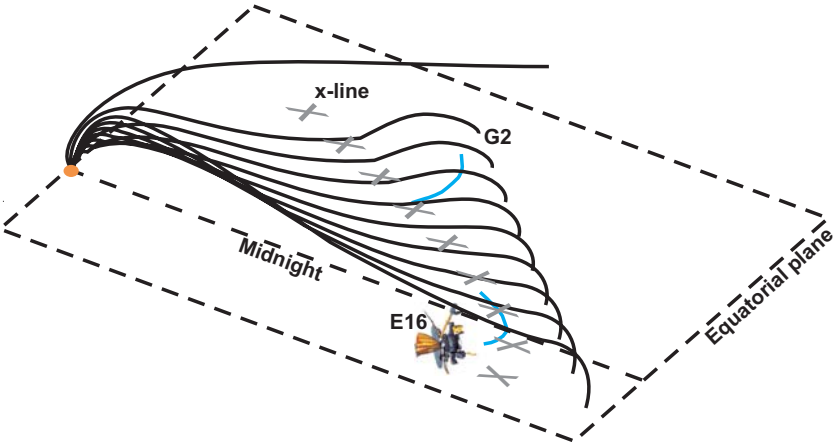

Figure 3.12: Topology of the magnetic field lines in the in the nightside Jovian magnetosphere. The grey crosses show the x-line derived by Woch et al. (2002). The blue lines are tracks of the G2 and E16 orbits. They show the trajectories of Galileo during the time presented in Figure 3.9 (orbit G2) and Figure 3.10 (orbit E16). The x-line and trajectories are plotted in real proportions. The black lines represent the possible configuration of the magnetic field lines during the mass- loading process. The field lines become stretched in the region planetward of the x-lines (shown in Figure 3.10). A "dipolarization" of the magnetic field lines is observed during the formation of plasmoid when Galileo is located tailward of the plasmoid center (see Figure 3.9).

first example implies that Galileo was located tailward of the plasmoid center, when the plasmoid was forming. The different nature of the magnetic field variations implies a different plasma sheet configuration which obviously depends on local time. It is known that the flux tubes are less stretched on the dusk side than on the dawn side (Kivelson and Khurana 2002). At the same radial distance the current sheet thickness at dusk is twice as thick as at dawn. The varying radial location of the x-line with local time derived by Woch et al. (2002) can be explained by the different thickness of the plasma sheet: the tearing instability, for example, occurs when the current sheet becomes thinner than a certain threshold which is of the order of the ion gyroradius (Pritchett et al. 1991). Thus this condition can be satisfied closer to the planet in the dawn region than at midnight in accordance with the x-line position found at 70 R_J in the predawn region and at 130 R_J at midnight (Woch et al. 2002).

The magnetic field data suggest that during the "quiet" period the plasma sheet is stretching in both regions planetward of the x-line location and tailward plasmoid-like structures form. But the signatures of this plasmoid-like structure at midnight are not as prominent as at dawn. At midnight the thin plasma sheet is gradually stretched out by the centrifugal force and not confined by the solar wind pressure. The configuration of the plasma sheet is "flat" and in the pre-dawn the plasma sheet configuration is slightly "dumb-bell-like". A possible cause might be due to compression of the flux tubes by the dawn-side magnetopause. Independently from the occurrence of reconfiguration event such a general local time dependence of the topology was derived from magnetic field data (Kivelson and Southwood 2005). The topology of this configuration is presented in

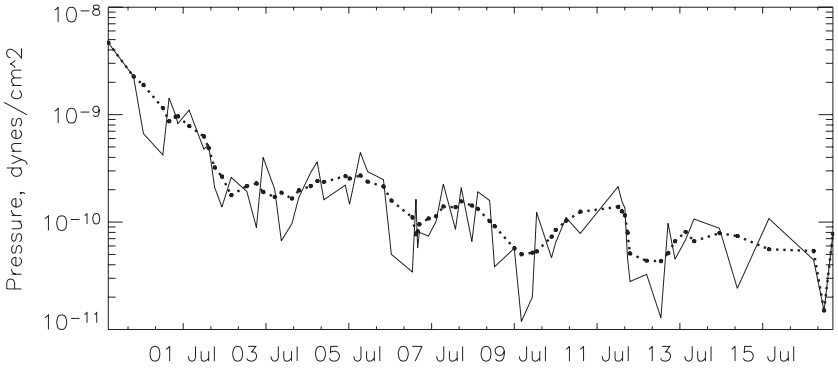

Figure 3.13: Plasma pressure for the time period 1997 DOY 180 04:00 to DOY 197 16:30. The dotted lines present the smoothed plasma pressure.

Figure 3.12.

3.3.2 Plasma pressure evolution

As it was discussed in Section 3.1, the ion pressure evolution is difficult to monitor at time periods with burst events. In order get a rough idea of the plasma pressure evolution a segment of the C9 orbit was chosen. This segment presents a Galileo pass through the middle and outer magnetosphere in the pre-midnight sector and is almost free of burst events. The few occurring were excluded from the ion pressure calculations. Figure 3.13 shows the periodical dynamics of the plasma pressure for the time period in 1997 from day 180 04:00 to day 197 16:30. Figure 3.14 presents a close-up view of a time interval of Figure 3.13 which exemplifies the variation of various parameters during the periodic stretching of the magnetotail (the stretching is seen from the decrease of the south-north magnetic field component and the high energy ion flux drops). It shows the fluctuations of the plasma pressure the particle flux and the south-north magnetic field component. The changes of the magnetic pressure do not coincide with the plasma pressure fluctuations. The high energy ion flux drops and the tailward stretching of the magnetic field lines correspond to the increase of the particle pressure. These phases have the same characteristics as the growth phase of a terrestrial substorm. Thereafter one can observe the increase of the particle flux and a "dipolarization" of the magnetic field (from the south-north magnetic field component). Towards the end of this phase the plasma pressure substantially decreases. These features are characteristic for the expansion phase of a terrestrial substorm. Thus, general features of the Jovian reconfiguration process are very similar to the characteristic of the terrestrial substorms. At the same time the same signatures (the plasma sheet stretching, plasma pressure increase) can indicate a mass-loading – unloading process. A signature of mass-loading of the flux tubes could be an increasing plasma pressure during the loading phase. The stretching of the mass-loaded flux tubes by the centrifugal force leads to increased cross-tail currents. This is in contrast to the Earth's case where an enhanced cross-tail electric field increases the plasma convection towards Earth during the growth phase and this plasma convection leads to an increased plasma pressure (Cheng 2004).

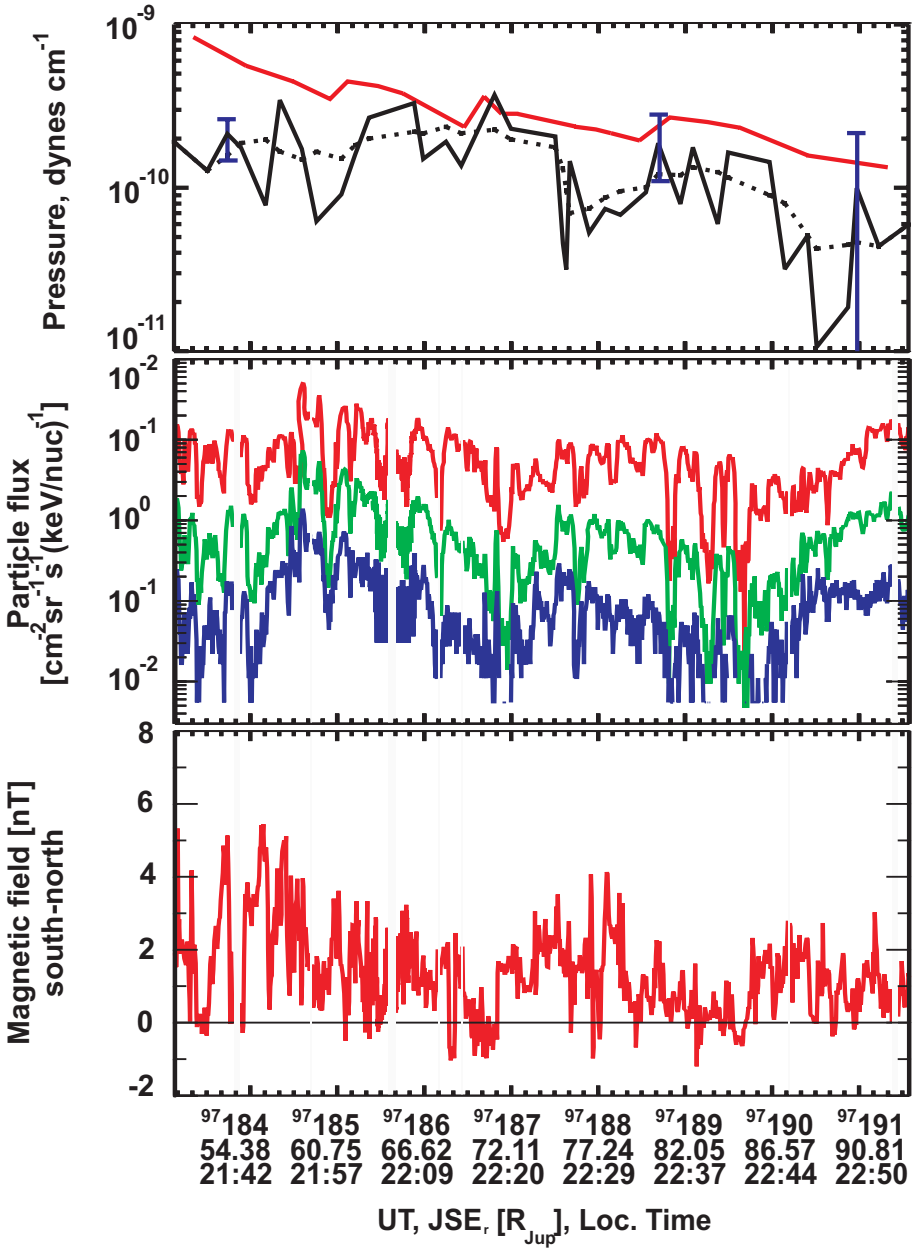

Figure 3.14: Plasma pressure (black), the dotted line present the smoothed plasma pressure and magnetic pressure (red) (top panel); the proton flux for tp1, tp2 and tp3 energy channels (second panel) and the south-north magnetic field component for the time period 1997 DOY 183 03:00 to DOY 191 14:00. The time periods marked in grey are phases associated with the loading phase of the Jovian magnetosphere.

3.3.3 Periodical substorms at Jupiter and Earth

While usually the terrestrial substorms appear as sporadic singular events, periodical terrestrial substorms have been observed (see Section 1.2.2). Let us compare the periodical terrestrial substorms and the periodical Jovian reconfiguration events. To demonstrate the

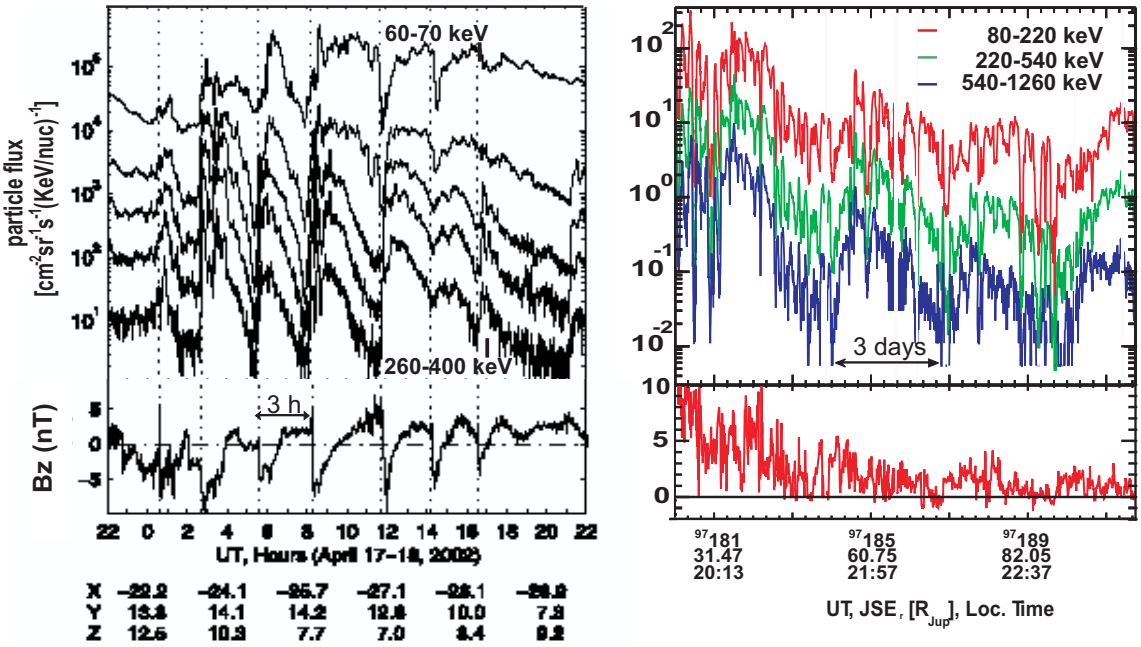

Figure 3.15: A comparison of the proton fluxes and the meridional component of the magnetic field (in GSE, respectively SIII) during the periodic magnetospheric substorms at Earth (17-18 April, 2002), left; and at Jupiter (DOY 180-191, 1997); right. The plot for the terrestrial case is taken from Huang et al. (2003).

similarities of the proton flux behavior and of the south-north magnetic field component, Figures 3.15 and 3.16 compare periodical events at Earth and Jupiter.

Figure 3.15 presents an example with striking similarities of the proton flux variations in the terrestrial and Jovian magnetotails. In both cases high energy fluxes drop stronger than lower energy fluxes. In both cases the magnetic field shows quasi-periodical fluctuations which, however, differ in form. The magnetic field of the terrestrial magnetotail shows a plasma sheet "dipolarization" during the flux drops. The magnetic field of the Jovian magnetotail shows a stretching of the plasma sheet. The lack to detect a "dipolarization" or a plasma sheet stretching depends on the spacecraft location and was discussed in Section 3.3.1.

Figure 3.16 compares a different Jovian periodic event with the same terrestrial event as in Figure 3.15. This time the flux dropouts are not as clear as in the previous example but instead the behavior of the magnetic field is very similar. The gradual "dipolarization" of the plasma sheet during the time of flux decreases are followed by an abrupt thinning of the plasma sheet during the times of sharp particle flux increases.

Therefore, both the periodical substorms at Earth and Jupiter undergo similar processes leading to high energy flux dropouts during the growth phase. The interpretation of the high energy flux dropouts is the following: energetic ions drift against the electric

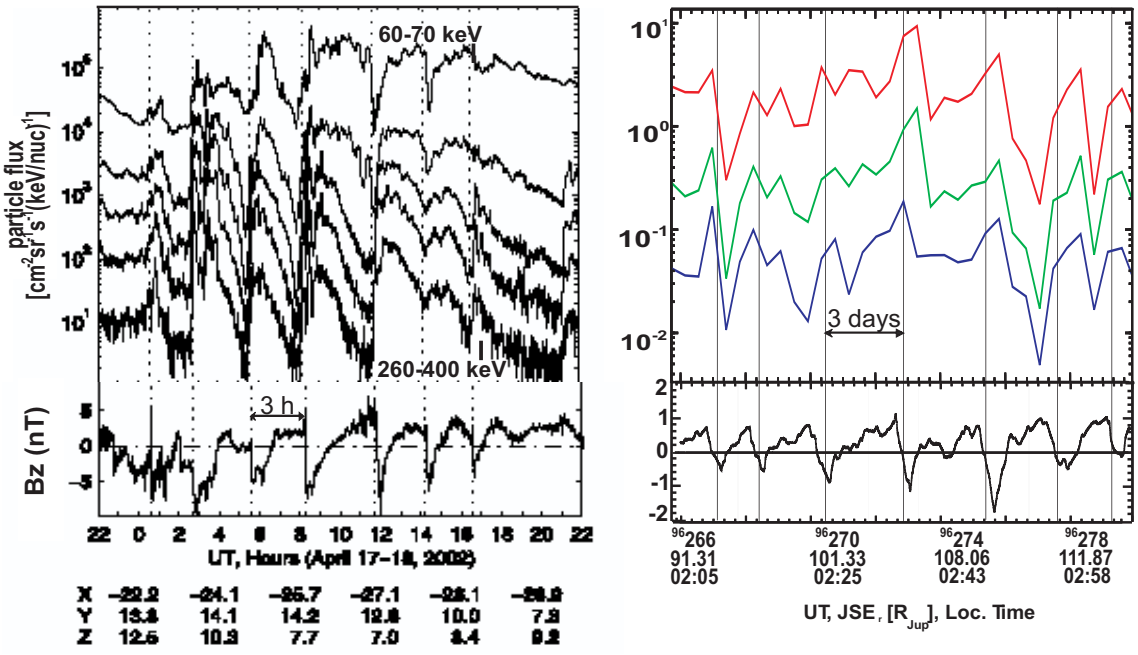

Figure 3.16: A comparison of the proton fluxes and the meridional component of the magnetic field of the periodic magnetospheric substorms at Earth (17-18 April, 2002) and at Jupiter (DOY 266-282, 1996), in the same format as in Figure 3.15. The plot for the terrestrial case is taken from Huang et al. (2003).

field induced by the stretching of the tail magnetospheric field and undergo a significant betatron deceleration (Sauvaud et al. 1996, Woch et al. 1998). Thus the stretching of the magnetic field leads to high energy flux decrease.

The comparison of the periodical substorms at Earth and Jupiter shows a striking similarity. This suggests that the same cyclic mechanisms of energy loading and unloading affects both magnetospheres. However, the sources of energy seem to be different.

3.4 Reconfiguration process - features in details

In this section we will present further detailed features of the Jovian reconfiguration / mass release processes and compare them (where applicable) with terrestrial substorms.

3.4.1 Characteristics of ion burst events

Mass release processes are associated with ion flow burst events. The radially outward and inward ion bursts selected from the anisotropy data were detected when the spacecraft crossed the current sheet center ($B_r = 0$), the sheet/lobe boundary layers and the lobe region (B_r approximately constant). This allows to conclude that the release of the plasma affects all magnetotail regions.

It seems possible to apply the model of Richardson et al. (1987), see Section 1.2, to the mass-release process at Jupiter. One may expect to observe in contest with the plasmoid-associated ion bursts three typical phases (in analogy to the Earth's substorms) the formation of Plasma Sheet Boundary Layers, Plasmoids and Post Plasmoid Plasma Sheet (PPPS). In the Jovian magnetosphere, the Plasma Sheet Boundary Layers (PSBL) are identified by an increase of the particle flux in the sheet/lobe boundary layers (compared to the particle flux in the current sheet center). The formation and evolution of the PSBL is well shown in the substorm-like event on day 270 00:00 in 1996 (see Figure 3.2). The first strong southward and then northward field tilts together with a high ion intensity is considered as a signature of plasmoids. The continually northward directed magnetic field and the slow decrease of the ion intensity is considered as a signature of the PPPS (Richardson et al. 1987).

A detailed view of an ion flow burst and the associated magnetic field variation for the time interval 06:00 to 10:30 on day 268, 1996 is presented in Figure 3.17. The magnetic field components exhibit signatures of leading corotation for most of the time period between 06:00 and 09:15. Thereafter the configuration attains again the usual lagging state.

At 07:15 the radial component of the ion directional flow anisotropy starts to increase. Simultaneously, indicated by the first vertical line, the data show the onset of magnetic field fluctuations. The 3 to 8 min period of these fluctuations is comparable to several gyroperiods of heavy ions. The gyroperiods of protons, O^{2+}, S^{3+} are $\sim$ 16, 125 and 375 s, respectively for a lobe magnetic field intensity of 4nT. Analogous low frequency oscillations associated with terrestrial substorms have a characteristic period of 15 to 25 s or several proton gyroperiods. At Earth such oscillations are interpreted as a signature for the onset of a substorm (Ohtani et al. 1998). Magnetic fluctuations on a time scale of an ion gyroperiod suggest that ions play an important role in the excitation of the fluctuations related to the substorm onset. The fluctuations in the meridional and azimuthal components are slightly dominating those in the radial component which indicates that the currents flow preferentially in the equatorial plane. The magnetic fluctuations at Earth last around 2 to 3 min (Ohtani et al. 1998); at Jupiter they last $\sim$ 45 min. It is still unknown even for the terrestrial case which mechanisms trigger these fluctuations. Takahashi et al. (1987) suggested that the spacecraft observed radial oscillations of the position of a nearby neutral line accounting for the reversal of the sign of the magnetic field. On the other side instabilities that occur in a thin current sheet can also produce such magnetic field oscil-

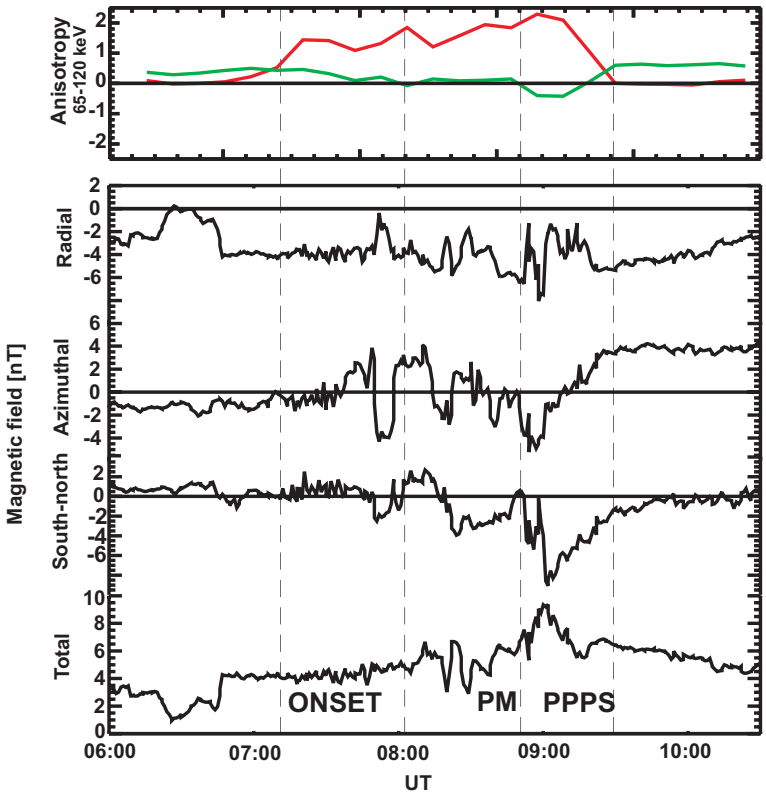

Figure 3.17: First panel: First order ion anisotropies in the radial (red, where positive is the outward direction and corotational (green) direction;). Second panel: The magnetic field variations during a reconfiguration event for the time period DOY 268 06:00 to DOY 268 10:30 in 1996. The vertical lines divide the magnetic field data in time periods comprising the onset oscillations, the plasmoids (PM) and the Post Plasmoid Plasma Sheet (PPPS).

lations. For example the tearing mode instability is one of the substorm trigger models in which kinetic ions play an essential role. Schindler (1974) suggested that ions are unmagnetized near the current sheet because their gyroradius is comparable to the field line curvature radius, and such ions destabilize the configuration and lead to ion tearing mode. The current sheet disruption model shows that a substorm can be triggered by the kinetic cross-field-streaming instability where unmagnetized ions play an important role (Ohtani et al. 1998) or by the kinetic ballooning instability which can be driven unstable in the enhanced cross-tail current sheet region due to the high plasma β, pressure gradient and enhanced tail-like magnetic curvature (Cheng 2004).

At 07:47 the signatures of a plasmoid are visible in the south-north magnetic field component. At 09:00 a strong northward tilt of the magnetic field component together with a a gradual decrease of the particle flux (not shown) are observed, which could be a signature of the PPPS. The expansion phase (from $\sim$ 08:00 to $\sim$ 10:00) which includes the formation of plasmoid and the PPPS lasts around 2 hours whereas at Earth it typically lasts only around 30 min. The azimuthal component of the flow anisotropy starts to dominate again at 09:27 and is back to the pre-disturbance level shortly thereafter.

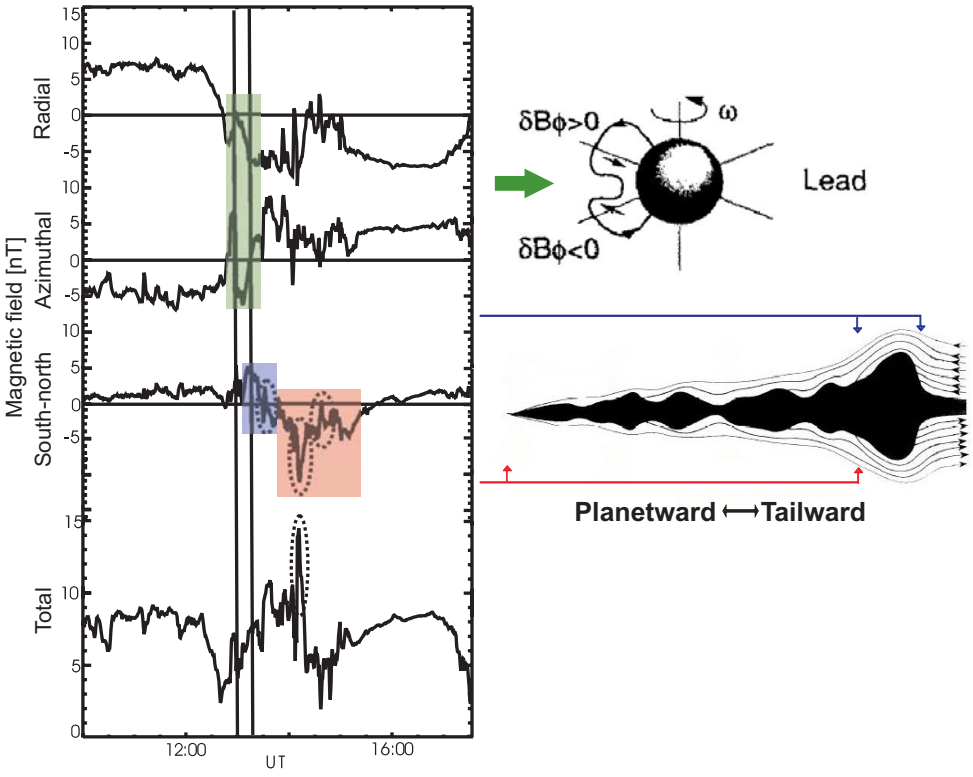

Figure 3.18: The magnetic field variations during a current sheet crossing tailward of a reconnection line for the time period DOY 264 10:00 to DOY 264 17:30 in 1996. Distortions of the field which can be attributed to plasmoids or wavy structure in the post plasmoid plasma sheet are encircled by dashed lines. The vertical lines indicate the time period when the magnetic field was swept forward out of the meridional plane. This type of configuration is sketched at the top right. The sketch at the bottom right shows the structure of a plasmoid and the post-plasmoid plasma sheet (adapted from Mukai (2000)). The plot was constructed by binning the ion flow burst samples into 0.5-hour-wide intervals.

Another event (Figure 3.18) shows the fine structure of the magnetic field during a Jovian mass-release event. Superimposed on a consistently northward inclined field a series of small-scale disturbances occur. These are either sporadic increases of the magnetic field intensity (above lobe levels) primarily due to a substantial increase of the south-north component or bipolar deflections in the south-north component. This implies that also in the PPPS plasmoid-like structures form (see the sketch of Mukai (2000) in Figure 3.18). At the onset and in the course of a mass release process one can often observe magnetic field changes from a swept-back to a swept-forward configuration. The leading configuration is consistent with the field rotating faster than corotation which indicates a transfer of momentum from high to low altitudes. Thus the planet's ionosphere gains momentum from the magnetospheric plasma (Dougherty et al. 1993). Such events have been discussed by Russell et al. (1998) as an indication for small-scale reconnection events. In contrast to that we presented evidence that these events are part of a global mass reconfiguration process.

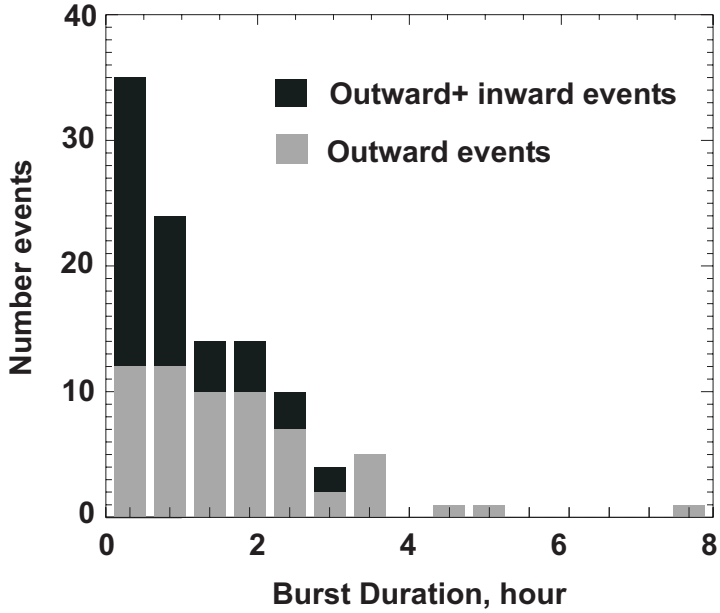

Figure 3.19: Occurrence rate of the flow burst events versus event duration. Black bars show the total number of the burst events (outward, inward) and grey bars present the amount of radially outward directed events. The plot was constructed by binning the data into 30 min intervals.

Each such reconfiguration and substorm-like event consists of radially outward and/or radially inward ion burst events. In the set of the substorm-like events from Table 3.1, there were 48 radially inward and 61 radially outward bursts identified. From this set, the general magnetic field variations during the burst events can be deduced. The radially inward bursts are associated with a positive meridional component of the magnetic field $B_\theta > 0$ and radially outward bursts (excluding the plasmoids with bipolar signature) are associated with $B_\theta < 0$, according to the topology of the magnetotail configuration during substorms.

Figure 3.19 displays the occurrence rate of the bursty events versus the event duration. The average duration of the inward events is 1 ± 0.7 hours and 1.8 ± 1.3 hours for the outward events. The duration of radially inward burst events is twice shorter than for radially outward events. A possible conclusion is that the outward mass-release process takes longer than the radially inward transport of emptied flux tubes. Another interpretation is that the radially inward bursts are generally closer to the x-line because it is supposed that the x-line is moving radially outward during the "disturbed" phase. This also explains why the radially inward bursts are commonly observed towards the end of the "disturbed phase".

The following study will concentrate on those ion burst events which are associated with plasmoid signature in the magnetic field.

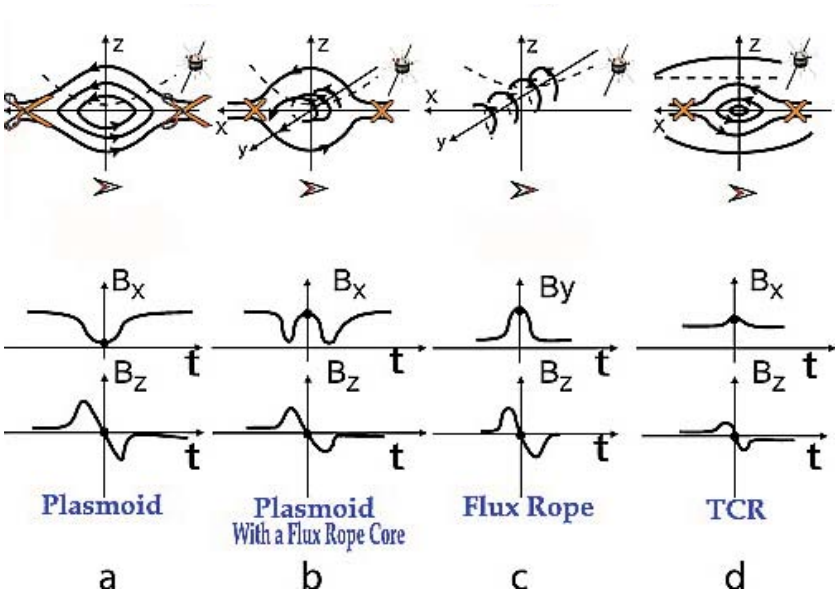

Figure 3.20: Magnetic structures detected in the terrestrial magnetotail as (a) Plasmoid, (b) plasmoid with a flux rope core, (c) Flux rope and (d) TCR in the magnetotail. Credit: (Zong et al. 2004).

3.4.2 Characteristics of plasmoids

In two dimensions the typical observational signatures of a plasmoid have been defined by a bipolar magnetic deflection the meridional direction B_θ, B_z. This magnetic signature is usually associated with high-speed tailward directed energetic ion and electron beams (Zong et al. 2004). Such a large tailward-moving loop-like magnetic structure is generated as the result of X-type reconnection in the near magnetotail (Hones 1979). The examination of the three dimensional topology and morphology of plasmoids in the Earth's magnetotail showed that they possess rather complicated configurations (see in Figure 3.20, Zong et al. 2004). From left to right the four sketches present (a) the original 2-dimensional Hones scenario, (b) a helical flux rope embedded in an outer closed loop magnetic field, (c) a helical flux rope and (d) a travelling compression region (TCR) which is detected as moving magnetic imprint of a plasmoid in the lobes.

Magnetic signatures of Jovian plasmoids were discussed by Russell et al. (1998). The main signature appears as a bipolar deflection of the meridional component, similar as in the case of Earth. However, a major difference occurs due to the fast rotation of Jupiter. The conservation of the angular momentum leads to predictable perturbations in the azimuthal component of the magnetic field as the magnetized plasma is convected either toward or away from Jupiter by reconnection. The angular velocity of the plasma initially increases inward of the reconnection point, causing a corotational lead, and as a consequence the magnetic field sweeps forward out of the meridional plane. Outward from this point the angular velocity of the plasma declines and the field is swept backward out of the meridional plane (see examples in Figures 1.7, 3.3, 3.18).

To recognize the signatures of flux ropes in the magnetic field data of Jupiter is an even

more complicated task because the corotational lag of the magnetic field and the wobbling of the plasma sheet introduce further magnetic field variations, which are superimposed on the flux rope signature.

There is another magnetic feature which can also be detected in the magnetotail. A tailward moving plasmoid in the central plasma sheet will temporarily compress the magnetic flux in the tail lobes because the cross-sectional area of the lobe is reduced. A structure with a transient increase in the lobe field strength and a deflection of the magnetic field vector, first northward and then southward in Earth's case, and first southward and then northward in Jupiter's case, is called TCR (Slavin et al. 2003). TCRs in the Jovian magnetotail will be discussed later in Section 3.4.3.

Velocity of plasmoids

It is expected that the plasma confined in a plasmoid has the same speed for different species which is the macroscopic plasma flow velocity. To derive this flow velocity, ion burst events associated with a strong bipolar signature in the B_θ component of the magnetic field were analysed. Furthermore the field configuration has to be sufficiently stable to allow to identify an anisotropy parallel or perpendicular to B. We limit our study to those events which then have a field-aligned anisotropy (the ion directional flow anisotropy component in the magnetic field direction) close to zero. In these events the ions move essentially perpendicular to the instantaneous magnetic field direction. Figure 3.21 presents a comparison of the derived velocity for different ion species for such burst events in different plasma sheet regions. In the lobe region mostly field-aligned beams (a dominating field-aligned anisotropy) are observed but also signatures of two plasmoid-like events which are probably TCRs. The latter two are included in Figure 3.21. Obviously the flow burst events which satisfy the above conditions have approximately the same velocities for the different ion species. Most of the plasmoid signatures are observed in the central plasma sheet (17 events) and in the plasma sheet boundary layers (11 events). In Figure 3.22 we present the occurrence rate of plasmoids with respect to the ion bulk velocity measured in the plasmoid. The plot was constructed by binning the plasmoid velocities into 100-km s^{-1} − wide intervals. The range of velocities and the velocity distribution are very similar to the results found for high speed flows in the terrestrial plasma sheet (Baumjohann et al. 1990). The most typical plasmoid speed is in a range between 400 and 500 km s^{-1} and the mean speed of the plasmoids is 461 ± 173 km s^{-1} in the current sheet, 463 ± 142 km s^{-1} in the plasma sheet boundary and 887 ± 142 km s^{-1} in the lobe region. In contrast to that the local plasma speed in non-plasmoid intervals is about ~ 250 km s^{-1}.

Duration and length of plasmoids

The distribution of the duration of plasmoids is presented in Figure 3.23. The figure was constructed by first determining the difference between the end time and start time of the plasmoids as shown in the four examples in Figure 3.20, and then by binning these events into 10-min-wide intervals. The 10-min-width is the minimum meaningful width of the bins. For this study the events with the most prominent bipolar signature were chosen. It is necessary to avoid the mixture of less prominent events with e. g.

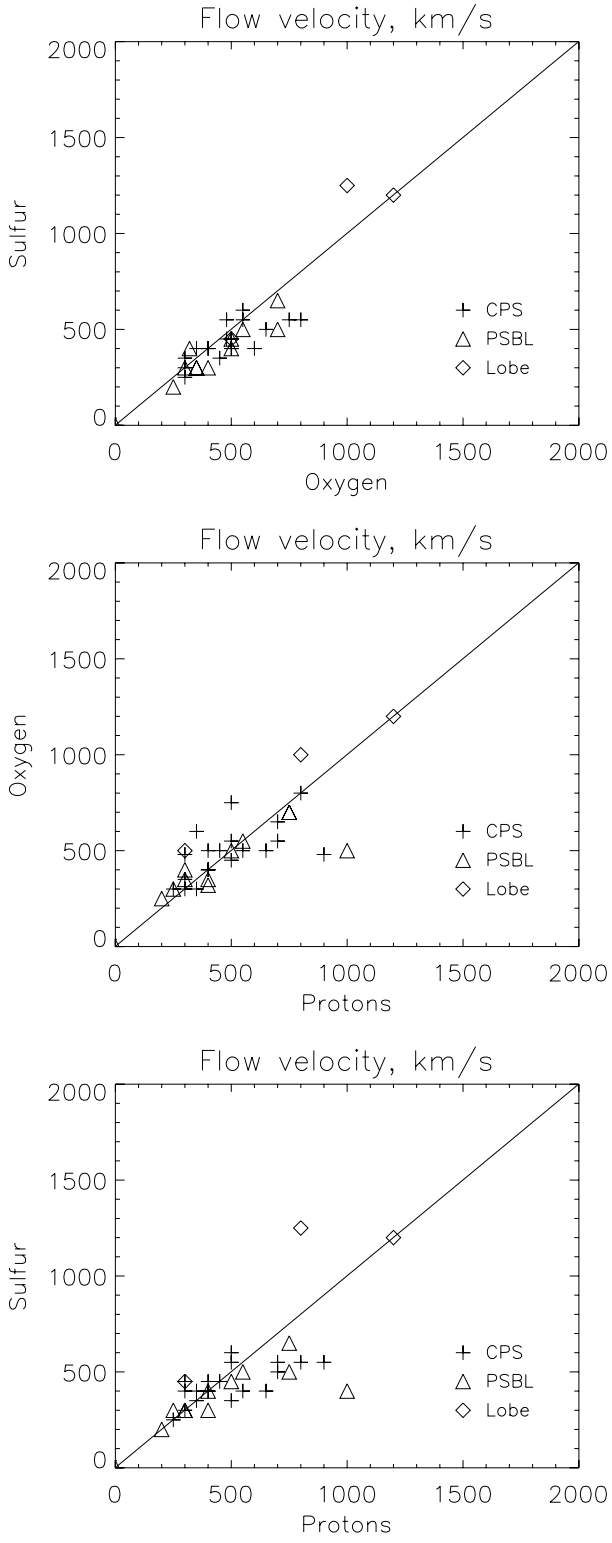

Figure 3.21: Velocity distribution for plasmoid events. S, O and protons plotted versus each other in the different regions of the magnetotail, i.e. the current sheet center, the plasma sheet boundary layers and the lobe regions.

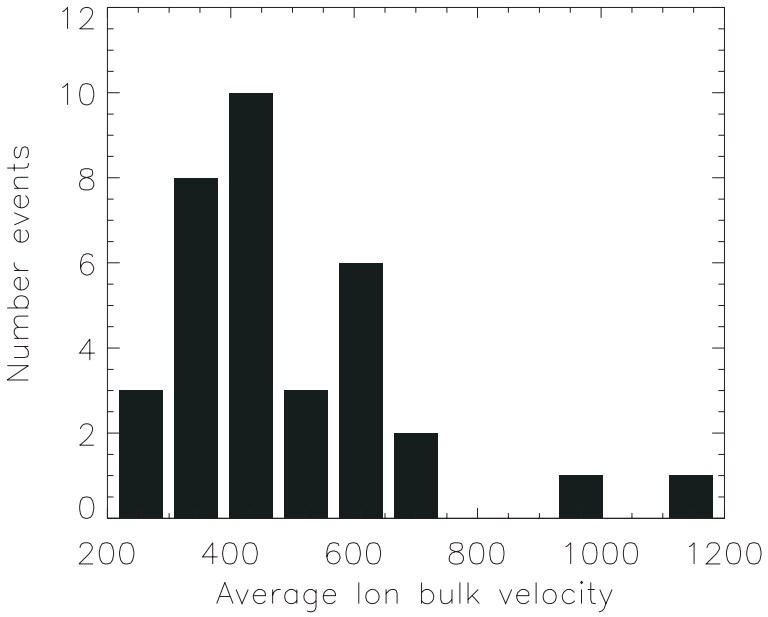

Figure 3.22: The occurrence rate of plasmoids versus to the ion bulk velocity measured in the plasmoid.

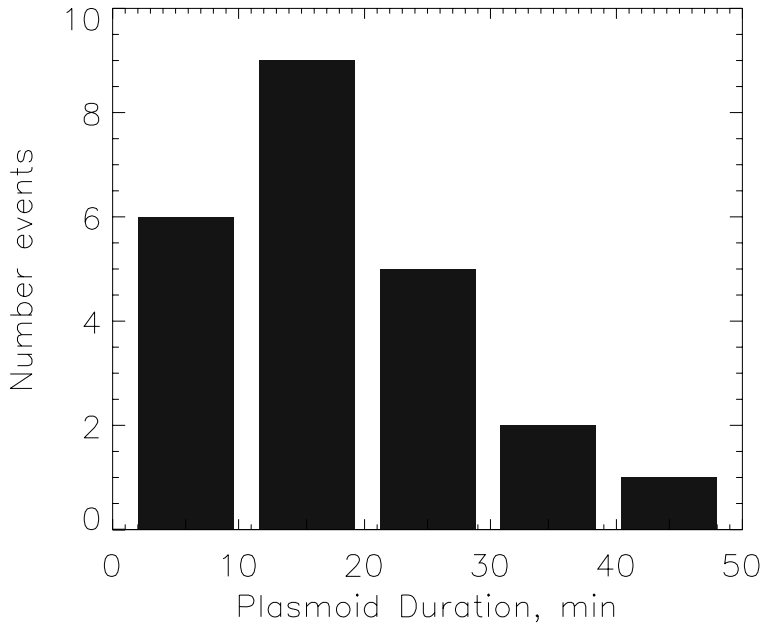

Figure 3.23: The occurrence rates of plasmoids versus the duration of the events.

surface waves. The number of events included in this statistics is less than in the case of the velocity statistics because of the availability of the high-resolution magnetic field data. It is necessary to take into account that the events with durations longer than 30 min could not be included because that the current sheet crossing by the spacecraft takes around 30 minutes. The majority of plasmoid events lasts between 10 and 20 minutes.

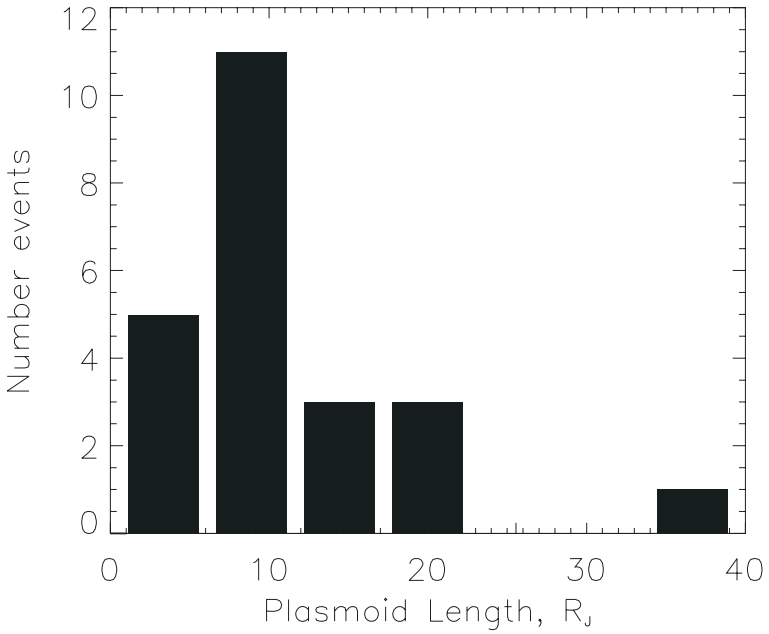

Figure 3.24: The occurrence rates of plasmoids versus the length of the events. The panel was constructed by binning these events into 5-R_J-wide intervals.

For comparison the typical duration at Earth is $\sim$ 1.5 min (Ieda et al. 1998).

The length of plasmoids is calculated by multiplying the plasmoids downtail velocities over the plasmoid duration in each event (presented in Figure 3.24). Most events have a length in the range between 5 and 10 R_J, with the mean plasmoid length being around $9 \pm 2.6 R_J$. The length of the Jovian plasmoids compared with the current sheet thickness is similar as for terrestrial plasmoids: from about 5 to 10 R_J length for a typical 2 R_J current sheet thickness in equilibrium state at Jupiter and $\sim$ 4 to 10 R_E length for a typical 1 R_E current sheet thickness at Earth (Ieda et al. 1998, Huang et al. 2003).

Table 3.4.2 presents the plasmoid duration, the plasmoid speed and the plasmoid length versus the radial distance from Jupiter. In this case all chosen events were located in the predawn sector observed during the orbit G2 in 1998. The radial distance was divided into two ranges (because of poor statistics): 85 - 100 R_J the region close to the x-line, and a region at 100 - 115 R_J, further away from the x-line.

Table 3.3: Characteristic quantities of the Jovian plasmoids versus the radial distance.

	85 - 100 R_J	100 - 115 R_J
Plasmoid duration	$\sim 20 \pm 7.7$ min	$\sim 24 \pm 5$ min
Plasmoid speed	$\sim 440 \pm 30$ km s^{-1}	$\sim 561 \pm 50$ km s^{-1}
Plasmoid length	$\sim 7.4 \pm 2.9\ R_J$	$\sim 11 \pm 2.4\ R_J$

This rough estimation shows that in the near x-line region plasmoids are slightly accelerated in the downtail direction and are more expanded. The same behavior is observed at the Earth's magnetosphere where Ieda et al. (1998) showed that the average length of plasmoids depends on the downtail distance, varying from $4R_E$ in the near tail to $10R_E$ in the distant tail. However, conclusions to be drawn for the plasmoid evolution in the Jovian magnetotail are very limited, because the Galileo coverage is restricted in the downtail regions to rather close distances from the x-line.

Alfvén Mach number of plasmoids

To compare the speed of plasmoids V_p with the Alfvén speed V_A the Alfvén Mach number M_A can be estimated as follows (Goedbloed and Poedts 2004)

$$M_A = \frac{V_p}{V_A}, \quad V_A = 2.18 \times 10^{16} \sqrt{\frac{Z}{A}} \frac{B}{\sqrt{n}}, \tag{3.1}$$

with $n(\equiv n_e \simeq Zn_i)$ where n_e is the electron density, n_i the ion density and Z the ion charge number (multiples of e) and with A the ion mass number (multiples of m_p) and B the magnetic field. The values of the electron number density n_e are derived from the cut-off frequency of the electromagnetic waves using Galileo PWS data. The values for the magnetic field B are taken in the lobe region, the average ion mass number A is assumed as 16 and the ion charge Z = +2 as the average value for the Jovian magnetotail (Geiss et al. 1992). Figure 3.25 shows the Alfvén speeds for the individual plasmoids in the three plasma sheet regions. The error of the Mach number estimations is $\sim$ 50% and that of the flow velocity $\sim$ 25%. In the figure it is visible that most plasmoids show close to Alfvénic flows ($M_A \simeq 1$). Only few events, mainly in the current sheet center reach super-Alfvénic speeds. This result also confirms the similarity of the Jovian substorm-like process with the terrestrial ones where plasmoids are moving with Alfvénic speed.

Convection electric field during the plasmoid release

Plasmoids moving in the central plasma sheet with a dominant velocity component perpendicular to the instantaneous magnetic field. They are characterized by a dipolarization of the central plasma sheet and are associated with strong electric fields $\mathbf{E} = -\mathbf{V} \times \mathbf{B}$. The average electric potential in the central plasma sheet during the plasmoid release can be estimated as follows $E = -(\sqrt{V_x^2 + V_y^2}) \cdot B_\theta$. It is studied that in the vicinity of the x-line (from x-line to 25 R_J) the degree of dipolarization does not depend on the distance from the x-line. Also the change of the velocity with distance to the x-line is not very prominent. Thus one can assume an average ion bulk velocity of $\sim$ 500 km s^{-1} and an average ΔB_θ of $\sim$ 3.3 nT which result in an average convection electric field of $\sim$ 1.6 mV m $^{-1}$. This average value is comparable to values for the reconfiguration events at Earth and is around one order of magnitude higher than the ambient Jovian value of the convection electric field which is approximately 0.25 mV m $^{-1}$.

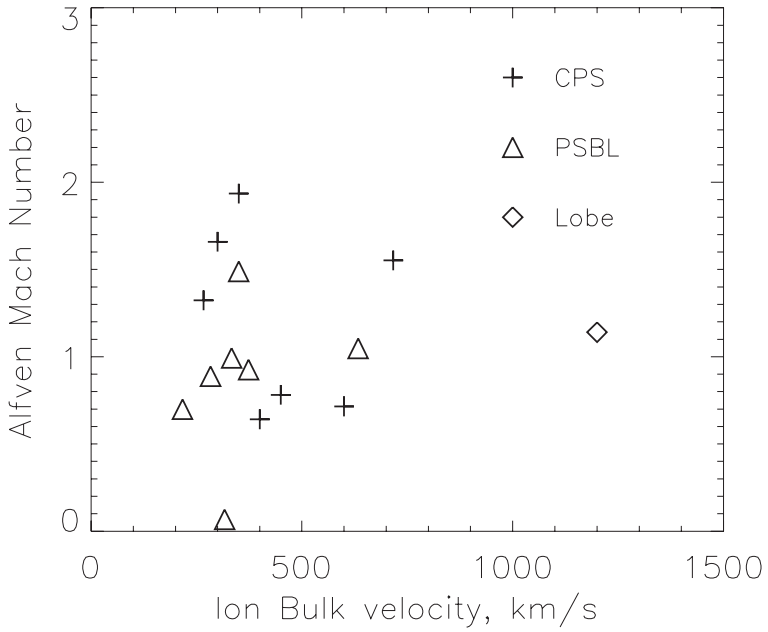

Figure 3.25: Alfvén Mach number $M_A = V_p/V_A$ of plasmoids in the three plasma sheet regions against the ion flow speed.

3.4.3 Determination of a substorm onset

A typical substorm-like event in the Jovian magnetosphere is shown in Figure 3.26. This event occurred in the time interval from day 97 151, 06:00 to day 97 154, 02:00. In this time Galileo was located in the midnight sector of the magnetotail (0116 LT) at R = 100 R_J. The first panel displays omnidirectional ion intensities in seven energy channels covering the energy range from 22 keV to 3.2 MeV. The second panel shows the radial and azimuthal component of the ion directional flow anisotropy of 65-120 keV ions. The next four panels present the magnetic field magnitude and its components in the SIII-system. First signatures of a mass-release process are observed at day 152, 07:00 with an unusual (for the lobe region) increase of the particle intensities (see vertical dashed line (1) in Figure 3.26). The corotational flow is disrupted by a strong tailward directed anisotropy spike. At day 152, 10:00 the next bursty flow ion anisotropy event arrives with bipolar features in the south-north magnetic field component. About 16 hours later another group of tailward directed bursts occurs and then in the subsequent plasma sheet encounter radially inward directed bursts are observed.

More details for the first burst event are presented in Figure 3.27 where omnidirectional ion intensity in six energy channels and the intensity of protons in three channels (first panel), the intensity of electrons in eight channels and the total magnetic field and its components are displayed.

The omnidirectional ion intensity and the intensity of the protons exhibit an energy dispersion in the sense that first the intensities of high energy ions increase. At 06:50 UT, on day 152 an increase of electron intensities in the lobe region can be interpreted as substorm onset. The higher energy ions arrive nearly simultaneously (within the time resolution of the measurements). Medium energy protons and ions arrive 10 minutes later.

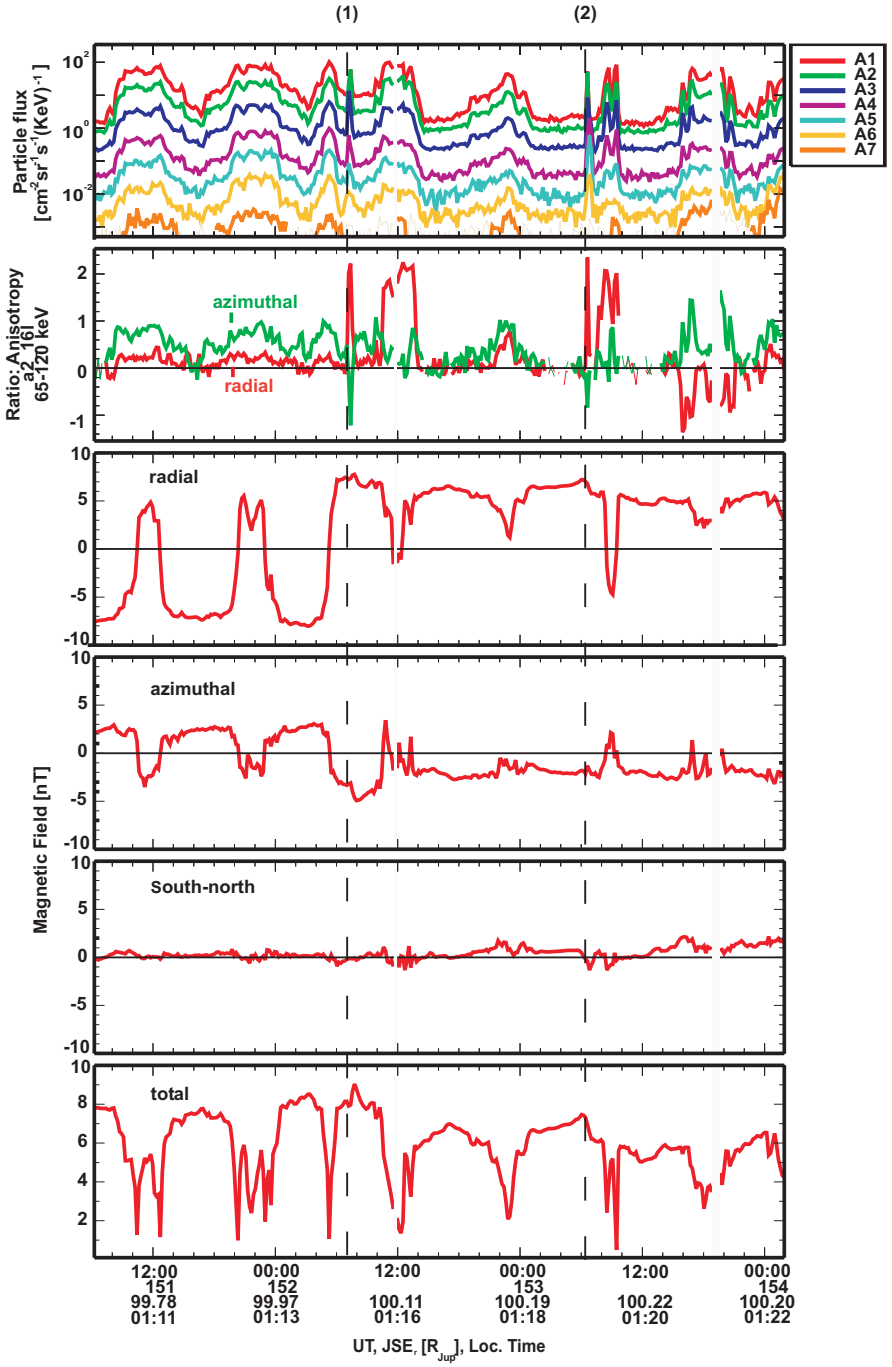

Figure 3.26: Energetic particle and magnetic field observations on Galileo orbit G8 from DOY 151, 06:00 to DOY 154, 02:00 in 1997. From top to bottom are displayed: omni-directional ion intensities (0.042-3.2 MeV) (first panel); first order ion anisotropies in the radial (positive is outward) and corotational direction (second panel); the magnetic field components in SIII coordinates (third to fifth panel) and its magnitude (sixth panel).

Assuming that the electrons are released at the reconnection site during the reconnection onset the distance of Galileo to the reconnection line can be roughly estimated from the

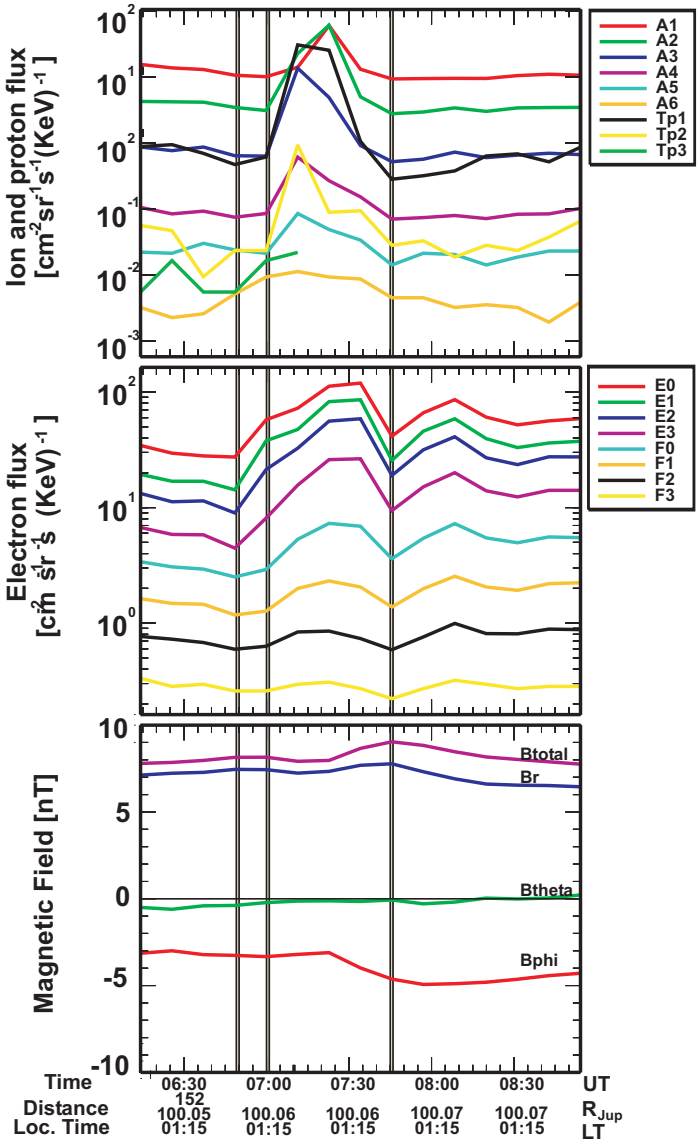

Figure 3.27: Energetic particle and magnetic field observations on Galileo orbit G8 from DOY 152, 06:00 to DOY 152, 09:00 in 1997. From top to bottom are displayed: omnidirectional ion intensities (22 - 825 keV, 8 energy channels) and proton intensities (80 - 1250 keV, 3 energy channels) (first panel); omnidirectional electron intensities (15 - 884 keV, 8 energy channels) (second panel); the magnetic field and its components in SIII coordinates (third panel). The first vertical line outlines the arrival of the electrons (15 - 93 keV) the second line the arrival of the protons (220 - 1250 keV) and the third line the arrival of the plasmoid.

proton delay time. The proton spike consists of a field-aligned beam and thus the proton field-aligned speed can be estimated from the proton energy. Protons with an energy of 132 keV (estimated as the geometric mean of the tp1 channel which is best defined), i.e. a speed of $\sim$ 5100 km s^{-1} arrive about 10 min later. This yields to a distance of 40 $R_J \pm$ 20 R_J and implies the formation of the x-line at $\sim$ 60 R_J from the planet. Alternatively, the

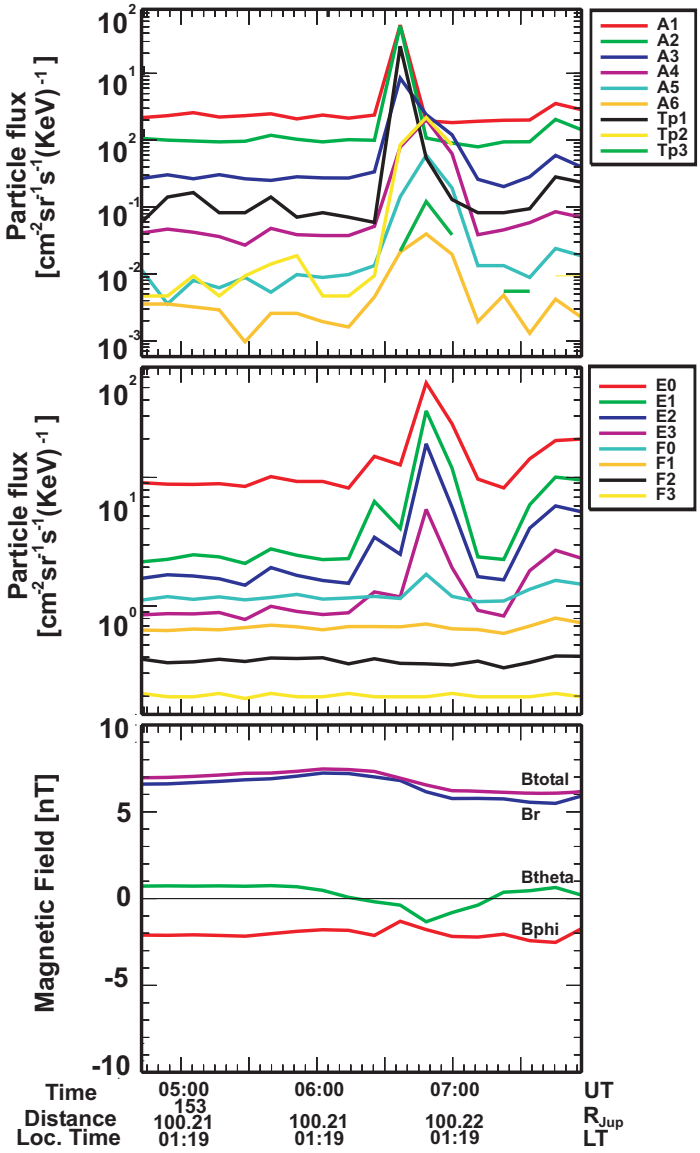

Figure 3.28: Energetic particles and magnetic field observations on Galileo orbit G8 from DOY 153, 04:30 to DOY 153, 08:00 in 1997, same format as Figure 3.27.

distance to the x-line can be estimated from the flow energy dispersion. Ions measured in a1 channel (mainly protons) with a geometric mean energy of 52 keV (speed of $\sim$ 3200 km s^{-1}) arrive $\sim$ 11 min later. This gives a distance of 20 $R_J \pm$ 10 R_J and an x-line formation at $\sim$ 80 R_J. Thus both methods give consistent results within the limitation of the methods due to the poor time resolution.

At 07:25 UT the beginning of a TCR is observed. The center of the TCR is observed at 07:45 UT, i. e. about 55 min after reconnection onset. If this plasmoid was moving from the x-line to Galileo ($\sim 20 R_J$) with a speed 500 km s^{-1} (during this time period the exact speed is not possible to estimate) it has a time delay of 50 min. That is in correspondence with the time delay from the substorm onset to the arrival of the plasmoid's center.

During this event another TCR is observed at DOY 153 06:20, (denoted by dashed

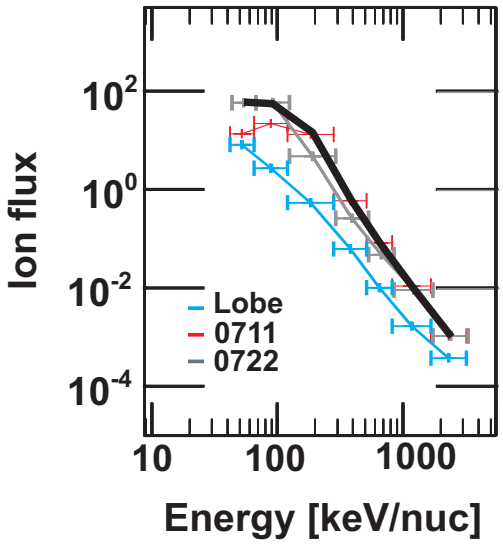

Figure 3.29: Energy spectra for ions in a quiet time during the lobe encounter on DOY 152 03:00 (blue), and in the burst times DOY 152 07:11 (red) and 07:22 (grey). The thick black line shows an envelope of the energy spectra during the burst event.
The drop in ion flux occurs at about 100 keV/nuc.

line (2) in Figure 3.26 and for details see Figure 3.28). First the radial component of the magnetic field is possibly compressed by an arriving plasmoid and the electrons and later also the ions are observed. The energetic particle injections are associated with the northward turn of the meridional magnetic field component. This particular event shows a reverse dispersion when first low energy ions and later high energy ions are observed. Additionally, the electrons arrive after the ions. The reversed dispersion implies a different spatial distribution of the ions and electrons which could be caused by the generation of the cross-tail current or by an azimuthal expansion of the field-aligned currents of the substorm wedge (Birn et al. 1997).

Figure 3.29 presents the time development of the burst spectra for the burst event shown in Figure 3.26 and an envelope of these individual spectra (thick black line) in comparison with a spectra taken in the lobe region preceding the event (blue line). The plasma heating for all ion channels and especially a strong acceleration of the low energy ions are observed while a drop of the ion flux at 100 keV/nuc is obvious. In analogy to the terrestrial case this drop can be due to a potential drop produced by field-aligned currents which are produced during the substorm. Podgorny et al. (2003) found that the potential drop produced by a substorm field-aligned current circuit is $\sim$ 50-100 kV. The potential drop EL is estimated by $EL = B_{tot}B_\theta/(2\pi\sigma ne)L$. In the current sheet during the above considered burst event the total magnetic field B_{tot} is $\sim$ 8 nT, the meridional magnetic field component B_θ $\sim$1 nT, the plasma density is n $\sim$0.01 cm^{-1}. With a typical current sheet thickness during a substorm of σ $\sim$0.5R_J, the potential drop at a distance L=100R_J will be $\sim$ 150 kV which is close to the voltage which can be deduced from the ion spectra presented in Figure 3.29.

3.5 General view of the reconfiguration events

Based on 34 investigated events the present study allows to establish the fundamental properties of the reconfiguration process. A reconfiguration event consists of a quasi-periodic transition between two elementary different states of the magnetotail. The general topology and properties of these two phases are sketched in Figure 3.30.

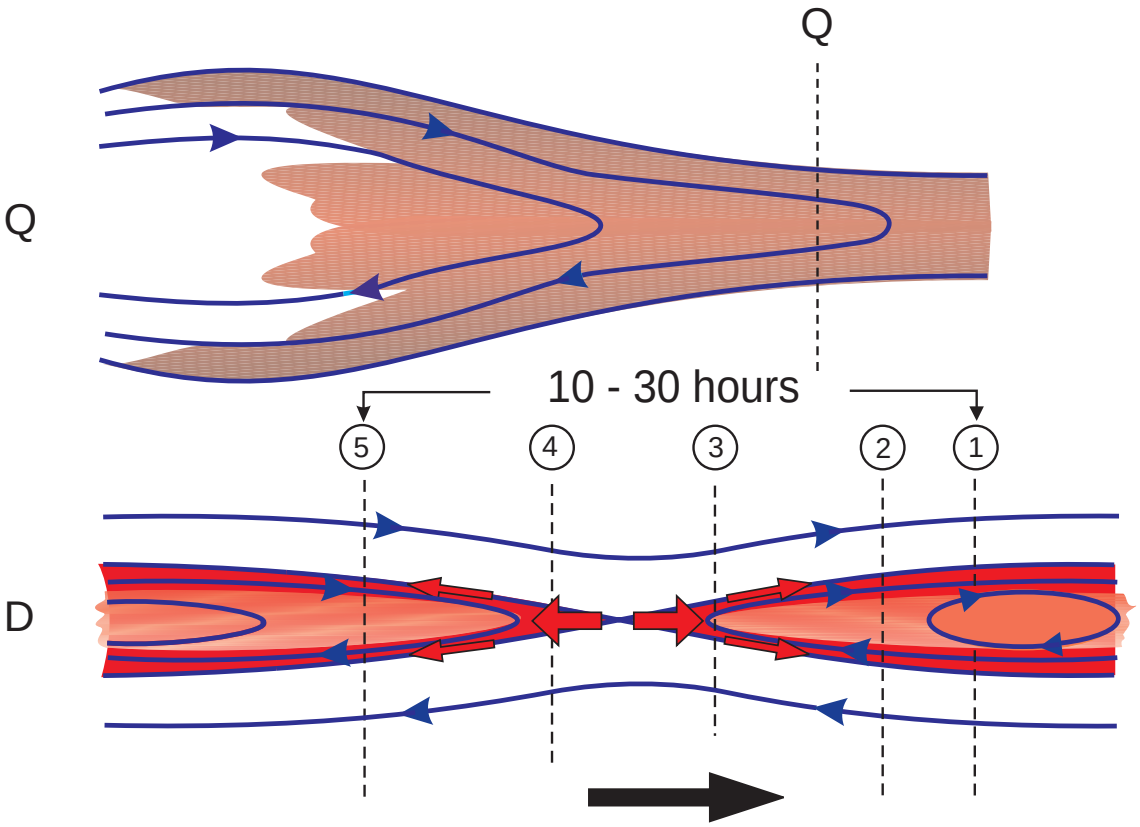

Figure 3.30: A sketch of the two basic states of the Jovian magnetotail. Top: "Quiet" state; bottom: disturbed state (details see text). The dashed lines and numbers correspond to the respective current sheet crossings labelled D1 to D5 in Figure 3.2 (Kronberg et al. 2005).

In the initial "quiet" state the plasma flow is directed in the corotational direction. The plasma sheet is thick, i.e., largely expanded in latitude around the current sheet and without a distinct boundary towards the lobe region. Depending on the location with respect to distance and local time (see Section 3.3.1) the plasma sheet is affected by gradual stretching or thickening (in the region of plasmoid formation). Thus the "quiet" state of Jupiter's magnetosphere is not an equivalent to the "ground state" of the Earth's magnetosphere. Due to continuous loading with energy the "quiet" state in the Jovian magnetosphere is very similar to the "growth" phase during terrestrial substorms. Apart from the gradual stretching or thickening (in the region of plasmoid formation) the current sheet itself resides in a state without significant large or small-scale disturbances.

In addition, the magnetic field is in a swept-back configuration, as expected for angular momentum transfer to the magnetospheric plasma (Russell et al. 1998, Dougherty et al. 1993). The ion intensities in the plasma sheet center are initially at a low level. The "quiet" phase usually persists for 3 to 5 Jupiter rotations.

Towards the end of the "quiet" phase the ion intensity rises, the flow velocity slowly increases both in the corotational direction as well as in the radial outward direction. The "quiet" phase ends with a breakdown of the corotational pattern of the plasma flow and the magnetotail transits into the "disturbed" phase.

At a given location the transit occurs abruptly within minutes. In the disturbed phase the particles are initially streaming tailward. In the course of the events the streaming direction reverses to planetward streaming. A continuous thinning of the plasma sheet is observed, with the strongest confinement of the plasma around the current sheet reached at the point of the flow reversal. Distinct boundary layers at the plasma sheet - lobe interfaces evolve which consist of intense, high-velocity particle beams. To first order the magnetic field topology shows a current sheet configuration. However, during the period of tailward streaming the magnetic field in the plasma sheet has a persistent northward tilt, i.e. opposite to what is expected from the normal planetary field orientation. After reversal of the flow direction, the tilt changes back to a southward tilt. Additionally transient, small-scale disturbances are superimposed over the average field configuration.

The observed particle and field characteristics are consistent with a reconnection scenario. Whereas in the "quiet" phase the plasma convection in the corotational direction is sustained in the magnetotail, in the disturbed phase the magnetotail has evolved into a configuration which enables the onset of reconnection and allows for the release of plasma. That reconnection is indeed occurring is primarily evidenced by the distinct tailward- and inward-streaming particle beams. They are presumably observed on field lines which have recently been reconnected. Furthermore, characteristic magnetic field distortions, most readily explained by the passage of plasmoid-like structures, confirm on-going reconnection.

The reconnection topology is neither spatially nor temporally static. Inherent to the plasma release process is an apparent outward motion of the reconnection region, with the result that the actual active x-line is generally first planetward of the observation point, then progresses through it, and finally ends up at a location tailward of the observation point.

The general characteristics of the "disturbed" phase is very similar to the features of the "expansion" phase during the Earth's substorms. Thus the Jovian "disturbed" phase can be compared with the terrestrial "expansion" phase.

3.5.1 Temporal, spatial scales and other characteristics

The configuration favoring reconnection is maintained from several hours to several tens of hours, with a maximum detected duration of 30 hours and an average of approximately 15 hours. This means, the reconnection configuration is observed usually for several - in some cases up to six - consecutive current sheet crossings.

Table 3.5.1 presents a summary of the typical durations of the main substorm phases at Jupiter in comparison with those at Earth. Apparently the duration of the substorm phases at Jupiter is more than an order of magnitude longer than at Earth.

Table 3.4: Typical duration of the main substorm phases at Jupiter and Earth.

Phase	Jupiter	Earth
Growth phase ("quiet" phase at Jupiter)	$\sim$ 48 hours	1 hour
Onset	$\sim$ 45 min	$\sim$ 1 min
Expansion ("disturbed" phase)	$\sim$ 15 hours	0.5 hour

Generally the release phase in the Jovian magnetosphere consists of several releases of individual plasmoids embedded the post plasmoid plasma sheet. This implies multiple x-line formations (see events in Figures 3.2, 3.5, 3.7).

A summary of some basic parameters of the Jovian substorm-like processes in comparison to the Earth's substorms is presented in the Table 3.5.1. The table shows that the mass-release processes in the Jovian magnetosphere have larger spatial scales than Earth's substorms. The basic quantities, however, such as the speed of the bursty bulk flows, the convection electric field and associated potential drop are in the same range. It shows that the basic mass and flux release processes are very similar in both magnetospheres. The relatively small scale of the plasmoids in Jupiter's magnetotail has to be compared with the large-scale topology favoring reconnection that persists for up to several planetary rotations during the reconfiguration events. The reconnection process certainly affect the major part of the Jovian magnetotail.

The apparent tailward motion of the reconnection topology which can be deduced from the flow reversal from tailward to inward seems to be an intrinsic feature of the reconfiguration / mass release events. A flow reversal in this sense is observed for the large majority of events. It suggests that inherently the breakup of flux tubes first starts relatively close to the planet. In the course of the mass release process the x-line retreats further downtail whereas the inward mass-emptied region might already return to the "quiet" corotational state. The outward motion could be associated with a progression of the local time sector being affected by the process towards dusk. Such a combination of outward and azimuthal motion of the reconnection region could explain the average location of the x-line deduced in statistical studies (Woch et al. 2002), which was shown to be located closer to the planet at pre-dawn compared to pre-midnight.

[1]The values for the bursty bulk flows are taken from Angelopoulos et al. (1994).

[2]The values of the potential drop created by the field-aligned current system during terrestrial substorms are taken from Angelopoulos et al. (1994) and Podgorny et al. (2003).

Table 3.5: Characteristic quantities of Jovian substorm-like processes in comparison with Earth's substorms.

Quantity	Jupiter	Earth
Burst duration		
inward	$\sim$ 1 hour	$\sim$10 min[1]
outward	1.8 hour	$\sim$ 370 s[1]
Plasmoid speed	$\sim$ 350 - 500 km s^{-1}	$\sim$ 400 - 700 km s^{-1}
Plasmoid duration	$\sim$ 10 - 20 min	$\sim$ 1.5 min
Plasmoid length	$\sim$ 9 R_J	10 R_E
Convection electric field	$\sim$ 1-2 mV m^{-1}	$\sim$ 2 mV m^{-1}
Potential drop[2]	$\sim$ 100-150 keV	$\sim$ 50-100 keV

3.5.2 Relation to auroral phenomena

The overall auroral activity at Jupiter is well correlated with the disturbance level of the magnetic field in the Jovian magnetosphere (Prangé et al. 2001). The activity shows a variability with time scales of several days. Thus these observations also suggest that a dynamic process with cyclic nature affects the Jovian magnetosphere. A detailed relation of individual auroral features with various signatures of the mass release process has yet to be established. However, it is tempting to speculate that isolated auroral spots frequently observed poleward of the main auroral oval, the so-called 'Nightside Polar Spots' (Grodent et al. 2004), may be the auroral imprints of transient reconnection events. The apparent magnetic conjugacy of the two phenomena and their compatible duration corroborates such a relation. It has been suggested that the sub-corotational part of the dark polar region - an ionospheric region at dawn void of auroral emissions (Stallard et al. 2001, Grodent et al. 2003b) - is connected to the return flow of emptied flux tubes (Cowley et al. 2003) from the Vasyliūnas' x-line. On other hand, it could also be speculated that the upward current necessarily associated with the braking of the fast return flow in the high-pressure subcorotational regime in the middle magnetosphere could lead to intensive emissions. Those may be associated with the so-called auroral dawn storms (Clarke et al. 1998) or multiple dawn arcs (Grodent et al. 2003a).

Due to the orbital characteristics of the Galileo trajectory the mass release events could be identified in the magnetotail region. However, the occurrence of plasma release events may not necessarily be restricted to the Jovian magnetotail. They might occur also on the dayside specifically during times of magnetospheric expansion, when outward stretching of mass-loaded flux tubes is no longer prevented by solar wind pressure forces. Thus mass release events might also account for dayside auroral intensifications.

4 Modelling of the periodic reconfiguration process

In the previous chapter it was shown that the Jovian magnetosphere is affected by a process similar to the substorms at Earth. However it was also shown that this Jovian reconfiguration process is most likely driven by internal sources. Moreover, whereas at Earth periodically recurring substorms are rather rarely observed, the reconfiguration process at Jupiter seems to be intrinsically quasi-periodical. It is of interest to model the periodic reconfiguration processes in the Jovian magnetosphere, in order to confirm the assumptions that substorm-like processes at Jupiter can be internally driven, to explain why they are periodically recurring and to derive an intrinsic time constant of the process. In this section a simple modified version of the Vasyliūnas model will be presented which allows an explanation of the periodic nature of the Jovian reconfiguration events.

4.1 Introduction to the model

Our model assumes that the observed quasi-periodic variations of the middle and outer magnetosphere of Jupiter are cyclic processes driven by internal dynamics. Starting from an initial mass-loaded state (see Figure 4.1) further mass-loading leads to a continuous stretching of the tail magnetic field configuration due to the increasing moment of inertia of the tail plasma and the centrifugal force (the second panel of Figure 4.1). This implies a situation where the field lines become more and more anti-parallel. At a certain moment of time the stretched out magnetic field line configuration undergoes magnetic reconnection and consequently formation of an x-line and plasmoid release becomes feasible (third panel of Figure 4.1). The forth panel of Figure 4.1 shows the configuration after plasmoid formation and mass-release which is basically the same as the initial mass-loaded state shown in the first panel. Now further mass-loading leads to newly stretched field lines and the process starts again. In this manner the magnetosphere can undergo quasi-periodically different states. The crucial parameter to be estimated is the intrinsic time constant of the tail stretching from the initial state up to the configuration that favores reconnection.

In generation of reconnection and plasmoids the tearing-mode instability is a possible candidate. It is a resistive instability in the plasma which is associated with a topological change of the magnetic field.

During the stretching of the magnetotail the meridional component of the magnetic field in the current sheet center will decrease. Let us now consider the collisionless ion tearing instability. The stretching of the current sheet can lead to the state when its thickness will become smaller than a typical ion gyroradius. Consequently the ions do not

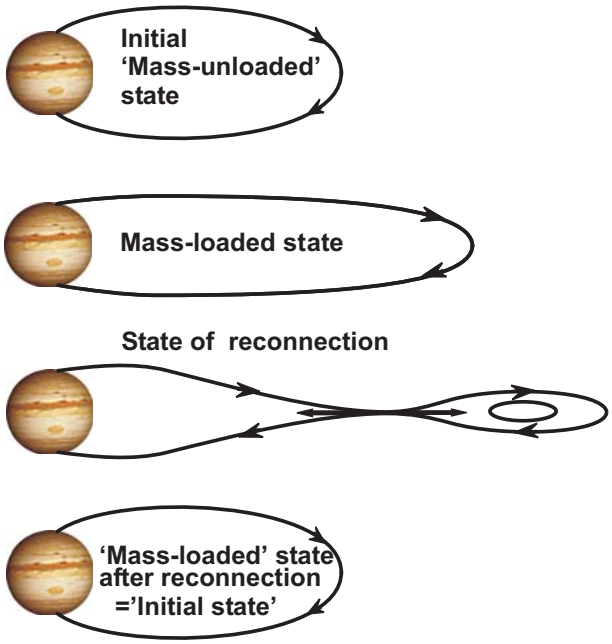

Figure 4.1: A sketch demonstrating the periodical nature of the reconfiguration process in the Jovian magnetosphere. The top panel shows the initial largely "mass-unloaded" state prior to excessive mass-loading from the internal sources. The second panel exhibits a stretching of the configuration as a consequence of continuous mass-loading and the centrifugal force. The third panel presents a reconnection state which leads to formation of x-line and mass-release in a form of plasmoids. This state is reached after sufficient thinning of the plasma sheet allowing for spontaneous reconnection. The forth panel shows the configuration after reconnection. The Jovian magnetosphere undergoes periodic changes between the first and the third state.

gyrate anymore around the magnetic field lines and the ion motion becomes chaotic. These chaotic ions can in turn become resonant with a tearing mode (the ion Landau resonance). This instability can occur when the following condition is satisfied (Wiechen and Schindler 1991):

$$Q = \frac{B_\theta}{B_r}\left(\frac{d}{r_{ion}}\right)^{\frac{5}{2}},$$

here d is the typical plasma sheet thickness, r_{ion} is the typical gyroradius, B_θ is the meridional magnetic field component in the current sheet center and B_r is the typical magnetic field in the lobe. The possibility of such a tearing-mode instability in the Jovian magnetosphere was discussed by Zimbardo (1993). Collisionless ion tearing modes can grow in a thin quasineutral sheet with the thickness in the order of an ion gyroradius. In the Jovian magnetotail with a typical current sheet thickness of 2 R_J and $B_r \sim 4$ nT (Khurana and Kivelson 1989) the mode has a growth rate of $\gamma = 0.03 \cdot \Omega_{ion} = 1 \cdot 10^{-3}\mathrm{s}^{-1}$ and a growth time of $t_{growth} = \gamma^{-1} = 11$ min, where Ω_{ion} is the cyclotron frequency (Zimbardo 1993).

4.2 Basic Equations

To describe the hypothetical processes in the Jovian magnetosphere a spherical coordinate system is chosen, where the observer is rotating together with the largely azimuthal, (sub) corotational plasma flow. The velocity of the plasma $\mathbf{v}$ in the inertial system is given by

$$\mathbf{v} = \mathbf{v}' + \mathbf{\Omega} \times \mathbf{r}', \tag{4.1}$$

where $\mathbf{v}'$ is velocity of plasma in the rotational system of reference and hence $\mathbf{v}' = 0$ in this consideration, $\mathbf{\Omega}$ is the angular velocity, here the angular velocity of planet Jupiter and $\mathbf{r}'$ the radial distance. Using the Equation

$$\frac{d\mathbf{v}}{dt}\Big|_{Inertial} = \frac{d\mathbf{v}}{dt}\Big|_{Rotational} + \mathbf{\Omega} \times \mathbf{v}$$

and Equation (4.1) an expression which connects the force density in the inertial system with the force density in the rotational system is obtained:

$$\frac{d\rho\mathbf{v}}{dt}\Big|_{Inertial} = \frac{d(\rho\mathbf{\Omega} \times \mathbf{r}')}{dt} + \rho\mathbf{\Omega} \times (\mathbf{\Omega} \times \mathbf{r}'), \tag{4.2}$$

where ρ is the mass density. The local stress balance in this co-rotating system, following Vasyliūnas (1983), can be written as

$$\dot{\rho}\mathbf{\Omega} \times \mathbf{r} + 2\rho\mathbf{\Omega} \times \dot{\mathbf{r}} + \rho\mathbf{\Omega} \times (\mathbf{\Omega} \times \mathbf{r}) + \nabla \cdot \mathbf{P} = \mathbf{j} \times \mathbf{B_0}. \tag{4.3}$$

where $\mathbf{r} = \mathbf{r}'$ is the radial distance, $\mathbf{P}$ the plasma pressure tensor, $\mathbf{j}$ the electric current density, $\mathbf{B_0}$ the magnetic field strength, while the dot denotes the local time derivative in the co-rotating system. Note that mass-loading is allowed in Equation (4.3) by including the local time derivative of the mass density. In the following consideration the Coriolis term $2\rho\mathbf{\Omega} \times \dot{\mathbf{r}}$ is neglected under assumption that the predominant plasma velocity is azimuthal. In order to determine the transverse part of $\mathbf{j}$, Equation (4.3) is multiplied with $\mathbf{B_0}$:

$$\dot{\rho}(\mathbf{\Omega} \times \mathbf{r}) \times \mathbf{B_0} + \rho\mathbf{\Omega} \times (\mathbf{\Omega} \times \mathbf{r}) \times \mathbf{B_0} + \nabla \cdot \mathbf{P} \times \mathbf{B_0} = (\mathbf{j} \times \mathbf{B_0}) \times \mathbf{B_0}. \tag{4.4}$$

The derivation proceeds by considering the local stress balance in the ϕ, r (equatorial) plane. The pressure is assumed to be isotropic. As the time dependent changes are observed at the current sheet center primarily in the south-north magnetic field component, the B_ϕ component will be neglected in the following. At the current sheet center $B_r = 0$ (please note that $(\partial B_r)/(r\partial\theta)$ can not be equal 0), this leads to

$$\dot{\rho}(\mathbf{\Omega} \times \mathbf{r}) \times \mathbf{B_0} = -\dot{\rho}\mathbf{\Omega}(\mathbf{B_0}\mathbf{r}) + \dot{\rho}\mathbf{r}(\mathbf{B_0}\mathbf{\Omega}) \simeq \dot{\rho} r B_\theta \Omega \mathbf{e_r},$$

$$\rho\mathbf{\Omega} \times (\mathbf{\Omega} \times \mathbf{r}) \times \mathbf{B_0} = \rho(\mathbf{\Omega}(\mathbf{\Omega}\mathbf{r}) - \mathbf{r}\Omega^2) \times \mathbf{B_0} \simeq \rho\Omega^2 B_\theta r \mathbf{e}_\phi,$$

$$(\mathbf{j} \times \mathbf{B_0}) \times \mathbf{B_0} \simeq -\mathbf{e_r} j_r B_\theta^2 - \mathbf{e}_\phi j_\phi B_\theta^2,$$

$$(\nabla \cdot P) \times \mathbf{B_0} \simeq \frac{\partial P}{r\partial\theta} B_\theta \mathbf{e_r} - \frac{\partial P}{\partial r} B_\theta \mathbf{e}_\phi$$

and Equation (4.4) reads

$$\dot{\rho} r B_\theta \Omega \mathbf{e_r} + \rho \Omega^2 B_\theta r \mathbf{e}_\phi + \frac{\partial P}{r \partial \theta} B_\theta \mathbf{e_r} - \frac{\partial P}{\partial r} B_\theta \mathbf{e}_\phi = -j_r B_\theta^2 \mathbf{e_r} - j_\phi B_\theta^2 \mathbf{e}_\phi. \tag{4.5}$$

Thus there are two components of the electric current density in the equatorial plane, a radial and an azimuthal one. The radial component is proportional to the mass-loading rate $\dot{\rho}$, is closed via field-aligned currents in the Jovian ionosphere, and serves to support corotation (Hill et al. 1983).

The azimuthal current is determined by the gradients of the magnetic field in radial and field-aligned direction:

$$\mu_0 j_\phi = \frac{\mu_0 \rho \Omega^2 r}{B_\theta} - \frac{\mu_0 \partial P}{B_\theta \partial r} = \frac{\partial B_\theta}{\partial r} - \frac{1}{r} \frac{\partial B_r}{\partial \theta}, \tag{4.6}$$

where μ_0 is the magnetic permittivity. The magnetic field data show that in the magnetotail spatial variations of B_θ in the radial direction are 100 times smaller than the meridional variations of B_r, therefore $(\partial B_\theta)/(\partial r)$ may be neglected (see also, Khurana and Kivelson 1989). Thus, the azimuthal current density is related to the radial magnetic field via

$$\mu_0 j_\phi \simeq -\frac{1}{r} \frac{\partial B_r}{\partial \theta} \simeq \frac{\mu_0 \rho \Omega^2 r}{B_\theta} - \frac{\mu_0 \partial P}{B_\theta \partial r}. \tag{4.7}$$

Furthermore assuming $|\partial B_r / r \partial \theta| \sim |B_r|/d$, where d denotes a typical scale of the magnetic field normal to the Jovian current sheet, equation (4.7) reads

$$-\frac{B_r}{d} \simeq \frac{\mu_0 \rho \Omega^2 r}{B_\theta} - \frac{\mu_0 \partial P}{B_\theta \partial r},$$

or

$$-\frac{B_r B_\theta}{\mu_0 d} \simeq \rho \Omega^2 r - \frac{\partial P}{\partial r}. \tag{4.8}$$

The last expression describes the azimuthal component of the local stress balance in the equatorial plane.

4.3 Estimation of the typical time constant

In order to derive the typical time constant of the Jovian reconfiguration process one has to first estimate the terms in expression 4.8.

Magnetic field

First we consider the evolution of the magnetic field. The change of the magnetic field components with distance can be estimated in different ways. One possibility is to use the dependencies derived by Khurana and Kivelson (1989). Here the magnetic field components B_r (in the lobe) and B_{theta} (at the equator) are:

$$\begin{aligned} B_r &= 6.12 \cdot 10^3 r^{-1.54}, \\ B_\theta &= 2.5 \cdot 10^4 r^{-2.4}, \end{aligned} \tag{4.9}$$

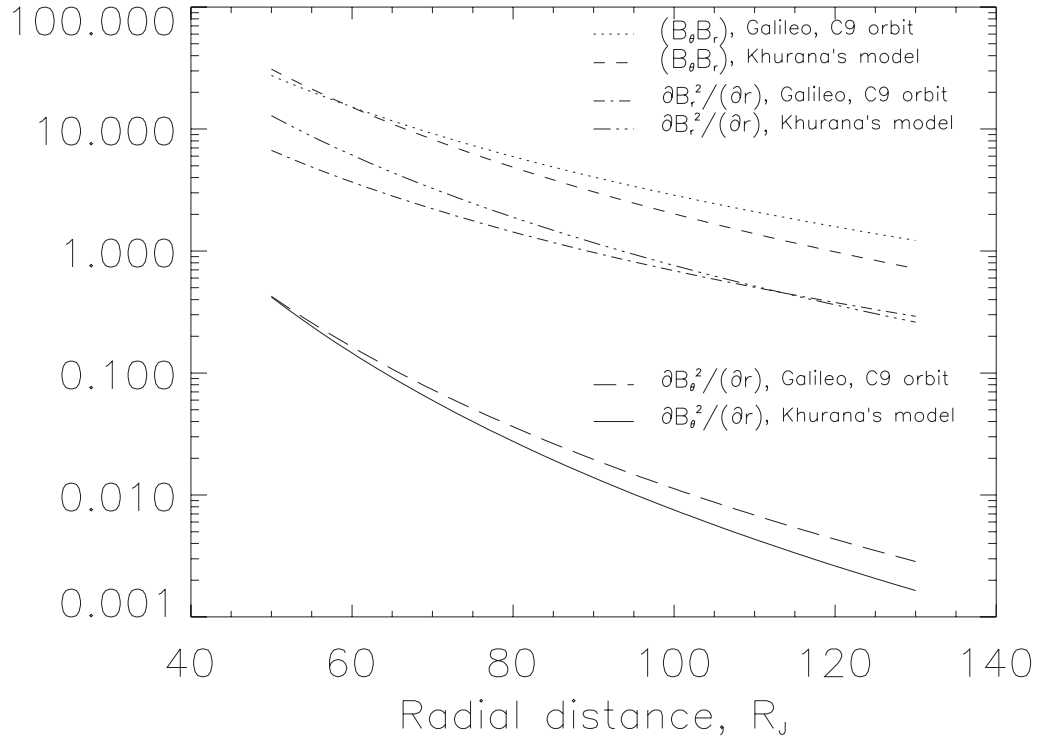

Figure 4.2: The change of the magnetic field components versus radial distance. The comparison of Khurana and Kivelson (1989) results and observations on Galileo orbit C9.

where B_r is in nT and r in R_J.

Another possibility is to use in situ measured data for a characteristic orbit. As an example the data from the Galileo C9 orbit is chosen. This orbit is located in the midnight sector and shows clear plasma sheet thinning signatures over a large radial interval. The magnetic field in the lobe has been fitted by a power law

$$B_r = 1.04 \cdot 10^3 r^{-1.14}.$$

For the B_θ component at the equator the power law fit yields

$$B_\theta = 9.14 \cdot 10^3 r^{-2.12}.$$

Here the units are the same as in Expression 4.9.

Figure 4.2 shows the comparison of the magnetic field change versus radial distance derived from the Galileo data (C9 orbit) and taken from Khurana and Kivelson (1989) model. The magnetic field changes are quite similar, but the derived power laws from the data of the C9 orbit give slightly higher values than those from Khurana and Kivelson (1989). This fact can be explained by difficulties in obtaining exact values of B_θ in the current sheet center and of B_r in the lobe region, (see Khurana and Kivelson 1989). Another reason could be the local time variation in the magnetic field.

Both of these estimations of the magnetic field will be used in the following.

Thickness of the plasma sheet and the centrifugal force

The half thickness d of the current sheet in the case of a pressure anisotropy can be estimated by (Khurana and Kivelson 1989)

$$d = \frac{|B_\theta B_r|}{\mu_0(-\rho\Omega^2 r + \frac{1}{2\mu_0}\frac{\partial}{\partial r}(B_r^2 + B_\theta^2))}. \tag{4.10}$$

In the denominator the contribution of the gradient of the meridional magnetic field component, $\partial B_\theta^2/\partial r$ in comparison to the gradient of the radial magnetic field component $\partial B_r^2/\partial r$ is negligible in the magnetotail as seen in Figure 4.2. To estimate the maximum current sheet half thickness, Khurana and Kivelson (1989) dropped the term with the centrifugal force because when publishing their work the mass density distribution was not well established.

Here we include the centrifugal force. For its estimation it is necessary to know the mass density and the angular velocity. The mass density according to Frank et al. (2002) can be described by: $\rho = 2.5 \cdot 10^{-25} r^{-1.28}$, assuming that the average ion mass is $16 \cdot m_p$, where m_p is the proton mass. The angular velocity is calculated as $\Omega = v^2/r$, where v is the azimuthal velocity with an average 200 km s^{-1} in the magnetotail (Krupp et al. 2001).

In Figure 4.3 two different approximations of the gradient of the radial magnetic field component are presented. In addition, the centrifugal force is shown for comparison. Khurana and Kivelson (1989) assumed in their calculations that the pressure balance is equal to unity and therefore

$$\frac{\partial P}{\partial r} \sim \frac{1}{2\mu_0}\frac{\partial}{\partial r}B_r^2. \tag{4.11}$$

This approximation is valid because the plasma sheet thickness is estimated in a steady state. Figure 4.3 demonstrates that the centrifugal term and the pressure terms from Khurana and Kivelson (1989) and the Galileo data are of the same order in the distant magnetotail. Therefore, using the similarity of the centrifugal term and pressure term and implying that the pressure term changes due to the mass-loading process, we can assume that

$$\frac{\partial P}{\partial r} \simeq \frac{1}{2\mu_0}\frac{\partial}{\partial r}B_r^2 \simeq -\mu_0\rho\Omega^2 r. \tag{4.12}$$

The temporal variations of both terms are supposed to be similar: the centrifugal force increases due to the mass-loading, while the increase of the gradient of the radial magnetic field component is shown indirectly (the radial magnetic field component increases with time during the loading time period) in Figure 3.10. Thus the expression of the current sheet half thickness 4.10 can be simplified as:

$$d = \frac{|B_\theta B_r|}{\mu_0(-\rho\Omega^2 r + \frac{1}{2\mu_0}\frac{\partial}{\partial r}B_r^2)} = -\frac{|B_\theta B_r|}{2\mu_0\rho\Omega^2 r}. \tag{4.13}$$

Figure 4.4 presents three estimates of the current sheet half thickness, one is from the Khurana and Kivelson (1989) model without centrifugal force, the two other estimations include the centrifugal force with the use of the magnetic field data derived from the Galileo C9 orbit and with the use of the magnetic field data from the Khurana and Kivelson (1989) model.

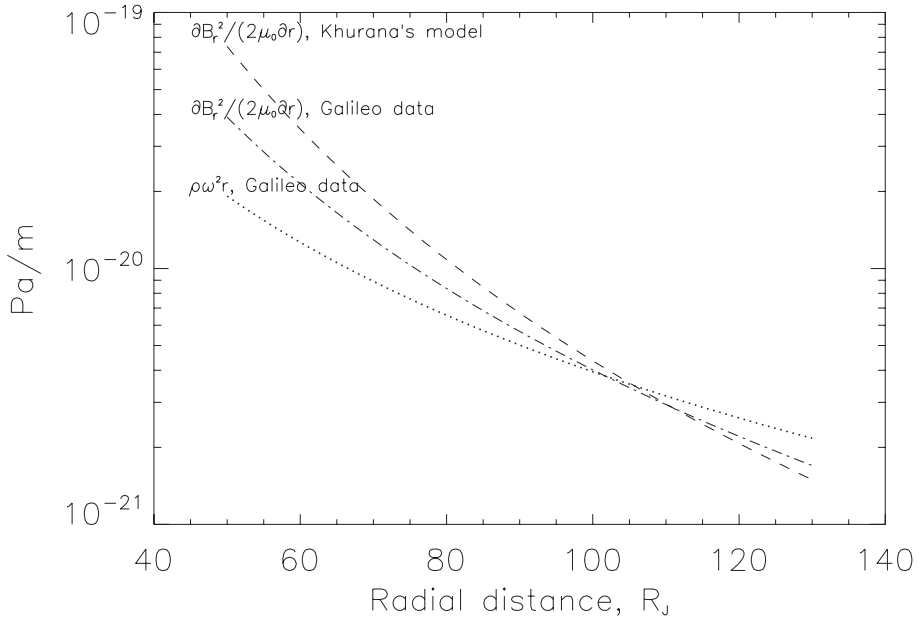

Figure 4.3: The centrifugal term (dotted thick line) and the pressure term expressed through the magnetic field using Khurana and Kivelson (1989) model, (dashed line) and data from Galileo C9 orbit, (dashed-dotted line).

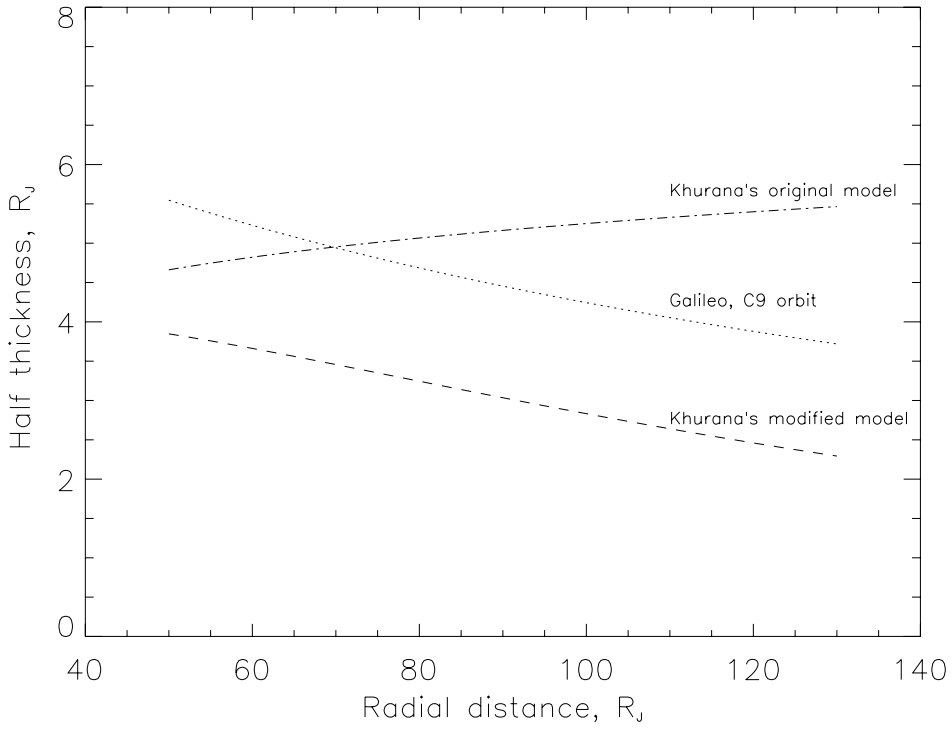

Figure 4.4: The thickness of the current sheet versus radial distance obtained by the different approaches described in the text.

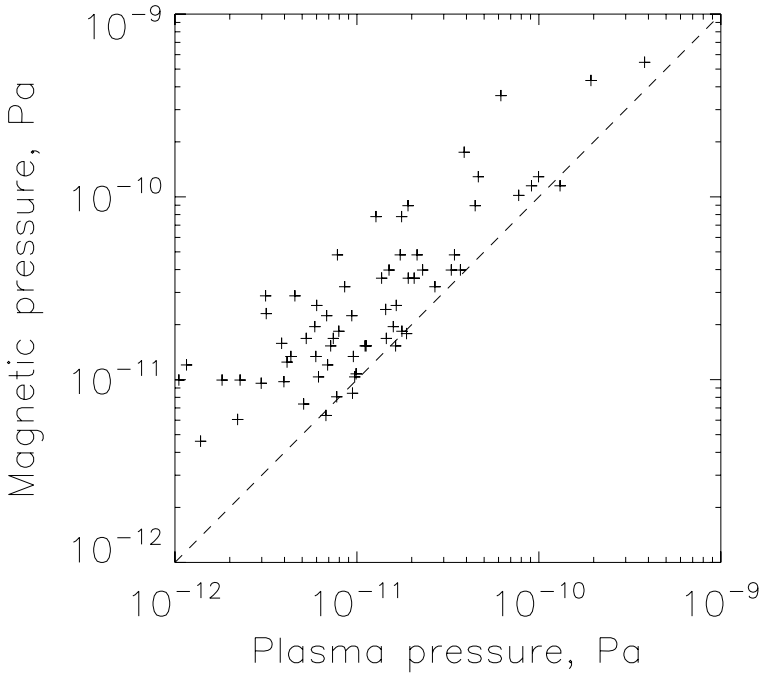

Figure 4.5: The relation of the plasma pressure in the current sheet center to the magnetic pressure in the lobe region. The dashed line denotes where the plasma pressure is equal to the magnetic pressure.

Pressure

Now let us return to the expression 4.8. While studying the dynamical behavior of the Jovian magnetosphere it is not evident that one can make the same approximation with respect to the pressure as in Expression 4.11. This assumption is only valid when the pressure balance is approximately constant and close to unity. Figure 4.5 presents the values of the plasma pressure in the current sheet centers derived from the EPD instrument and the magnetic pressure in the lobe regions for the C9 orbit. It shows that the stress balance indeed stays approximately constant with the correlation coefficient $\gamma = 0.89$, just the magnetic pressure is slightly higher than the plasma pressure. However, this difference is expected because the plasma pressure derived from the EPD instrument is only the partial plasma pressure (see discussion in Section 2.7.3). Therefore the pressure can be approximated as $\frac{\partial P}{\partial r} \sim \frac{1}{2\mu_0}\frac{\partial}{\partial r}B_r^2$. Under the considered conditions and by using the results from Figure 4.3 one can approximate the pressure also as $\frac{\partial P}{\partial r} \simeq -\mu_0 \rho \Omega^2 r$.

Time constant derivation

With relation 4.5 we can define the ratio α between the product of both the radial and the meridional magnetic field components and the typical scale of the magnetic field

normal to the Jovian current sheet (current sheet thickness):

$$\alpha = \left| \frac{B_\theta B_r}{\mu_0 d} \right| \simeq 2\rho\Omega^2 r. \tag{4.14}$$

This ratio $|(B_\theta B_r)/(\mu_0 d)|$ is independent of the sign of the field components and this shows that the temporal evolution of the current sheet topology is driven by mass-loading in rotating flux tubes. The stretching of the current sheet is caused by the Lorentz force influences the parameter α. The Lorentz force $\mathbf{j} \times \mathbf{B}$ is supposed to increase in the current sheet center because the stretching of the current sheet leads to an increased current density.

The expression for the current sheet thickness 4.13 and the expression 4.14 are similar. This is not surprising because both expressions are derived from the local stress balance.

The main aim of our conceptual model is to calculate the time, which the magnetotail needs to change from a dipolarized to a stretched-out situation. Therefore we need to find the temporal variation of the current sheet topology parameter α

$$\frac{d\alpha}{dt} = 2\dot{\rho}\Omega^2 r. \tag{4.15}$$

Here the temporal evolution of the Lorentz force is assumed to be linear. The data show that the temporal variation of B_θ and B_r can be roughly approximated by a linear fit, (cf. Figure 4.6).

The product $B_\theta \cdot B_r$ is monotonously decreasing in the time interval $[0, \infty]$ (see Figure 4.6), consequently the current sheet thickness d is also decreasing monotonously. The stretching of the current sheet can also be seen from the decreasing of the ratio B_θ/B_r (cf. the last panel in Figure 4.6). Close to the time when this ratio approaches the threshold for ion tearing instability (marked by the horizontal line) the usual southward directed magnetic field of the current sheet changes to a northward directed field. After this configurational change the radially outward ion burst follows (see the first burst in Figure 3.10).

The example presented in Figure 3.10 is one of the best. In other cases all ratios of B_θ/B_r show a decrease with time (time starts when the previous reconfiguration event is over), but this ratios do not always exceed the Zimbardo's threshold (=0.025) just before the likely beginning of the reconfiguration event. The value of the ratio can be maximum three times higher than the threshold. The reason is presumably that we do not register the actual ratio just prior to the reconfiguration event onset. Due to the limited temporal resolution of the magnetic field data and mainly because it is impossible to detect the magnetic field values simultaneously in the current sheet center and the lobe region. Furthermore, Galileo is not necessarily taken measurements fully in the lobe region. Thus the lobe field might be underestimated. Also the linear approximation of the magnetic field increase/decrease is a rather rough approach.

Using the linear approximation a robust estimation of the typical time constant of the stretching process τ can be written as:

$$\tau \simeq \frac{\alpha^{rec} - \alpha^0}{2\dot{\rho}\mu_0\Omega^2 r} \simeq \frac{\frac{B_r^{rec} B_\theta^{rec}}{d^{rec}} - \frac{B_r^0 B_\theta^0}{d^0}}{2\dot{\rho}\mu_0\Omega^2 r}, \tag{4.16}$$

where the terms with "0" correspond to the initial state of the magnetotail configuration (i.e. just after the preceding disturbed state), the terms with "rec" imply values taken just before the disturbed period starts. By using Formula 4.10, τ can be written as:

$$\tau \simeq \frac{2\mu_0\rho_{rec}\Omega^2 r - 2\mu_0\rho_0\Omega^2 r}{2\dot{\rho}\mu_0\Omega^2 r} = \frac{(\rho_{rec} - \rho_0)}{\dot{\rho}}. \tag{4.17}$$

In comparison of the expressions for τ, it is important to discern that the typical time constant in expression 4.16 depends on the initial current sheet configuration, the angular velocity and the mass-loading rate. It is also determined by the configuration of the current sheet at which the generation of the reconnection process is possible. With the help of 4.17 we get τ as a function. And in expression 4.17 τ depends only on the initial mass density, mass-loading rate and the threshold mass density at which the reconnection process could be generated.

Reconnection conditions

The reconnection process can be triggered by micro instabilities in thin current sheets when $d \sim r_{ion}$, where r_{ion} is the ion Larmor radius (Pritchett et al. 1991), and the magnetic field is distended as $|B_\theta/B_r| \leq 0.025$, where B_r is measured outside of the current sheet and B_θ within the equatorial plane (Zimbardo 1993). It was shown in Section 3.3.1 that the last condition is fulfilled just before the reconnection process starts.

Now let us consider the current sheet thickness at which the reconnection process becomes initiated. The ion Larmor radius is equal to

$$r_{ion} = \frac{v_\perp}{\Omega_{ion}} = 9.47 \times 10^{-7} \frac{\sqrt{A}}{Z} \frac{\sqrt{T}}{B},$$

where $v_\perp = v_{th}$ is the thermal velocity of ions, Ω_i is the ion cyclotron frequency, A is the ion mass number (in multiples of m_p), T is the temperature in Kelvin, Z is the ion charge number and B is the magnetic field strength in the lobe region in Tesla. Thus for typical plasma temperature in the Jovian magnetotail in the order of 10^8 K (Frank et al. 2002) and a typical magnetic field strength in the lobe region of 4 nT the gyroradii of the most abundant ions are about 0.1 R_J for sulfur 3+ and oxygen 2+ and 0.05 R_J for protons.

In the following we show that the current sheet thickness in the Jovian magnetotail can indeed become very thin. It will be estimated from Equation 4.10 using data from the E16 orbit (1998 248-249 DOY). This time interval is chosen because it shows the signatures of the current sheet thinning followed by reconnection. The magnetic field components are $B_r^{rec} = 4.35$ nT and $B_\theta^{rec} = 0.04$ nT (see Table 3.3). The azimuthal velocity is $v =$ 200 km s^{-1} (to calculate the angular velocity $\Omega = v^2/r$) and the mass density is assumed as 1.3·10^{-21} kg m^{-3} (Frank et al. 2002). So at a distance of 124 R_J the thickness of the current sheet just prior to the reconnection onset was $\sim$ 0.17 R_J which is of the order of the ion gyroradius. The time resolution and the wobbling of the current sheet do not allow to detect the real thickness directly before reconnection starts. Thus the above value constitutes an upper limit. In our estimation of the current sheet thickness only one parameter is defined not well enough: the mass density. The mass density can be twice higher or twice smaller but the current sheet thickness will still be of the order of the ion gyroradius.

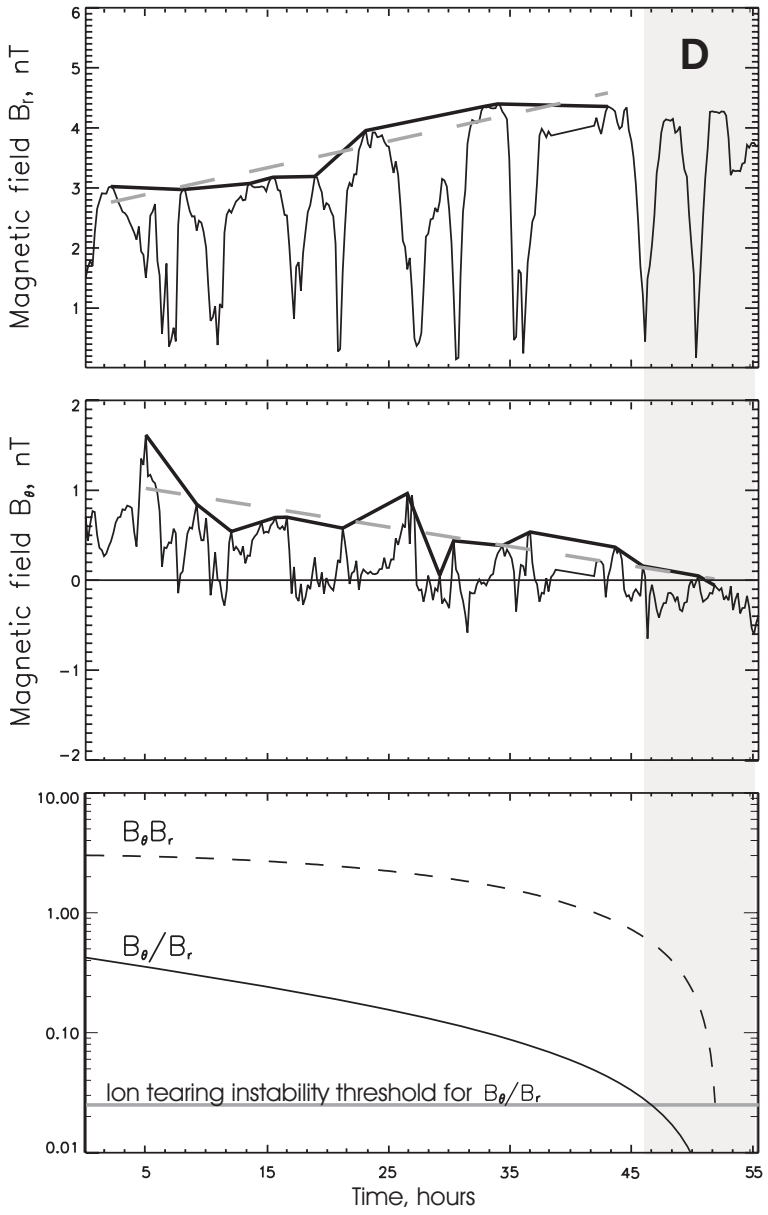

Figure 4.6: Top panel: the absolute value of the radial magnetic field component. The thick line shows an envelope of local maximum values of the magnetic field in the lobe region and the dashed line shows the linear fit of the envelope. Second panel: the south-north component of the magnetic field, where the thick line shows an envelope of local maximum values of the azimuthal magnetic field (in the vicinity of the current sheet center) and the dashed line shows the linear fit to this envelope. Third panel: the ratio of the linear fit of the south-north magnetic field component to the linear fit of the envelope of the radial magnetic field component. The horizontal line marks the threshold for the ion tearing instability (Zimbardo 1993) and the dashed line shows the time development of a product of the radial magnetic field component and the meridional magnetic field component. The data was taken in the time interval between DOY 235, 00:00 to DOY 237, 00:08 in 1998, (this corresponds to the first "quiet" interval in Figure 3.10). The grey area marks the disturbed state.

Mass-loading rate

To estimate the average change of the mass density in the Jovian magnetosphere $\dot{\rho} = \dot{m}/V$, it is necessary to define the mass-loading rate $\dot{m}$ and the mass-loaded plasma sheet volume V.

Estimations of the mass-loading rate is in the range between 100 and 600 kg s^{-1}, with an assumption of 250 kg s^{-1} as the most likely value, (see Section 1.1.1).

The partial volume of the Jovian magnetosphere which is affected by plasma loading is approximated by a cylindric volume $V = \pi h r^2$ where h is the height of the cylinder given by the average plasma sheet thickness which can be estimated as $h = 5R_J$ (Khurana et al. 2004). The cylinder radius r is assumed to be around $90R_J$ which is the radial distance from Io up to the probable neutral line location in the pre-dawn region (Woch et al. 2002). With these estimates the ion mass loading rate is in the order of $\dot{\rho} = 6 \cdot 10^{-27}$kg $(m^3 s)^{-1}$.

Estimation of the typical time constant

The estimation of the typical time constant can be made using either expression 4.16 or expression 4.17.

Estimation 1 (from Formula 4.16)

The values of the magnetic field and the current sheet thickness are presented in Table 4.3. The determination of the angular velocity was shown above.

Table 4.1: Typical values of the current sheet configuration in the midnight magnetotail.

B_r^{rec}	B_r^0	B_θ^{rec}	B_θ^0	d^{rec}	d^0
4.5 nT	3.5 nT	0.1 nT	1.1nT	0.148 R_J ($\sim$ 1 ion gyroradius)	2.5 R_J, 4 R_J

With these parameters the estimation of the typical time constant versus the mass-loading rate using expression 4.16 is presented in Figure 4.7. The time constant for various mass-loading rates and two initial current sheet thicknesses are displayed. The shaded area indicates the observed time constants, i. e., the characteristic repetition rate of the reconfiguration events.

The derived time constant τ has a value of ~ 3.5 days for a mass-loading rate of 250 kg s^{-1} and for a current sheet thickness of 2.5 R_J, which is in good agreement with observations. However, it should be noted that both the initial current sheet thickness as well as the mass-loading rate are not well constraint.

Estimation 2 (from Formula 4.17)

Here the estimation of the typical time constant is provided using expression 4.17 where the time constant depends on the initial mass density, the mass-loading rate and the

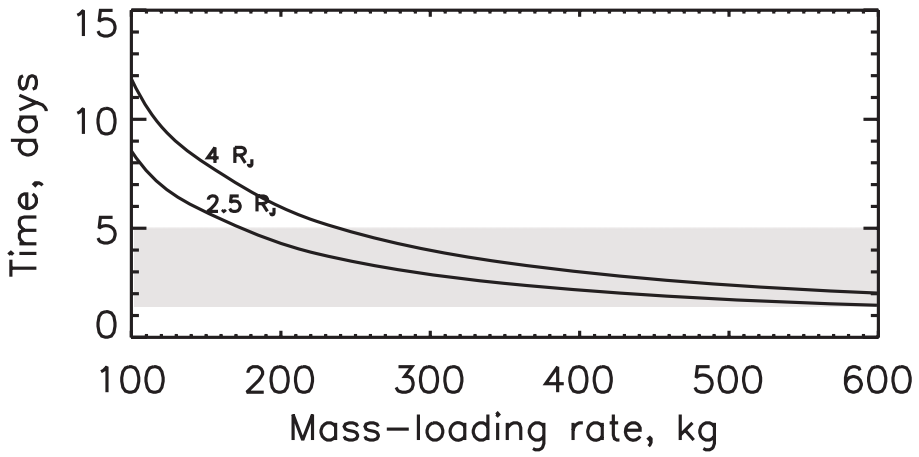

Figure 4.7: The time constant of the Jovian magnetosphere needed for mass loading until reconnection onset versus the ion mass-loading rate. Values of 4 R_J and 2.5 R_J are used for a current sheet thickness after the disturbed time period in the magnetotail region (initial current sheet thickness). The shaded area is the observable time constant.

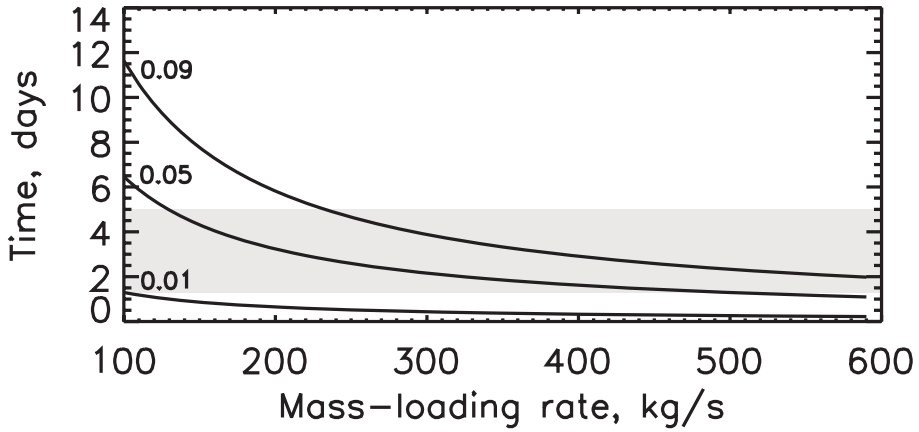

Figure 4.8: The time constant of the Jovian magnetosphere versus the mass-loading rate of the ions. As parameter we used the difference of the number density from the initial to the pre-reconnection state, $\delta n = 0.09, 0.05, 0.01$ cm^{-3}. The shaded area is the observable time constant.

mass density just before the reconnection starts. The difference of the initial number density and the number density just before the beginning of the reconnection in Expression 4.17 can be approximated as $\delta n = (\rho_{rec} - \rho_0) \cdot m_p \cdot 16$. Using the approximate values of δn from the number density values derived by Frank et al. (2002) the result of the estimation is shown in Figure 4.8.

Both estimations made above show similar results, as expected.

4.4 Discussion

It can be seen that the simple conceptual model presented here is able to explain the observations well if the mass-loading rate is of the order of a few hundred kg s^{-1}.

The basic assumptions for our estimations are:

(1) The radial and meridional magnetic field components as well as the current sheet thickness vary linearly with time.

(2) The angular velocity is assumed to be constant in time. This is corroborated by observations which show no clear indication of an angular velocity change.

(3) The pressure is isotropic and the pressure gradient term is equal to the centrifugal term in the stress balance as shown by observations.

The result of this simple conceptual model for the Jovian reconfiguration process is basically the same as the result of the "minimal substorm model" of Freeman and Morley (2004) with difference only regarding the energy sources. Equations 4.15 and 1.2 are basically equivalent. Thus $\alpha_0 \sim \rho_0$ is a prototype of an energy state F that the magnetotail would like to exist in, $\alpha_{rec} \sim \rho_{rec}$ is a prototype of a critical energy threshold C and $d\alpha/dt \sim \tau \cdot (\dot{\rho}\Omega^2 r)$ is a prototype of DP, where P is solar wind power and D is a constant related to a substorm periodicity. Therefore the parameter α_0 as well F in the Earth case is determined by the solar wind boundary conditions. The parameter α_{rec} is determined by the conditions for the current sheet configuration favoring reconnection, i.e., the current sheet thickness is of the order of the ion gyroradius and by the distention of the magnetic field. The parameter $d\alpha/dt$ basically depends on the mass-loading power and the centrifugal force. Thus it is an internal energy source. Thus the $\dot{\rho}$ in the magnetotail region strongly depends on the mass-loaded volume and hence as well on the solar wind conditions.

Therefore it is suggested that the main driving mechanism of the Jovian periodical substorms is the mass-loading of the rotating flux tubes with some external influence imposed by the solar wind conditions.

5 Summary and Outlook

The energetic particle and high-resolution magnetic field data from the Galileo orbits which cover the time interval from mid-1996 to end of 2002 were scanned for the occurrence of particle flow burst events, i.e. intervals with significant deviation of the particle flow from the usual corotational direction. From these we selected the 34 most prominent events for further analysis. Essentially they comprise those events which last longest while short-lasting events consisting of singular flow spikes were discarded. This choice was conditioned by the resolution of the EPD instrument which does not allow to study particle features on short time scales. Also the main aim of this study is the investigation of the large-scale processes. So the 34 periods with flow bursts are usually associated with considerable structural changes of the plasma sheet that indicate a general configuration change of the Jovian magnetotail. These events are referred to as reconfiguration events.

We have presented a detailed study on these events which allows to at least partly answer fundamental questions not only with respect to the nature of the burst / reconfiguration events but more generally on process governing the Jovian magnetosphere. These are:

- What is the nature of the observed radially outward and inward ion bursts / reconfiguration events in the Jovian magnetotail?

The detailed analysis of individual reconfiguration events shows that the reconfiguration process in the magnetotail consists of a transition from a "quiet" state to a "disturbed" state. The initial "loading" phase is characterized by plasma convection at a moderate speed in the corotational direction and by a gradual stretching of the Jovian plasma sheet configuration. In the release phase reconnection through a thinned current sheet leads to radially inward and outward plasma flows and the ejection of plasmoids. This phase is associated with signatures of radio emissions of auroral origin.

- Do substorm-like processes occur in the Jovian magnetosphere? What are the similarities and what are the differences to terrestrial substorms?

This study exemplifies that these events are very similar to terrestrial substorms in terms of the characteristic features. In analogy with the terrestrial substorm process the initial "loading" phase resembles characteristics of the growth (loading) phase and the "disturbed" phase (unloading) resembles the expansion phase of terrestrial substorms. The transition between these two states (in terrestrial substorm terminology called onset) of the substorm-like processes in the Jovian magnetosphere occur very rapidly like in the terrestrial case.

The recovery phase of the Jovian reconfiguration process seems to be very short in relation to the other phases similar as in the terrestrial case. The recovery phase of the Jovian reconfiguration process coincides with the beginning of the next loading phase. Thus the recovery phase is not defined as a distinctive phase.

A closer look at the substorm-like processes in the Jovian magnetosphere also reveals further features similar to the terrestrial substorms, such as the onset of magnetic fluctuations on a time scale of an ion gyroperiod in the magnetotail, plasma sheet boundary layer formation, signatures of travelling compression regions and the formation of a post plasmoid plasma sheet. The signatures of cross-tail and field-aligned current generations during the reconfiguration process (e. g. potential drop, reversed dispersion of ions and electrons, timing of reconfiguration events) support the substorm scenario.

The substorm-like configuration with x-line formation is backed up by a statistical study of the magnetic field configuration. There are evidences for multiple x-line formation phenomena like multiple releases of plasmoids.

The topological morphology of the reconfiguration process shows that the formation of the x-line, as deduced in a statistical study by Woch et al. (2002), could be explained by a different plasma sheet thickness in different local time sectors. The relatively thick plasma sheet in the midnight sector is presumably able to reconnect only at a more distant point from the planet than the relatively thin plasma sheet in the predawn region. Thus different signatures of magnetic field changes are observed at distinct positions relative to the x-line. If the spacecraft is located planetward of the x-line then the signatures of the current sheet stretching (seen in the magnetic field and the spectral index) are observed. When the spacecraft is located tailward of the x-line signatures of current sheet dipolarization (or plasmoid formation) are observed. Another topological feature is the apparent tailward motion of the reconnection topology that can be deduced from the flow reversal from tailward to inward. It seems to be an intrinsic feature of the reconfiguration / mass release events.

The investigated quantitative characteristics of the mass-release process show that the processes in the Jovian magnetosphere are about 10 times longer and larger in spatial scales than in the terrestrial one. The duration of the onset could be different due to different ion species abundance in the magnetospheres. Thus the reconnection growth rate is slower if the instability (tearing) is driven by heavier ions. At the Jovian magnetosphere the heavy ions as sulfur and oxygen more likely drive the instabilities because their gyroradius is larger and more comparable to the current sheet thickness. The quantities of the electric field and the velocities are similar to those during terrestrial substorm. Also the plasmoids in the Jovian magnetosphere are moving with Alfvénic speed as in the terrestrial case.

- What is the role of the solar wind and the interplanetary magnetic field in driving substorm-like processes at Jupiter?

Despite of the overall similarities of the terrestrial substorm and the Jovian reconfiguration process there is an important difference which let us to conclude that the Jovian reconfiguration process is fundamentally different from the terrestrial one. The Jovian reconfiguration process is inherently periodic. The cycle of topological stretching + dipolarization repeats every several days. Storage of magnetic energy in the lobe region by

interaction with the interplanetary medium seems not to be the prime driver of the reconfiguration process. Rather, the Jovian reconfiguration process is internally driven. The most prominent argument for an internally driven process is, of course, the intrinsic periodicity itself. Most regions of the Jovian magnetosphere covered during the Galileo mission undergo quasi-periodic modulations with a time period of several days. These modulations appear as periodically recurring ion flow bursts associated with disturbances in the meridional component of the magnetic field in the Jovian magnetotail, as changes of the ion spectral index and convection pattern as well as plasma sheet thickness in the middle magnetosphere. Each individual cycle of these modulations is believed to represent a global reconfiguration of the Jovian magnetosphere. Furthermore, in contrast to the Earth's case for most of the events no substantial magnetic flux increase during the presubstorm phase is observed rather the derived plasma pressure is gradually increasing during the "quiet state". This can be interpreted as a signature of mass-loading.

For these reasons it can be stated that the role of the solar wind as an energy source is of less importance for Jovian substorms than for terrestrial substorms. Instead, it can be envisaged that plasma loading of fast rotating magnetic flux tubes and the associated centrifugal forces drive the reconfiguration process.

- Why do these release processes occur periodically? Which mechanism is responsible for the release of plasma into the interplanetary space?

In order to confirm the observational conclusions a simple conceptual model for this periodic process was developed. It assumes that the ion-mass loading from internal plasma sources and the fast planetary rotation causes magnetotail field line stretching due to centrifugal forces. This leads to the development of a magnetotail configuration favoring magnetic reconnection. It is established that the condition for the onset of a tearing mode instability is satisfied just before each disturbed period of the reconfiguration process. It is shown that the current sheet thickness at that time is comparable to a heavy ion gyroradius. It is suggested that the tearing instability causes both plasmoid formation and their release with continuing mass loading leading to renewed stretching of tail field lines. The model yields that the intrinsic time constant of the Jovian reconfiguration process depends primarily on internal parameters like the mass-loading rate and is affected by the external solar wind conditions (the initial mass density). This model shows that the suggested intrinsic mechanism can explain the observed periodicities of several days of the Jovian substorm-like process.

- Are there fundamental commonalities with substorms and periodical substorms occurring at Earth?

The similarity of the processes at Jupiter and Earth supports the idea of Baker et al. (1999) that the substorm process is an energy loading-unloading process. The energy accumulated from different sources needs to be released. In the case of the Jovian magnetosphere it is its internal energy supplied by mass loading of flux tubes. Since the mass loading occurs more or less continuous this leads to an inherently periodic process. The repetition period is depending on the energy input and the ability of the magnetosphere to reconfigurate itself. Thus the repetition period of the Jovian reconfiguration events as well as occasionally observed periodical terrestrial substorms (as concluded by Freeman

and Morley 2004) depend on the energy input in to the magnetosphere, the solar wind boundary conditions and a critical energy threshold. The evolution of the Jovian reconfiguration process resembles a bifurcation as suggested by Schröer et al. (1994) for the terrestrial substorms case, i. e. the magnetotail collapses catastrophically and the highly stressed reconfiguration changes to the relaxed dipolar state. In this sense Jovian periodical substorms can be identified as a configurational instability as it was suggested by Baker et al. (1999) for the terrestrial case.

The carried out study suggests to investigate further the problem of the Jovian magnetosphere dynamics from different aspects.

- The developed model can be improved by implementing terms which were neglected in the simplified approach as for example the pressure anisotropy. It would be also interesting to take into account non-linearized time evolution of the terms in the local stress balance in the current sheet center.
- The dynamics of the Jovian magnetosphere (including the effects of mass loading) could be investigated with the help of time dependent MHD-simulations. To do do one has to construct first an equilibrium which includes the centrifugal force.
- Using a constructed magnetic field model from Belenkaya (2004) where the electric fields and plasma motions caused by Jupiter's rotation and the solar wind MHD generator it would be interesting to include the mass-loading via the change of the current strength, and then compare the results of our model with the current increase in the Belenkaya (2004) model which will lead to reconnection in the magnetotail.

If the results are successful it would be interesting to apply the model to Saturn's magnetosphere. Similar reconfiguration processes might also occur in Saturn's magnetosphere, because Saturn like Jupiter is a rapidly rotating planet with significant internal mass sources. The Energetic Neutral Atoms observations by Krimigis et al. (2005) detected that the nightside source varies with 11 hours periodicities. MHD simulations from Hansen and Gombosi (*private communication*) also predict periodical variations in Saturn's magnetotail. Preliminary results of our model predict time variations of about 10 hours.

Furthermore, further observational constrains on the Jovian reconfiguration process will be provided by the planned NASA mission JUNO with its Jovian Auroral Distributions Experiment and Juno Ultraviolet Spectrograph. They will allow to establish the contest between tail processes and the Jovian aurora, specifically to identify particle source population responsible for aurora generation. These could bring new understanding of the reconfiguration processes at Jupiter.

Bibliography

Angelopoulos, V., Kennel, C. F., Coroniti, F. V., Pellat, R., Kivelson, M. G., Walker, R. J., Russell, C. T., Baumjohann, W., Feldman, W. C., Gosling, J. T., 1994, Statistical characteristics of bursty bulk flow events, J. Geophys. Res., 99, 21 257–21 280

Bagenal, F., 1997, Ionization source near Io from Galileo wake data, Geophys. Res. Lett., 24, 2111–2114

Baker, D. N., Pulkkinen, T. I., Angelopoulos, V., Baumjohann, W., McPherron, R. L., 1996, Neutral line model of substorms: Past results and present view, J. Geophys. Res., 101, 12 975–13 010

Baker, D. N., Pulkkinen, T. I., Büchner, J., Klimas, A. J., 1999, Substorms: A global instability of the magnetosphere-ionosphere system, J. Geophys. Res., 104, 14 601–14 612

Balogh, A., Dougherty, M. K., Forsyth, R. J., Southwood, D. J., Smith, E. J., Tsurutani, B. T., Murphy, N., Burton, M. E., 1992, Magnetic field observations during the ULYSSES flyby of Jupiter, Science, 257, 1515–1518

Baumjohann, W., 1991, Die Erdmagnetosphäre, pp. 105–118, Plasmaphysik im Sonnensystem

Baumjohann, W., Paschmann, G., Luehr, H., 1990, Characteristics of high-speed ion flows in the plasma sheet, J. Geophys. Res., 95, 3801–3809

Belenkaya, E. S., 2004, The Jovian magnetospheric magnetic and electric fields: Effects of the interplanetary magnetic field, Planet. Space Sci., 52, 499–511

Birn, J., Thomsen, M. F., Borovsky, J. E., Reeves, G. D., McComas, D. J., Belian, R. D., 1997, Characteristic plasma properties during dispersionless substorm injections at geosynchronous orbit, J. Geophys. Res., 102, 2309–2324

Chamberlain, J. W., Hunten, D. M., 1987, Book-Review - Theory of Planetary Atmospheres, Science, 238, 96–+

Charbonneau, P., 1995, Genetic Algorithms in Astronomy and Astrophysics, Astrophysical Journal Supplement, 101, 309–+

Cheng, C. Z., 2004, Physics of Substorm Growth Phase, Onset, and Dipolarization, Space Science Reviews, 113, 207–270

Clarke, J. T., Jaffel, L. B., Gérard, J., 1998, Hubble Space Telescope imaging of Jupiter's UV aurora during the Galileo orbiter mission, J. Geophys. Res., 103, 20 217–20 236

Clauer, C. R., Cai, X., 2005, Similarities and differences between storm-time saw-tooth events and typical signatures of magnetospheric substorms, IAGA Abstracts, pp. IAGA2005–A–00 949

Cooper, J. F., Johnson, R. E., Mauk, B. H., Garrett, H. B., Gehrels, N., 2001, Energetic Ion and Electron Irradiation of the Icy Galilean Satellites, Icarus, 149, 133–159

Cowley, S. W. H., Bunce, E. J., Stallard, T. S., Miller, S., 2003, Jupiter's polar ionospheric flows: Theoretical interpretation, Geophys. Res. Lett., 30, 24–1

Dessler, A. J., 1983, Physics of the Jovian magnetosphere, Physics of the Jovian Magnetosphere

Dougherty, M. K., Southwood, D. J., Balogh, A., Smith, E. J., 1993, Field-aligned currents in the Jovian magnetosphere during the ULYSSES flyby, Planet. Space Sci., 41, 291–300

Dungey, J. W., 1961, Interplanetary Magnetic Field and the Auroral Zones, Physical Review Letters, 6, 47–48

Frank, L. A., Paterson, W. R., Khurana, K. K., 2002, Observations of thermal plasmas in Jupiter's magnetotail, J. Geophys. Res., 107, 1–1

Freeman, M. P., Morley, S. K., 2004, A minimal substorm model that explains the observed statistical distribution of times between substorms, Geophys. Res. Lett., 31, 12 807

Fukazawa, K., Ogino, T., Walker, R. J., 2005, Dynamics of the Jovian magnetosphere for northward interplanetary magnetic field (IMF), Geophys. Res. Lett., 32, 3202

Galopeau, P., Boudjada, M., 2005, Solar wind control of Jovian auroral emissions, J. Geophys. Res., 110, A09 221

Ganushkina, N. Y., Kubyshkina, M. V., Pulkkinen, T. I., 2005, Modeling of magnetic field and particle flux variations during saw-tooth events on October 21-22, 2001 storm, IAGA Abstracts, pp. IAGA2005–A–01 215

Geiss, J., Gloeckler, G., Balsiger, H., Fisk, L. A., Galvin, A. B., Gliem, F., Hamilton, D. C., Ipavich, F. M., Livi, S., Mall, U., 1992, Plasma composition in Jupiter's magnetosphere - Initial results from the Solar Wind Ion Composition Spectrometer, Science, 257, 1535–1539

Goedbloed, H., Poedts, S., 2004, Principles of Magnetohydrodynamics, Cambridge

Grodent, D., Clarke, J. T., Kim, J., Waite, J. H., Cowley, S. W. H., 2003a, Jupiter's main auroral oval observed with HST-STIS, J. Geophys. Res., 108, 2–1

Grodent, D., Clarke, J. T., Waite, J. H., Cowley, S. W. H., Gérard, J.-C., Kim, J., 2003b, Jupiter's polar auroral emissions, J. Geophys. Res., 108, 6–1

Grodent, D., Gérard, J.-C., Clarke, J. T., Gladstone, G. R., Waite, J. H., 2004, A possible auroral signature of a magnetotail reconnection process on Jupiter, J. Geophys. Res., p. A05201

Gurnett, D. A., Kurth, W. S., Hospodarsky, G. B., Persoon, A. M., Zarka, P., Lecacheux, A., Bolton, S. J., Desch, M. D., Farrell, W. M., Kaiser, M. L., Ladreiter, H.-P., Rucker, H. O., Galopeau, P., Louarn, P., Young, D. T., Pryor, W. R., Dougherty, M. K., 2002, Control of Jupiter's radio emission and aurorae by the solar wind, Nature, 415, 985–987

Hill, T. W., Dessler, A. J., Maher, L. J., 1981, Corotating magnetospheric convection, J. Geophys. Res., 86, 9020–9028

Hill, T. W., Dessler, A. J., Goertz, C. K., 1983, Magnetospheric models, pp. 353–394, Physics of the Jovian Magnetosphere

Hones, E. W., 1979, Transient phenomena in the magnetotail and their relation to substorms, Space Science Reviews, 23, 393–410

Huang, C., Foster, J. C., Reeves, G. D., Le, G., Frey, H. U., Pollock, C. J., Jahn, J.-M., 2003, Periodic magnetospheric substorms: Multiple space-based and ground-based instrumental observations, J. Geophys. Res., 108, 16–1

Huang, C., Le, G., Reeves, G. D., 2004, Periodic magnetospheric substorms during fluctuating interplanetary magnetic field B_z, Geophys. Res. Lett., 31, L14 801

Huang, C.-S., 2002, Evidence of periodic (2-3 hour) near-tail magnetic reconnection and plasmoid formation: Geotail observations, Geophys. Res. Lett., 29, 42–1

Ieda, A., Machida, S., Mukai, T., Saito, Y., Yamamoto, T., Nishida, A., Terasawa, T., Kokubun, S., 1998, Statistical analysis of the plasmoid evolution with Geotail observations, J. Geophys. Res., 103, 4453–4466

Joy, S. P., Kivelson, M. G., Walker, R. J., Khurana, K. K., Russell, C. T., Ogino, T., 2002, Probabilistic models of the Jovian magnetopause and bow shock locations, J. Geophys. Res., 107, 17–1

Kan, J. R., Sun, W., 1996, Substorm expansion phase caused by an intense localized convection imposed on the ionosphere, J. Geophys. Res., 101, 27 271–27 282

Kane, M., Williams, D. J., Mauk, B. H., McEntire, R. W., Roelof, E. C., 1999, Galileo Energetic Particles Detector measurements of hot ions in the neutral sheet region of Jupiter's magnetodisk, Geophys. Res. Lett., 26, 5–8

Khurana, K. K., 1992, A generalized hinged-magnetodisc model of Jupiter's nightside current sheet, J. Geophys. Res., 97, 6269–6276

Khurana, K. K., 2001, Influence of solar wind on Jupiter's magnetosphere deduced from currents in the equatorial plane, J. Geophys. Res., 106, 25 999–26 016

Khurana, K. K., Kivelson, M. G., 1989, On Jovian plasma sheet structure, J. Geophys. Res., 94, 11 791–11 803

Khurana, K. K., Kivelson, M. G., Vasyliunas, V. M., Krupp, N., Woch, J., Lagg, A., Mauk, B. H., Kurth, W. S., 2004, The configuration of Jupiter's magnetosphere, pp. 593–616, Jupiter. The planet, satellites and magnetosphere. Edited by Fran Bagenal, Timothy E. Dowling, William B. McKinnon. Cambridge planetary science, Vol. 1, Cambridge, UK: Cambridge University Press, ISBN 0-521-81808-7, 2004, p. 593 - 616

Kivelson, M. G., Khurana, K. K., 2002, Properties of the magnetic field in the Jovian magnetotail, J. Geophys. Res., 107, 23–1

Kivelson, M. G., Southwood, D. J., 2005, Dynamical consequences of two modes of centrifugal instability in Jupiter's outer magnetosphere, J. Geophys. Res., 110, A12 209

Kivelson, M. G., Khurana, K. K., Means, J. D., Russell, C. T., Snare, R. C., 1992, The Galileo magnetic field investigation, Space Science Reviews, 60, 357–383

Kivelson, M. G., Khurana, K. K., Russell, C. T., Walker, R. J., 1997, Intermittent short-duration magnetic field anomalies in the Io torus: Evidence for plasma interchange?, Geophys. Res. Lett., 24, 2127–2130

Krimigis, S. M., Armstrong, T. P., Axford, W. I., Bostrom, C. O., Fan, C. Y., Gloeckler, G., Lanzerotti, L. J., Hamilton, D. C., Zwickl, R. D., 1980, Energetic /approximately 100-keV/ tailward-directed ion beam outside the Jovian plasma boundary, Geophys. Res. Lett., 7, 13–16

Krimigis, S. M., Carbary, J. F., Keath, E. P., Bostrom, C. O., Axford, W. I., Gloeckler, G., Lanzerotti, L. J., Armstrong, T. P., 1981, Characteristics of hot plasma in the Jovian magnetosphere - Results from the Voyager spacecraft, J. Geophys. Res., 86, 8227–8257

Krimigis, S. M., Mitchell, D. G., Hamilton, D. C., Krupp, N., Livi, S., Roelof, E. C., Dandouras, J., Armstrong, T. P., Mauk, B. H., Paranicas, C., Brandt, P. C., Bolton, S., Cheng, A. F., Choo, T., Gloeckler, G., Hayes, J., Hsieh, K. C., Ip, W.-H., Jaskulek, S., Keath, E. P., Kirsch, E., Kusterer, M., Lagg, A., Lanzerotti, L. J., LaVallee, D., Manweiler, J., McEntire, R. W., Rasmuss, W., Saur, J., Turner, F. S., Williams, D. J., Woch, J., 2005, Dynamics of Saturn's Magnetosphere from MIMI During Cassini's Orbital Insertion, Science, 307, 1270–1273

Kronberg, E. A., Woch, J., Krupp, N., Lagg, A., Khurana, K. K., Glassmeier, K.-H., 2005, Mass release at Jupiter: Substorm-like processes in the Jovian magnetotail, J. Geophys. Res., 110, A03 211

Krupp, N., Woch, J., Lagg, A., Wilken, B., Livi, S., Williams, D. J., 1998, Energetic particle bursts in the predawn Jovian magnetotail, Geophys. Res. Lett., 25, 1249–1252

Krupp, N., Lagg, A., Livi, S., Wilken, B., Woch, J., Roelof, E. C., Williams, D. J., 2001, Global flows of energetic ions in Jupiter's equatorial plane: First-order approximation, J. Geophys. Res., pp. 26 017–26 032

Ladreiter, H. P., Zarka, P., Lacacheux, A., 1994, Direction finding study of Jovian hectometric and broadband kilometric radio emissions: Evidence for their auroral origin, Planet. Space Sci., 42, 919–931

Lagg, A., 1998, Energiereiche Teilchen in der inneren Jupitermagnetosphäre: Simulation und Ergebnisse des EPD-Experimentes an Bord der Raumsonde Galileo, Ph.D. thesis, University of Innsbruck

Lopez, R. E., Lui, A. T. Y., Sibeck, D. G., Takahashi, K., McEntire, R. W., 1989, On the relationship between the energetic particle flux morphology and the change in the magnetic field magnitude during substorms, J. Geophys. Res., 94, 17 105–17 119

Louarn, P., Roux, A., Perraut, S., Kurth, W., Gurnett, D., 1998, A study of the large-scale dynamics of the jovian magnetosphere using the Galileo plasma wave experiment, Geophys. Res. Lett., 25, 2905–2908

Louarn, P., Roux, A., Perraut, S., Kurth, W. S., Gurnett, D. A., 2000, A study of the Jovian "energetic magnetospheric events" observed by Galileo: role in the radial plasma transport, J. Geophys. Res., 105, 13 073–13 088

Lui, A. T. Y., 1996, Current disruption in the Earth's magnetosphere: Observations and models, J. Geophys. Res., 101, 13 067–13 088

Lyons, L. R., 1996, Substorms: Fundamental observational features, distinction from other disturbances, and external triggering, J. Geophys. Res., 101, 13 011–13 026

Mauk, B. H., Mitchell, D. G., McEntire, R. W., Paranicas, C. P., Roelof, E. C., Williams, D. J., Krimigis, S. M., Lagg, A., 2004, Energetic ion characteristics and neutral gas interactions in Jupiter's magnetosphere, J. Geophys. Res., p. A09S12

Mukai, T., 2000, Plasma Distribution Functions in Plasmoids: Geotail Observations, Advances in Space Research, 26, 415–424

Nishida, A., 1983, Reconnection in the Jovian magnetosphere, Geophys. Res. Lett., 10, 451–454

Ohtani, S., Takahashi, K., Higuchi, T., Lui, A. T. Y., Spence, H. E., Fennell, J. F., 1998, AMPTE/CCE-SCATHA simultaneous observations of substorm-associated magnetic fluctuations, J. Geophys. Res., 103, 4671–4682

Pavlos, G. P., Athanasiu, M. A., Anagnostopoulos, G. C., Rigas, A. G., Sarris, E. T., 2004, Evidence for chaotic dynamics in the Jovian magnetosphere, Planet. Space Sci., 52, 513–541

Podgorny, I. M., Podgorny, A. I., Minami, S., Rana, R., 2003, The mechanism of energy release and field-aligned current generation during substorms and solar flares, Adv. Polar Upper Atmos. Res.

Pontius, D. H., 1997, Radial mass transport and rotational dynamics, J. Geophys. Res., 102, 7137–7150

Prangé, R., Chagnon, G., Kivelson, M. G., Livengood, T. A., Kurth, W., 2001, Temporal monitoring of Jupiter's auroral activity with IUE during the Galileo mission. Implications for magnetospheric processes, Planet. Space Sci., 49, 405–415

Pritchett, P. L., Coroniti, F. V., Pellat, R., Karimabadi, H., 1991, Collisionless reconnection in two-dimensional magnetotail equilibria, J. Geophys. Res., 96, 11 523–+

Reiner, M. J., Fainberg, J., Stone, R. G., 1993, Source characteristics of Jovian hectometric radio emissions, J. Geophys. Res., 98, 18 767–+

Richardson, I. G., Cowley, S. W. H., 1985, Plasmoid-associated energetic ion bursts in the deep geomagnetic tail - Properties of the boundary layer, J. Geophys. Res., 90, 12 133–+

Richardson, I. G., Cowley, S. W. H., Hones, E. W., Bame, S. J., 1987, Plasmoid-associated energetic ion bursts in the deep geomagnetic tail - Properties of plasmoids and the postplasmoid plasma sheet, J. Geophys. Res., 92, 9997–10 013

Russell, C. T., 2001, The dynamics of planetary magnetospheres, Planet. Space Sci., 49, 1005–1030

Russell, C. T., McPherron, R. L., 1973, The Magnetotail and Substorms, Space Science Reviews, 15, 205–+

Russell, C. T., Khurana, K. K., Huddleston, D. E., Kivelson, M. G., 1998, Localized Reconnection in the Near Jovian Magnetotail, Science, 280, 1061–1064

Russell, C. T., Khurana, K. K., Kivelson, M. G., Huddleston, D. E., 2000a, Substorms at Jupiter: Galileo Observations of Transient Reconnection in the Near Tail, Advances in Space Research, 26, 1499–1504

Russell, C. T., Kivelson, M. G., Kurth, W. S., Gurnett, D. A., 2000b, Implications of depleted flux tubes in the Jovian magnetosphere, Geophys. Res. Lett., 27, 3133–3136

Sanderson, T. R., Page, D. E., 1974, Spherical harmonic analysis of satellite anisotropy measurements, Nuclear Instrumentation and Methods, 119, 177–182

Saur, J., Strobel, D. F., Neubauer, F. M., 1998, Interaction of the Jovian magnetosphere with Europa: Constraints on the neutral atmosphere, J. Geophys. Res., 103, 19 947–19 962

Saur, J., Strobel, D. F., Neubauer, F. M., Summers, M. E., 2003, The ion mass loading rate at Io, Icarus, 163, 456–468

Saur, J., Neubauer, F. M., Connerney, J. E. P., Zarka, P., Kivelson, M. G., 2004, Plasma interaction of Io with its plasma torus, pp. 537–560, Jupiter. The Planet, Satellites and Magnetosphere

Sauvaud, J. A., Beutier, T., Delcourt, D., 1996, On the origin of flux dropouts near geosynchronous orbit during the growth phase of substorms 1. Betatron effects, J. Geophys. Res., 101, 19 911–19 920

Schindler, K., 1974, A theory of the substorm mechanism, J. Geophys. Res., 79, 2803–2810

Schröer, A., Neukirch, T., Kiessling, M., Hesse, M., Schindler, K., 1994, Numerical bifurcation study of a nonlinear current sheet model, Physics of Plasmas, 1, 213–215

Schreier, R., Eviatar, A., Vasyliunas, V. M., Richardson, J. D., 1993, Modeling the Europa plasma torus, J. Geophys. Res., 98, 21 231–21 243

Scurry, L., Russell, C. T., Gosling, J. T., 1994, Geomagnetic activity and the beta dependence of the dayside reconnection rate, J. Geophys. Res., 99, 14 811–+

Slavin, J. A., Owen, C. J., Dunlop, M. W., Borälv, E., Moldwin, M. B., Sibeck, D. G., Tanskanen, E., Goldstein, M. L., Fazakerley, A., Balogh, A., Lucek, E., Richter, I., Reme, H., Bosqued, J. M., 2003, Cluster four spacecraft measurements of small traveling compression regions in the near-tail, Geophys. Res. Lett., 30, 7–1

Smith, E. J., Connor, B. V., Foster, G. T., 1975, Measuring the magnetic fields of Jupiter and the outer solar system, IEEE Transactions on Magnetics, 11, 962–980

Smyth, W. H., Marconi, M. L., 2003, Nature of the iogenic plasma source in Jupiter's magnetosphere I. Circumplanetary distribution, Icarus, 166, 85–106

Southwood, D. J., Kivelson, M. G., 2001, A new perspective concerning the influence of the solar wind on the Jovian magnetosphere, J. Geophys. Res., pp. 6123–6130

Stallard, T., Miller, S., Millward, G., Joseph, R. D., 2001, On the Dynamics of the Jovian Ionosphere and Thermosphere. I. The Measurement of Ion Winds, Icarus, 154, 475–491

Takahashi, K., Zanetti, L. J., McEntire, R. W., Potemra, T. A., Lopez, R. E., 1987, Disruption of the magnetotail current sheet observed by AMPTE/CCE, Geophys. Res. Lett., 14, 1019–1022

Thorne, R. M., Armstrong, T. P., Stone, S., Williams, D. J., McEntire, R. W., Bolton, S. J., Gurnett, D. A., Kivelson, M. G., 1997, Galileo evidence for rapid interchange transport in the Io torus, Geophys. Res. Lett., 24, 2131–2134

Tomás, A., Woch, J., Krupp, N., Lagg, A., Glassmeier, K.-H., Dougherty, M. K., Hanlon, P. G., 2004, Changes of the energetic particles characteristics in the inner part of the Jovian magnetosphere: a topological study, Planet. Space Sci., 52, 491–498

Vassiliadis, D., Klimas, A. J., Baker, D. N., Roberts, D. A., 1995, A description of the solar wind-magnetosphere coupling based on nonlinear filters, J. Geophys. Res., 100, 3495–3512

Vasyliūnas, V. M., 1983, Plasma distribution and flow, pp. 395–453, Physics of the Jovian Magnetosphere

Vasyliūnas, V. M., Frank, L. A., Ackerson, K. L., Paterson, W. R., 1997, Geometry of the plasma sheet in the midnight-to-dawn sector of the Jovian magnetosphere: Plasma observations with the Galileo spacecraft, Geophys. Res. Lett., 24, 869–872

Walker, R. J., Ogino, T., 2003, A simulation study of currents in the Jovian magnetosphere, Planet. Space Sci., 51, 295–307

Walker, R. J., Russell, C. T., 1985, Flux transfer events at the Jovian magnetopause, J. Geophys. Res., 90, 7397–7404

Wiechen, H., Schindler, K., 1991, Grundprozesse magnetosphärischer Aktivität, in: Glassmeier, K.-H., M. Scholer, Plasmaphysik im Sonnensystem, pp. 139–163, Mannheim

Williams, D. J., McEntire, R. W., Jaskulek, S., Wilken, B., 1992, The Galileo Energetic Particles Detector, Space Science Reviews, 60, 385–412

Woch, J., Krupp, N., Lagg, A., Wilken, B., Livi, S., Williams, D. J., 1998, Quasi-periodic modulations of the Jovian magnetotail, Geophys. Res. Lett., 25, 1253–1256

Woch, J., Krupp, N., Khurana, K. K., Kivelson, M. G., Roux, A., Perraut, S., Louarn, P., Lagg, A., Williams, D. J., Livi, S., Wilken, B., 1999, Plasma sheet dynamics in the Jovian magnetotail: Signatures for substorm-like processes?, Geophys. Res. Lett., 26, 2137–2140

Woch, J., Krupp, N., Lagg, A., 2002, Particle bursts in the Jovian magnetosphere: Evidence for a near-Jupiter neutral line, Geophys. Res. Lett., 29, 42–1

Woch, J., Krupp, N., Lagg, A., Tomás, A., 2004, The structure and dynamics of the Jovian energetic particle distribution, Advances in Space Research, 33, 2030–2038

Zimbardo, G., 1993, Observable implications of tearing-mode instability in Jupiter's nightside magnetosphere, Planet. Space Sci., 41, 357–361

Zong, Q.-G., Fritz, T. A., Pu, Z. Y., Fu, S. Y., Baker, D. N., Zhang, H., Lui, A. T., Vogiatzis, I., Glassmeier, K.-H., Korth, A., Daly, P. W., Balogh, A., Reme, H., 2004, Cluster observations of earthward flowing plasmoid in the tail, Geophys. Res. Lett., 31, L18 803

Acknowledgements

First of all my greatest thanks go to my scientific supervisors Dr. Joachim Woch and Dr. Norbert Krupp, who inspired and supported this work in every possible way, by ideas, lively discussions, humour and many other things.

My special thanks to Dr. Andreas Lagg for his readiness to help with the EPD software and programming problems.

I would like to deeply thank Professor Dr. Karl-Heinz Glassmeier for his assistance and ideas in the development of the theoretical model.

Also I would like to thank the PI of the EPD instrument D. Williams at JHU/APL, and the PI of the MAG instrument, M. Kivelson and S. Joy at IGPP/UCLA. The German contribution of the EPD Instrument was in part financed by the DLR (Deutsches Zentrum für Luft- und Raumfahrt e. V.) under contract No. 50 ON 0201. This work was financially supported by the Deutsches Zentrum für Luft- und Raumfahrt and the German Bundesministerium für Bildung und Forschung.

Many thanks to Dr. Krishan Khurana at IGPP/UCLA for his scientific comments which helped to better understand the problem. I am grateful to Dr. Paul Hanlon from the Imperial College for useful discussion and support with magnetic field data.

At MPS I am thankful to Mr. Monecke for his assistance in problems with software and hardware.

My thanks to Sybilla Siebert-Rust and Petra Fahlbusch for their help with paper work and making the life in Lindau easier. Here I would also give many thanks to Professor Dr. Klaus Jockers for his substantial help with life in Germany, for his help with the kindergarten and paper work.

I would like to express my gratitude to Professor Dr. Sami K. Solanki and Professor Dr. Ulrich Christensen that they made the work in the exiting research atmosphere of the Max-Planck-Institute for Solar System Research possible in the first place. Thanks to the IMPRS and in particular to Dr. Dieter Schmitt for his great coordination of the school.

Many thanks to my office colleges Ana Tomás and Katerina Radioti, to Luciano Rodriguez and Martin Tschimmel for their readiness to help and for lively conversations. It was simply great to work together!

The time I spent in Lindau has been great because I have found wonderful friends, friends with whom I could share the good and bad times in life. Many thanks to you!

Special thanks to Dr. Thomas Wiegelmann for his great help in all aspects of life, starting from science.

Many thanks to my parents for supporting me, for their unstipulated and infinite love! And my last but very cordial thanks to you my son Konstantin, for the wonderful moments, for your patience to your permanently working mama, sorry that this time was devoted not to you. But we both have grown and we both have learned a lot.

Curriculum Vitae

PERSÖNLICHE DATEN

Name	Elena Aleksandrovna Kronberg
Geburtsdatum	July 2, 1978
Geburtsort	Kemerovo/USSR
Familienstand	Geschieden, ein Kind: Konstantin, geb. am 7 May, 1999
Eltern	Aleksander und Tatiana Kronberg
Staatsangehörigkeit	Russin

SCHULBILDUNG

1985-1992	Grund-und Mittelschule N 84, Barnaul, Russland
1992-1995	Gymnasium N 123 mit Schwerpunkt Mathematik und Physik, Barnaul, Russland

STUDIUM

1995-1999	Bachelor in Physics with honors - Diploma Thesis: "Stochastic dynamics of relativistic electrons in the upper-hybrid wave field and transverse magnetic field", Altai State University, Barnaul, Russland
1999-2001	Master in Physics with honors - Diploma Thesis: "Stochastic dynamics of relativistic electrons in the vector-scalar wave field and in the static magnetic field", Altai State University, Barnaul, Russland
2001-2002	Promotionsstudium an der Altai State Universität, Barnaul, Russland

PROMOTION

Jan. 2003 - Dec. 2005	Stipendium des Max-Planck-Instituts für Sonnensystemforschung